Magnetic anisotropy of transition metal and lanthanide ions in pentagonal bipyramidal geometry

Jean-pascal Sutter, Virginie Béreau, Valentin Jubault, Kateryna Bretosh, Céline Pichon, Carine Duhayon

Magnetic Anisotropy of Transition Metal and Lanthanide Ions in Pentagonal Bipyramidal Geometry [§]

Jean-Pascal Sutter,[a]* Virginie Béreau,[a,b] Valentin Jubault,[a] Kateryna Bretosh,[a] Céline Pichon,[a] Carine Duhayon[a]

[a] *Laboratoire de Chimie de Coordination du CNRS (LCC-CNRS), Université de Toulouse, CNRS, Toulouse, France*
[b] *Université de Toulouse, Institut Universitaire de Technologie Paul Sabatier-Département de Chimie, Av. Georges Pompidou, F-81104 Castres, France*

Table of Content

Magnetic Anisotropy of Transition Metal and Lanthanide Ions in Pentagonal Bipyramid Geometry

The magnetic anisotropy associated with a PBP coordination sphere is examined on the basis of experimental and theoretical investigations; its origin and characteristics are described, and the effects of crystal field, structural distortion, and the second coordination sphere are discussed.
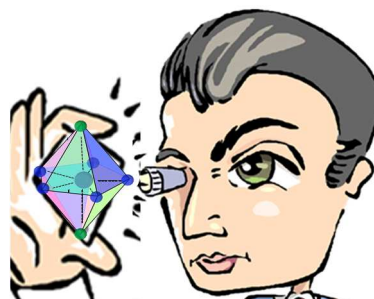
[§] Formalisms used in this paper:

Spin Hamiltonian with ZFS terms describing the magnetic anisotropy: $H = D[S_z^2 - S(S+1)/3] + E(S_x^2 - S_y^2) + \mu_B \boldsymbol{g} \cdot \boldsymbol{S} \cdot \boldsymbol{B}$, where D and E are the axial and rhombic ZFS parameters, S the spin, the last part corresponds to the Zeeman term, $\boldsymbol{B}$ stands for the magnetic field vector.

The exchange interactions are given in accordance with Hamiltonians of type $H = -J\boldsymbol{S_1} \cdot \boldsymbol{S_2}$ (example for a pair of spins)

Abstract :

The magnetic anisotropy associated to a pentagonal bipyramidal (PBP) coordination sphere is examined on the basis of experimental and theoretical investigations. The origin and the characteristics of this anisotropy are discussed in relation with the electronic configuration of the metal ions. The effects of crystal field, structural distortion, and second-coordination sphere, on the observed anisotropies for transition meal and lanthanide ions are outlined. For the Ln derivatives, we focus on compounds showing SMM-like behavior (i.e. slow relaxation of their magnetization) in order to highlight the essential chemical and structural parameters for achieving strong axial anisotropy. The use of PBP complexes to impart controlled magnetic anisotropy in polynuclear species such as SMMs or SCMs is also addressed.

This review of the magnetic anisotropies associated to a pentagonal bipyramidal coordination sphere for transition metal and lanthanide ions is intended to highlight some general trends that can guide the chemists in designing of a compound with specific properties.

Magnetic anisotropy is a key parameter of the behavior exhibited by magnetic materials. For instance, the hardness of a bulk magnet correlates with its magnetic anisotropy; the performance of a single molecule magnet (SMM) is highly dependent on large and strongly axial magnetic anisotropy, whereas for molecular Spin Qubits, small and in-plan magnetic anisotropy is preferable. The magnetic anisotropy emanates mainly from the metal centers constituting the compound; its characteristics (strength, axial or planar) depend on the metal ion, the electronic configuration, the coordination geometry, and the ligand field. It is therefore possible to impart magnetic anisotropy to a compound in a controlled way by chemical design.

Seven-coordinated metal complexes with pentagonal bipyramid-shaped coordination sphere (abbreviated to PBP hereafter) have emerged recently as an attractive option for achieving large magnetic anisotropy in a molecular unit.[1, 2] This applies for transition metal and lanthanide ions with suitable electronic configurations. In several cases, mononuclear complexes have been found to exhibit SMM-type behaviors. More generally, this coordination geometry allows easy access to a wide range of axial or planar magnetic anisotropy that depends mainly on the metal ion involved.

Access to PBP shaped coordination sphere can be straightforward. Following a strategy documented in the 70s,[3-5] this geometry can be designed using a suitable pentadente ligand (Figure 1) to occupy five equatorial coordination sites of the metal center.[6-8] The pentadentate ligand also confers to the complex a good structural robustness making possible the substitution of the labile ligands (solvents, anions) in axial positions without compromising the coordination geometry,[9] thus preserving the magnetic anisotropy. This allowed using these complexes as building blocks in the design of polynuclear systems such as SMM (Single Molecule Magnets) and SCM (Single Chain Magnets).
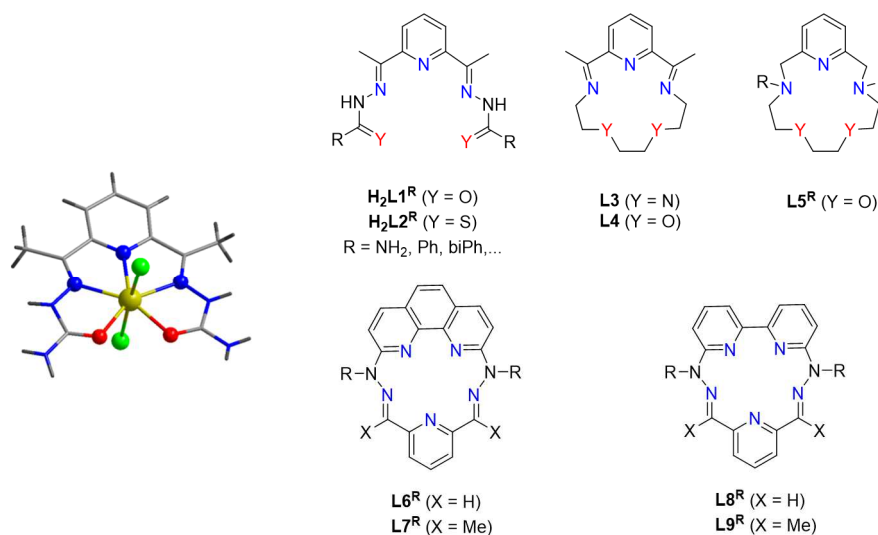

Figure 1. Selection of typical pentadentate ligands used in pentagonal bipyramidal complexes (for H_2L1^R see also *Appendix 1*).

The objective of this paper is to review the knowledge acquired on the magnetic anisotropy of transition metal and rare earth ions with PBP coordination sphere. A first section is devoted to the

transition metal complexes, where the origin of the magnetic anisotropy in PBP geometry will be introduced and the main experimental conclusions summarized for the most relevant metal ions. The use of such PBP complexes as building units to incorporate controlled magnetic anisotropy in polynuclear species is also illustrated. The second section focuses on lanthanide ions.

I. Transition metal ions with pentagonal bipyramidal coordination polyhedron

The qualitative splitting pattern of the d orbitals in ideal pentagonal bipyramidal crystal field (D_{5h}) is depicted in Figure 2a. It consists in two sets of two-degenerate orbitals, plus one orbital of higher energy. Such a situation is favorable for first-order spin-orbit coupling for electronic configurations leading to a filling of a degenerate level with 3 electrons. However, in real systems, the degeneracies are lifted due to distortion of the coordination sphere and unsymmetrical ligand field (Figure 2b-c).[10, 11] Therefore, spin-orbit coupling in the complexes results mainly from zero-field splitting (ZFS), and magnetic anisotropy is characterized by axial ZFS parameter D, and rhombic parameter E. It relies on coupling between ground electronic state and excited states, therefore electronic configuration and the energy of the electronic transitions dictate D. The value of D will be all the greater the smaller the energy gap between the ground state and the excited states. It follows that the strongest contribution to D will come from the coupling with the first excited states. For the electron transitions between orbitals with same magnetic quantum number, m_l,[12] the sign of the contribution to D is negative while transitions between orbitals of different m_l yield positive values. These simple considerations make it possible to anticipate the sign of D for a given electronic configuration. For instance, the orbital filling for a d^6 ion with high spin configuration (Figure 2b) leads to two electrons in the lowest energy orbital, d_{yz}, and one electron in each of the other four orbitals. The first excited quintet state results from the promotion of one electron from the d_{yz} orbital to the d_{xz} orbital, which are very close in energy, whereas second and third excited quintet (corresponding to the promotion of the electron to the $d_{x^2-y^2}$ and d_{xy} orbitals) are higher in energy.[13] Consequently, the strongest contribution to the D parameter is expected from the first excited state, and since m_l remains unchanged, this contribution is negative. An overall negative D value can therefore be anticipated for high-spin Fe^{II}, and this is supported by experimental data (*vide infra*). For a high-spin d^7 configuration (Figure 2c) typical for Co^{II}, the strongest contributions to the axial D parameter are expected from the excited quartet states resulting from the promotion of an electron from d_{xz} or d_{yz} orbitals to the $d_{x^2-y^2}$ orbital.[10] These contributions being positive, an overall positive D parameter can be expected for such a metal complex, which is indeed found experimentally. Of course, the actual magnitude of D will depend on all the contributions that are directly related to the effective energy diagram for the d orbitals. The latter relies on structural and chemical aspects.
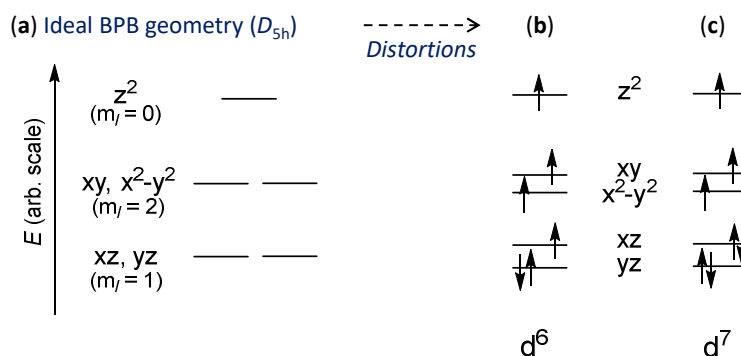
Figure 2. Orbital energy diagrams for (a) ideal pentagonal bipyramidal geometry (D_{5h}), and (b-c) in real systems after lifting of the degeneracy (qualitative sketches), with electron filling for Fe^{II} and Co^{II}, respectively.

The magnetic anisotropy reported for various electronic configurations are reviewed below and the effects of structural and chemical features will be discussed.

I.1 d^1 ions (V^{IV})

Few PBP metal complexes of d^1 electronic configuration have been reported and the characterization of their magnetic features remained basic. The presence of a single electron in the d-orbitals results in S = ½ spin state which excludes any ZFS, hence magnetic anisotropy. PBP V^{IV} is found in oxo-bridged bimetallic $[\mu\text{-O-}\{V(L2^{NH2})(MeOH)\}_2]^{2+}$ complex and its magnetic behavior is consistent with two S = ½ spin centers.[14]

I.2 d^2 ions (V^{III}, Mo^{IV}, W^{IV})

The presence of two electrons in the two low-lying orbitals (Figure 2) is anticipated to result in a ground spin state of S = 1 displaying magnetic anisotropy characterized by ZFS with a positive *D* parameter.

A very early example of heptacoordinated 3d^2 ion with an organic ligand set in PBP arrangement was K$_4$[V(CN)$_7$],[15] [16] but no information about its magnetic anisotropy is available. A detailed investigation of the ZFS parameters for V^{III} in PBP environment was performed for a series of complexes obtained with the pentadentate ligand H$_2$L1^{Ph} in various states of deprotonation (Table 1).[17] Combined magnetic, high-field EPR, and theoretical studies concluded in the absence of first-order spin-orbit coupling due to degeneracy lifting of the two lower energy levels and converged to anisotropy parameters *D* in the range of 3.9-4.5 cm^{-1}, and negligibly small E. The magnetic behavior for two complexes, $[V^{III}(tepa)(\mu\text{-}Sn_2Q_6)]$n (tepa stands for tetraethylenepentamine, Q = S or Se), featuring an open N5-pentadentade ligand and either S or Se atoms in the apical positions have been reported but no information on the magnetic anisotropy was provided.[18]

Significantly larger ZFS effects have been found for second and third row metal ions. A 4d complex with Mo^{IV}, $[Mo(L1^{Ph})Cl_2]$, was found to undergo a rapid decrease of its magnetic moment below 50 K

attributed to thermal depopulations of the excited M_S = +/-1 levels resulting from ZFS of the S = 1 triplet state.[19] The temperature dependence of the magnetic susceptibility (χ_M) was modeled considering a ZFS effect with D = 50 cm^{-1}, and it was noticed that a substantial temperature independent paramagnetism (TIP) contributed to the experimental behavior.

The effect of spin-orbit interaction is even more noticeable for 5d ions. The W^{IV} complex, [W(CN)$_7$]$^{3-}$, was found to exhibit a non-magnetic ground state at 2 K, and a $\chi_M T$ value increasing with T but reaching only 0.77 cm^{3}mol^{-1}K at 300 K. This value, below the contribution expected for an S = 1 spin, suggests a partial thermal population of first excited levels (with M_S = +/-1) even at 300 K, hence a large energy gap with ground level. The behavior was analyzed supposing ZFS of the S = 1 ground state and led to an axial parameter as large as D = 430 cm^{-1}.[20] Ligand Field calculations supported the magnitude of the ZFS energy.[19]

Complex	ZFS parameters (cm^{-1})		Ref.
	experimental	theory	
[V(H$_2$L1^{Ph})Cl$_2$]Cl	-	D = 3.9; E = 0.035	[17]
[V(HL1^{Ph})(NCS)$_2$]	-	D = 4.0; E = 0.09	[17]
[V(L1^{Ph})(MeOH)$_2$]Cl	D = 4.5; E = 0$^{(a)}$ D = 4.6; E = 0$^{(b)}$	D = 3.98; E = 0.06	[17]
[Mo(L1^{Ph})Cl$_2$]	D = 50; E = 0.025$^{(b)}$	D = 49.8; E = 0.025	[19]
(NBu$_4$)$_3$[W(CN)$_7$]	D = 330; E = 100$^{(b)}$ D = 430; E = 38$^{(c)}$	D = 279; E = 0.14	[19, 20]

(a) from HF-EPR data; (b) from magnetic susceptibility data; (c) from M versus H data

Table 1. Magnetic anisotropy in d^2 metal complexes

I.3 d^3 ions (Cr^{III}, Mo^{III}, W^{III}, Re^{IV})

Two situations can apply for a d^3 spin configuration in PBP geometry; either it is high spin and gives rise to a spin state S = 3/2, or it is low spin with S = ½.

The high-spin configuration has been found to apply in Cr^{III} PBP derivatives (Table 2). In an ideal PBP geometry, two electrons would be in the low-lying d_{xz} and d_{yz} orbitals and the third would be shared by the d_{xy} and $d_{x^2-y^2}$ orbitals (Figure 2). Such a situation would lead to significant axial anisotropy (D < 0); however, real compounds exhibit coordination dissymmetry in the pentagonal plane due to Jahn-Teller effect (Figure 3) that lifts the d_{xy} / $d_{x^2-y^2}$ orbitals degeneracy aimed at reducing the total energy of the system.[21, 22] As a result, magnetic anisotropy was evaluated to be very small with |D| in the order of 1-2 cm^{-1}.[22] Theoretical calculations performed for [Cr(HL1^{PhOMe})(Cl)$_2$] and [Cr(L1^{Ph})(CN)$_2$]$^-$ moieties indicated a negative D close to -1 cm^{-1}. [21, 23, 24] Such overall small magnetic anisotropy is rationalized by the energy difference of the d_{xy} and $d_{x^2-y^2}$ orbitals introduced by the Jahn-Teller distortion. The concomitant increase of the energy gap between the ground state and the first excited state, i.e. $(d_{xy})^1(d_{x^2-y^2})^0$ <-> $(d_{xy})^0(d_{x^2-y^2})^1$ reduces its negative contribution to D that becomes balanced by the positive contributions from the higher excited states.
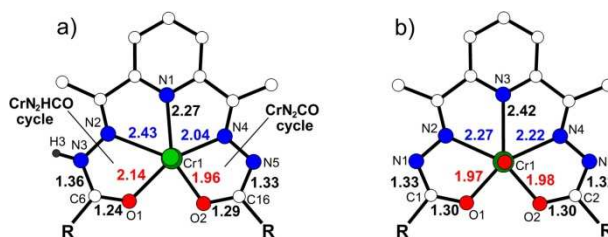
Figure 3. Comparison of the Cr^{III}-ligand bond length (Å) in the equatorial plane in (a) $[Cr(HL1^{PhOMe})Cl_2]$ and (b) $[Cr(L1^{PhOMe})(MeO)(MeOH)]$. (Reprinted from ref.[21] with permission from Elsevier, copyright 2021)

The known $4d^3$ and $5d^3$ ions with PBP coordination polyhedron have low spin configuration with an S = ½ ground spin state characterized by strongly anisotropic g parameters (Table 2). The isoelectronic cyanometallate complexes $[Mo^{III}(CN)_7]^{4-}$ and $[Re^{IV}(CN)_7]^{3-}$ are well investigated examples. Detailed magnetic studies down to 2 K have been reported for a structurally rigid complex, $NEt_4[Mo(L1^{Ph})Cl_2]$ and its behavior rationalized by ligand field calculations.[25] Such compounds are not expected to exhibit magnetic anisotropy (ZFS takes place only for S > ½) but unquenched orbital momentum occurs. Due to the orbital degeneracy and strong spin-orbit coupling, the ground state of the PBP complex is split into two Kramers doublets ($\varphi(\pm 1/2)$ and $\chi(\pm 1/2)$ in Figure 4). The ground-state Kramers doublet was found to exhibit strong magnetic anisotropy with spin and orbital momenta parallel to the apical direction of the complex.[25] This results in a highly anisotropic g tensor; for instance $g_\perp$ = 1.77 and $g_{//}$ =
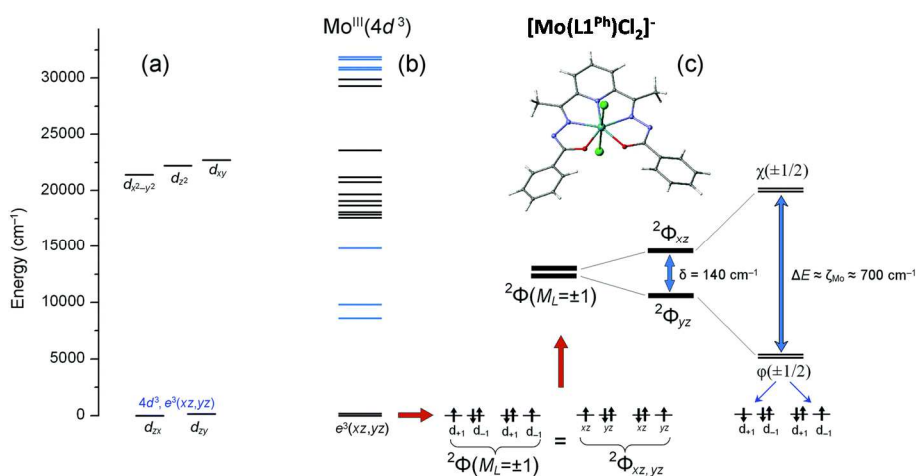

Figure 4 . Ligand field calculations for $[Mo^{III}(L1^{Ph})Cl_2]^-$: (a) 4d orbital energies of the complex. (b) Energy spectrum of the $4d^3$ LF states (Excited quartet spin states (S = 3/2) are marked with blue lines). (c) Electronic structure of the ground state of the complex. The ground state is the orbital doublet $^2\Phi(M_L = \pm 1)$ with unquenched orbital momentum $M_L = \pm 1$ resulting from the $e^3(xz,yz)$ doubly degenerate electronic configuration (where $d_{\pm 1} = (d_{xz} \pm id_{yz})/2^{1/2}$ are complex d-orbitals with the definite projection of the orbital momentum $m_l = \pm 1$). The $^2\Phi(M_L = \pm 1)$ doublet is split (by δ = 140 cm^{-1}) into two real components $^2\Phi_{xz} = (yz)^2(xz)^1$ and $^2\Phi_{yz} = (yz)^1(xz)^2$, which are further split by the spin–orbit coupling $\zeta_{Mo}\mathbf{LS}$ into the ground $\varphi(\pm 1/2)$ and excited $\chi(\pm 1/2)$ Kramers doublets. The ground Kramers doublet $\varphi(\pm 1/2)$ exhibits Ising-type magnetic anisotropy; the orbital composition of its wave functions is indicated. (Reproduced from Ref.[25] with permission from The Royal Society of Chemistry.)

3.89 have been obtained from EPR studies of solid $NaK_3[Mo^{III}(CN)_7]$, where Mo has PBP coordination sphere.[26] For the Re^{IV} homologue, $g_\perp = 1.759$ and $g_{||} = 3.66$ have been found.[27, 28] Somewhat less anisotropic g was observed for a PBP W^{III} derivative with mixed carbonyl/cyanide ligand set, cis-$[W(CN)_5(CO)_2]^{2-}$, but EPR was recorded in solution.[29]

Ab initio calculations performed for $[Mo(L1^{Ph})Cl_2]^-$ reveal large anisotropy for the magnetic susceptibility with a susceptibility along the Cl-Mo-Cl direction, χ_z, about two order of magnitude larger than the χ_x and χ_y components. Such a situation was found to favor highly anisotropic exchange interaction with 3d ions which can be source for magnetic anisotropy in polynuclear compounds.[30-32]

PBP d³ units in polynuclear compounds. These PBP complexes have been used in the preparation of polynuclear compounds because of the exchange interactions they can establish with the paramagnetic ions to which they are bound. For instance, 1-D compounds have been formed with $[Cr(L1^R)(CN)_2]^-$ and Mn^{II},[22] Fe^{II},[23] or Ni^{II},[33] the last two are ferromagnetic SCMs. Trinuclear [Cr₂Fe] complexes involving same Cr metallo-ligand and PBP Fe^{II} were found to behave as SMMs.[24]

The combination of PBP $[Mo(CN)_7]^{4-}$ and Mn^{II} units, which do not exhibit any magnetic anisotropy due to ZFS, can lead to compounds with a behavior characterized by magnetic anisotropy. For instance, $[Mo(CN)_7]^{4-}$ has been involved in several 3-D magnets, some with ferrimagnetic order for temperatures above 100 K.[34-36] A rather unexpected feature of these magnets containing S = ½ units and high-spin Mn^{II} is the large magnetic hysteresis loops they can exhibit. This correlates with the actual geometry of the $[Mo(CN)_7]^{4-}$ moieties in the framework,[37] with the largest magnetic anisotropy (i.e. large magnetic hysteresis) observed when Mo units exhibit a PBP shape.[38] Similarly, discrete or 1-D derivatives involving PBP $[Mo(CN)_7]^{4-}$ and Mn^{II} were found to behave as SMM or SCM but this is the case only when the Mn is connected to the CN-ligands in the apical positions of the Mo^{III}.[39-42] The actual origin of the magnetic anisotropy exhibited by these polynuclear species results from anisotropic Mo-Mn exchange interactions.[31] Same applies for 5d derivative $[Re(CN)_7]^{3-}$ in PBP geometry. Several pentanuclear $[M^{II}_4Re]$ complexes involving PBP $[Re(CN)_7]^{3-}$ and = Mn^{II}, Ni^{II}, and Cu^{II} were reported to exhibit magnetic anisotropy.[43, 44]

Complexes	Spin state	ZFS parameters $D(E)$ (cm^{-1})		Ref.
		Experimental	Theory[g]	
$[Cr(HL1^{NH2})(H_2O)_2]^{2+}$	3/2	–	–	45, 46
$[Cr(L8^{EtOH})(H_2O)_2]^{3+}$	3/2	–	–	47
$[Cr(HL1^{Ph})(H_2O)_2]^{2+}$	3/2	|2.2|		22
$[Cr(HL1^{Ph})(NCS)_2]$	3/2	1.3		22
$[Cr(L1^{Ph})(CN)_2]^-$	3/2	-0.88[b,c,d]	D = -0.99(0.23) to +0.92(0.27)	22-24
$[Cr(HL1^{PhOMe})Cl_2]$	3/2	-1.8	-1.06	21
		EPR		
$NaK_3[Mo^{III}(CN)_7]$	1/2	$g_{||}$ = 3.89, $g_\perp$ = 1.77[e]		26
$[Mo(L1^{Ph})Cl_2]^-$	1/2	–		25
cis-$[W(CN)_5(CO)_2]^{2-}$	1/2	g_x = 1.92, g_y = 1.89, g_z = 1.82[f]		29
$(NBu_4)_3[Re^{IV}(CN)_7]$	1/2	$g_{||}$ = 3.66, $g_\perp$ = 1.759[e]		27

(a) from HF-EPR data; (b) from magnetic susceptibility data; (c) from magnetization data; (d) unpublished results, (e) in solid state, (f) in solution, (g) CASSCF/NEVPT2 calculations

Table 2. Magnetic anisotropy in d³ metal complexes.

I.4 d^4 ions (Mn^{III})

Examples of high-spin d^4 complexes with PBP coordination sphere are scarce. The magnetic anisotropy for two Mn^{III} derivatives, $[Mn(L3)X_2]PF_6$ (X = Cl^-, Br^-) have been reported. These complexes have been obtained by oxidation of pre-existing PBP Mn^{II} complex $[Mn(L3)Cl(MeOH)]PF_6$ with either $NOPF_6$ or Br_2.[48] Their Curie constants of 2.95-3.0 $cm^3mol^{-1}K$ are in agreement with S = 2 spin state. Axial ZFS parameter of D = -2.11 cm^{-1} and -2.59 cm^{-1}, respectively for X = Cl and Br with $g_{||}$ = 1.95, $g_{\perp}$ = 1.98, were estimated from low temperature magnetic susceptibility behaviors.[49]

The very few reports on PBP Mn^{III} complexes could be ascribed to the limited stability of this higher oxidation state in pentagonal bipyramidal coordination sphere. For example, oxidation of the Mn^{II} complex formed with ligand L3 allowed isolation of the Mn^{III} derivative, whereas with homologous ligands but with ring sizes of [16] or [17] atoms spontaneous reduction was observed in the absence of oxidant. Similar observations were made for complexes based on the ligand H_2L1^R. Oxidation of the Mn^{II} complexes with Br_2 led to green solutions indicating oxidation to Mn^{III} but this color faded after a short time to orange color characteristic of the divalent complexes.[50]

I.5 d^5 ions (Mn^{II}, Fe^{III})

With half field d-shell, a high-spin $3d^5$ ion is expected to display weak magnetic anisotropy. EPR studies performed on Mn^{II} complexes have consistently yielded very small D parameters, typically below 0.1 cm^{-1} (Table 3). A typical example is $[Mn(L3)(H_2O)_2]\cdot2Cl$ for which extensive X and Q band EPR studies performed in the solid state for a diluted sample at 300 K and 77 K, led to an axial crystal-field parameter D = 0.07 cm^{-1}.[51] For $[Mn(L5^R)]^{2+}$ (R = 2-benzimidazolylmethyl),[52] a combined analysis of low temperature magnetic behavior and theoretical calculations resulted in negative D values (-0.30 and -0.12 cm^{-1}, respectively). Moreover, D was found rather insensitive to the nature of the ligands in the apical positions for the series of complexes $[Mn(L5^H)X_2]$ with X = Cl^-, Br^-, I^-, N_3^-, or NCS^-.[53, 54]

Fe^{III} complexes with PBP coordination sphere are readily stabilized by a pentadentate ligand and have high-spin electronic configuration.[59-63] Earlier Mössbauer results for a series of $[Fe(L3)X_2]^+$ derivatives suggested an effect of the apical ligands on the sign of D, with a change from positive (X = Cl^-, Br^-, I^-) to negative (X = NCS^-, N_3^-).[58, 64] EPR studies for derivatives with X = Cl^- and NCS^- pointed to small $|D|$ values in the order of 1 cm^{-1} while magnetic susceptibility investigations for X = I^- and NCS^- derivatives resulted in $|D|$ = 10.3 and 7.98 cm^{-1}, respectively.[65] A detailed investigation for $[Fe(L1^{NMe3})(NCS)_2]^+$ lead to values of $|D|$ = 1.67 and 1.57 cm^{-1} (from EPR and susceptibility data), whereas theoretical calculations confirmed a negative sign for this parameter.[61] The Mössbauer spectra at 4.2 K for $[Fe(L1^{NMe3})(NCS)_2]^+$ and $[Fe(L3)(NCS)_2]^+$ display marked differences, the first consists in a broad singlet whereas the second shows a six-line pattern. This latter is attributed to longer spin-spin relaxation times.[64]

Regardless of any interest in magnetic anisotropy, PBP Mn^{II} complexes have been widely used as building blocks for polynuclear structures.[9] The related Fe^{III} PBP derivatives seem to have attracted much less interest.[66]

Complexes	Spin state	ZFS parameters (cm^{-1})	Ref.
Mn(II)			
[Mn(H$_2$L1^{NH2})(NCS)$_2$]	5/2	D = 0.1, E/D = 0.25[a]	55
[Mn(L1^{PhNH2})(dmso)$_2$]	5/2	D = 0.1, E = 0.01, g = 2.0[b]	56
[Mn(L3)(H$_2$O)$_2$]·2Cl	5/2S	D = 0.07, E = 0.008, g = 2.11 ª	51
[Mn(L5^H)X$_2$]	5/2		
X = Cl$^-$		D = 0.017, E/D = 0.11[d]	53
X = Br$^-$		$\|D\|$ = 0.7[c]	54
X = I$^-$		$\|D\|$ = 0.4[c]	
X = N$_3^-$		$\|D\|$ = 0[c]	
X = NCS$^-$		$\|D\|$ = 0.1[c]	
[Mn(L5^R)](ClO$_4$)$_2$ (R = 2-benzimidazolylmethyl)	5/2	D = -0.3, g = 1.95[c] D = -0.071/ -0.0122, E/D = 0.07[d]	52
[Mn(quinol-NO3)(H$_2$O)$_3$]	5/2	D = -0.6, E = 0, g = 2.01[c]	57
Fe(III)			
[Fe(L3)Cl$_2$]ClO$_4$		$\|D\|$ = 0.3, E/D = 0.03[b]	58
[Fe(L3)X$_2$]ClO$_4$			59, 60
X = Br, I, NCS			
[Fe(L3)(NCS)$_2$]ClO$_4$		$\|D\|$ = 0.5, E/D = 0.13[b]	58
[Fe(L1^{NMe3})(NCS)$_2$]NCS	5/2	$\|D\|$ = 1.67, $\|E\|$ = 0.17, g = 2.05[a] D = -1.6, E = -0.4[d]	61
[Fe(L1^{NMe3})(NCS)$_2$]$_2$[Fe(NCS)$_5$(H$_2$O)]	5/2	$\|D\|$ = 1.57, $\|E\|$ = 0.16, g = 1.98[a] D = -1.6/-1.5, E/D = 0.23[d]	61

(a) EPR in solid state; (b) EPR in solution; (c) magnetic behavior; (d) theoretical calculations; quinol-NO3: 8-carboxymethoxy-2-quinolinecarboxylate

Table 3. Magnetic anisotropy in d^5 metal complexes.

I.6 d^6 ions (Fe^{II})

In PBP coordination sphere Fe^{II} has high-spin configuration with S = 2 (Figure 2) and was found to exhibit a magnetic anisotropy characterized by a negative D parameter (Table 4). This easy-axis anisotropy is perpendicular to the pentagonal plane of the PBP geometry, aligned along the X-Fe-X direction (X are the atoms in apical positions) as depicted in Figure 5 by the blue arrow.
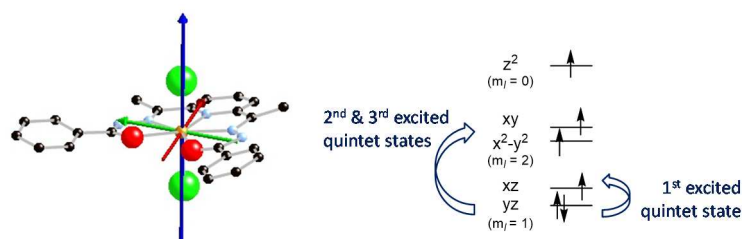
Figure 5. [Fe(H$_2$L1^{Ph})Cl$_2$] with its magnetic axes; easy-axis is depicted in blue, x and y are green and red, respectively (Reproduced from reference[13] with permission from Wiley-VCH, copyright 2022), and sketch showing the first three excited states which coupling with ground state give strongest contributions to D for PBP Fe^{II} complexes.

The first quantitative information on the axial ZFS parameter of Fe^{II} in this geometry was provided for [Fe(L3)(H$_2$O)$_2$]·2Cl with a D value of -17 cm^{-1} deduced from magnetization and high-field EPR

experiments.[67] Subsequent examples revealed that the magnetic anisotropy exhibited by Fe^{II} can vary significantly with the coordination environment of the metal center, D values ranging between -25 cm^{-1} and +7.9 cm^{-1} have been reported (Table 4). For instance, in a series of complexes with pentadentate ligand H_2L1^{Ph} in equatorial positions, the presence of either Cl or H_2O in the axial coordination sites of Fe^{II} resulted in a decrease of its magnetic anisotropy from D = -13.3 to -4.0 cm^{-1}, respectively.[13] Theoretical calculations showed that the main contribution to the negative D parameter is brought by a single excited state corresponding to the promotion of an electron from the d_{yz} to the d_{xz} orbital (Figure 5). Since ZFS is inversely proportional to the energy difference between the ground state and the excited states, D for a PBP Fe^{II} complex mainly depends on the energy gap between the two lowest quintet states (*i.e.* the ground and the first excited state). This energy difference can be related directly to the energy difference between the d_{xz} and the d_{yz} orbitals. Calculations performed for [Fe(H$_2$L1^{Ph})Cl$_2$] revealed close lying orbitals with an energy difference of *ca* 170 cm^{-1} while for [Fe(L1^{Ph})(MeOH)H$_2$O](BF$_4$)$_2$ this gap reaches *ca* 410 cm^{-1}. This situation has been rationalized by the π-interactions occurring between the Fe^{II} and the ligands in apical positions (Figure 6). For Cl$^-$, the lone pairs have two identical π-interactions with the metal ion in the *x* and *y* directions whereas for the O-ligands (H$_2$O or ROH) only a single π-interaction takes place, which differentiates the d_{xy} from the d_{yz} orbital. For this reason, the contribution from the first excited state to the overall D for [Fe(H$_2$L1^{Ph})Cl$_2$] is stronger than for [Fe(H$_2$L1^{Ph})(MeOH)H$_2$O]·2BF$_4$ with respectively -28.30 and -18.95 cm^{-1}; in agreement with the more negative D value found experimentally for the former complex. The same argument of symmetrical metal-ligands π-interactions was shown to hold for N-bonded cyanide ligands in [Fe(H$_2$L1^{Ph}){Ni(CN)$_4$}], which D is similar to that of [Fe(H$_2$L1^{Ph})Cl$_2$]. It may be noticed that the largest magnetic anisotropies have been reported for Fe complexes with N-coordinated nitrile groups in apical positions.[68, 69]
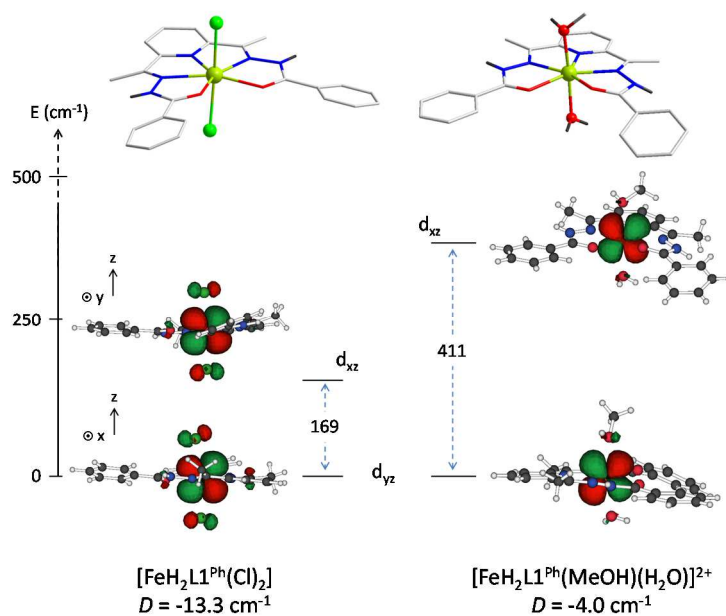
Figure 6. The two lowest molecular orbitals (optimized at the CAS(6,5)SCF level[13]) showing the ligand-Fe π-interactions for [Fe(L1^{Ph})Cl$_2$] (left) and [Fe(L1^{Ph})(MeOH)H$_2$O](BF$_4$)$_2$ (right) and their energy difference in cm^{-1}.

It is interesting to note that the quadrupole splitting (Δ) observed by Mössbauer spectroscopy for a series of [Fe(HL1^{Ph})X$_2$] complexes has been found to vary significantly depending on the ligands in

apical positions.[13, 70] Thus, a quadrupole splitting of Δ = 3.07 mm s^{-1} was observed when X = ROH while smallest splitting with Δ = 1.67 mm s^{-1} was found for X = Cl; for X = {Ni(CN)$_4$} an intermediate value of Δ = 2.29 mm s^{-1} was obtained. This effect of the apical ligands can be paralleled by the variations of D of these complexes which range from -4.0 cm^{-1} for X = ROH to -13.3 cm^{-1} for X = Cl, whereas an intermediate anisotropy with D = -10.7 cm^{-1} characterizes the complex with X = {Ni(CN)$_4$}.

An overall more negative D can be also achieved if the positive contributions to D arising for higher excited states are reduced. This possibility was illustrated with the complexes [Fe(H$_2$L1^{NHPh})X$_2$], where X = NCS$^-$, NCSe$^-$, or N(CN)$_2$$^-$ are ligands leading to weak π-interactions with the metal orbitals. Theoretical calculations revealed an energy difference of about 4000 cm^{-1} between the low lying d_{xz}/d_{yz} orbitals and the $d_{xy}/d_{x^2-y^2}$ orbital set;[69] a gap significantly larger than the ca 2600 cm^{-1} found for [Fe(H$_2$L1^{Ph})Cl$_2$].[13] For this series of complexes, D spanning from -14.3 to -25.9 cm^{-1} have been deduced from magnetic behaviors (Table 4).

Complexes	ZFS parameters (cm^{-1}) and g					SMM	Ref.
	experimental			Theory[c]		U_{eff}/k_B	
	D[a]	$|E|$	g	D	E	(applied H_{DC})	
[Fe(L3)(H$_2$O)$_2$]·2Cl	-17.2[b]	3.6	2.12	–		–	67
[Fe(tpa)(CF$_3$SO$_3$)]$^+$	-7.9	2.2	2.11	–		–	71
[Fe(L1^{Ph})(MeOH)(H$_2$O)]$^{2+}$	-4.0	–	2.28	-12.3	1.58	no	13, 70
[Fe(H$_2$L1^{biPh})(MeOH)Cl]Cl	-6.3	0.16	2.18	–		no	13
[Fe(H$_2$L1^R)Cl$_2$]							13, 70
R = Ph	-13.3	–	2.30	-21.6	0.85	n.a. (3 kOe)	
R = NH$_2$	-13.0	3	2.16	–	–	53 K (3 kOe)	
1D-[Fe(H$_2$L1^R){Ni(CN)$_4$}]							
R = Ph	-10.7	0.12	2.21	9.29	2.17	49 K (3 kOe)	13, 70
R = NH$_2$	-8.3	1.3	2.18	–	–	–	12
R = NHPh	-13.25	0.7	g_x, g_y = 2.21, g_z = 2.32	-13.99	2.0	61 K[d] (2.5kOe)	72
[Fe(H$_2$L1^{NHPh})X$_2$]							
X = NCS	-14.3	0.3	g_x, g_y = 2.13, g_z = 2.42	-13.9	1.9	21 K[d] (2 kOe)	69
X = NCSe	-22.7	0.4	g_x, g_y = 2.17, g_z = 2.25	-26.03	1.15	25 K[d] (2 kOe)	
X = N(CN)$_2$	-25.9	0.8	g_x, g_y = 2.21, g_z = 2.53	-43.19	0.99	25 K[d] (2 kOe)	
[Fe(L4)(H$_2$O)$_2$](methyl-Orange)$_2$	−3.7	0.02	g_x, g_y = 2.32, g_z = 1.92	–		n.a. (2 kOe)	73
[Fe(L5^R)](ClO$_4$)$_2$							
R = CH$_2$Py	-7.4	0	2.13	8.1	2.5	no	74
R = 2-bzimidazolylmethyl	+7.9[b]	1.7	2.06	7.41/7.55	1.48	no	52
[Fe(L5^{CH2COO})]	-9.6	0.06	2.11	-12.8	2.8	n.a. (4 kOe)	75
1D-[Fe(L5^H)($\mu_{1,3}$-N$_3$)]ClO$_4$	-11.7	–	2.13	-11.4	3.5		76
[Fe(L4)(MeCN)$_2$](BPh$_4$)$_2$	-17.1	0.6	g_x, g_y = 2.16, g_z = 2.42	-19.7	0.4	89 K[d] (1.5kOe)	68

(a) from magnetic behavior; (b) EPR data available; (c) CASSCF/NEVPT2 calculations ; (d) multiprocess relaxation analysis; tpa: 6,6'-(pyridin-2-ylmethylazanediyl)bis-(methylene)bis(N-*tert*-butylpicolinamide); n.a.: not available.

Table 4. Magnetic anisotropy in high-spin d^6 Fe^{II} complexes and their SMM characteristics.

A strong modulation on D was evidenced for PBP complexes based on ligand $L5^R$ where R groups are two moieties coordinated in the apical positions of Fe^{II}. For R = carboxylate the magnetic anisotropy was characterized by D = -9.6 cm^{-1} whereas a positive value of 7.9 cm^{-1} was obtained with R = benzimidazole.[52, 75] For the latter, the positive value for D was attributed to a distortion of the coordination polyhedron with respect to PBP geometry. This example well illustrates that the energy difference between the d_{xz} and the d_{yz} orbitals is also related to structural considerations. Thus it will be all the smaller when the ligand set in the equatorial positions form a regular pentagonal polyhedron and when this ligand field is more symmetrical. Consequently, magnetic anisotropy will increase the more the coordination polyhedron becomes closer to PBP geometry. Moreover, approaching degeneracy of the d_{xz} and the d_{yz} orbitals should also favor the emergence of first order spin-orbit coupling that might be the best way to reach substantial magnetic anisotropy in PBP Fe^{II} complexes.

SMMs: Several Fe complexes showed SMM-like behavior (Table 4), which is associated with their axial anisotropy. However, slow relaxation is usually observed only when a static magnetic field is applied. Since Fe^{II} has integer spin, rhombic anisotropy (E) leads to fast resonant quantum tunneling of magnetization (QTM) through degenerate energy levels. This fast relaxation of the magnetization can be efficiently reduced upon application of a magnetic field that lifts the degeneracy of the $\pm m_S$ levels. However, this may not be sufficient to observed SMM behavior even if complexes have similar D (see Table 4). Spin-dipolar interactions between neighboring centers in the lattice are also responsible for the relaxation. Such spin-lattice interactions are suppressed when the spin in the lattice have their easy axes all aligned along the same direction. This may be obtained by serendipity as a result of the crystal packing but can also be controlled by crystal engineering. For instance, the diamagnetic cyanometallate $[Ni(CN)_4]^{2-}$ has been used to organize PBP Fe^{II} complexes in 1D $[Fe(L1^R)\{Ni(CN)_4\}]$ arrays (Figure 7) and thus align the directions of the easy axis of all Fe centers in the same direction.[70, 72] SMM behavior characterized by U_{eff}/k_B= 49 K was obtained for $[Fe(L1^{Ph})\{Ni(CN)_4\}]$ whereas only fast relaxation was observed for $[Fe(L1^{Ph})Cl_2]$ that exhibits a very similar magnetic anisotropy but a crystal packing of tilted molecules.[70]
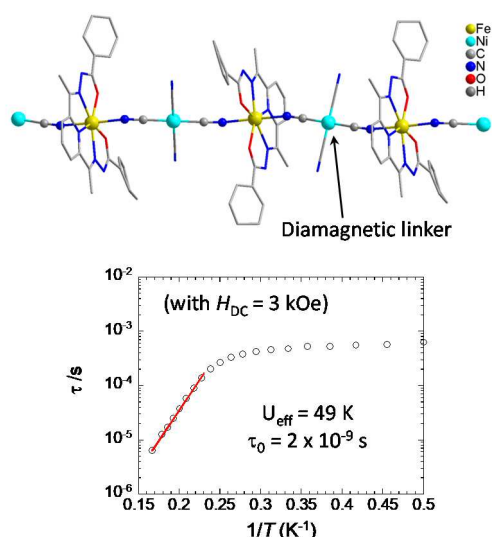

Figure 7. Crystal structure and temperature dependence of the relaxation time (τ) for 1D-$[FeL1^{Ph}\{Ni(CN)_4\}]$ (adapted from ref.[70] with permission from The Royal Society of Chemistry).

From Table 4 it can be noticed that U_{eff}/k_B may vary substantially even for complexes exhibiting similar magnetic anisotropy. In addition to the fact that different relaxation processes may possibly be involved, the way the temperature dependence of the relaxation time was analyzed may contribute. This is well illustrated by a report on $[Fe(L4)(MeCN)_2](BPh_4)_2$ for which modeling the linear variation of $\ln\tau = f(T^{-1})$ in the high-temperature part by the Arrhenius law gave U_{eff}/k_B = 50 K whereas analysis over the whole T-domain by a multi-process expression comprising the Arrhenius component yielded U_{eff}/k_B = 89 K.[68]

It must be mentioned that PBP Fe[II] complexes involving pentadentate ligands L3 or L4 with either NCS⁻ or CN⁻ ligands in the apical positions have been found to undergo a spin change from S = 2 to a diamagnetic state when lowering the temperature. This spin change was found to be related to a structural change from hepta- to hexa-coordination due to a rupture of linkage between Fe and one site of the pentadente ligand.[77] These derivatives are not concerned by magnetic anisotropy and therefore are not considered herein, a review on the topic can be found in the following reference.[9] However, it was found that the PBP geometry and high spin state of $[Fe(L3)(CN)_2]$ can be photo-regenerated at low temperature,[78] which should restore the magnetic anisotropy of Fe.

PBP Fe[II] as building unit: These Ising-type anisotropy Fe[II] complexes have been involved in the design of polynuclear nanomagnets (Table 5). A cyanide-bridged bimetallic complex, $[Fe(tpa)\{ReCl_4(CN)_2\}]$, characterized by a ferromagnetic Fe-Re interaction of 6 cm⁻¹ and a molecular ZFS D = -2.3 cm⁻¹, was shown to give rise to slow magnetic relaxation albeit with a small relaxation barrier.[71] Trimetallic [Fe[II]Cr[III]] complexes with different metal ion ratio have been reported. Compound $[\{Fe(L4)(H_2O)\}_2\{Cr(CN)_6\}]$ comprises two PBP Fe[II] centers in ferromagnetic interaction with a central Cr[III] (J = 7.4 cm⁻¹).[79] This compound exhibits SMM-type behavior with U_{eff}/k_B = 44.3 K. Several [FeCr₂] compounds with a single PBP Fe as source of magnetic anisotropy were shown to behave as SMM but with noticeable differences in U_{eff}/k_B despite very similar chemical features (Table 5).[23, 24] Theoretical insights revealed that the decrease of the energy barrier for demagnetization results from the bending of the Fe-NC linkages with respect to the normal of the pentagonal plane. Such bending was shown to affect both the magnetic anisotropy of the Fe center and the ferromagnetic Fe-Cr interactions.[24] Pentanuclear [Fe₃W₂] complexes obtained by association of $[Fe(H_2L1^R)(H_2O)_2]^{2+}$ and $[W(CN)_8]^{3-}$ were found to exhibit rather strong ferromagnetic Fe-W interaction (J = 30 cm⁻¹).[13] In these complexes the terminal PBP Fe centers have one of their apical positions occupied by a H_2O ligand that drastically reduces the magnetic anisotropy of these centers. Only central Fe site provides strong magnetic anisotropy which may account for the modest SMM-type behavior with U_{eff}/k_B of just 35 K in DC field.

PBP Fe[II] centers are found in several SCMs. A seminal example is the ferrimagnetic chain $[\{Fe(L3)\}_2\{Nb(CN)_8\}]$ characterized by U_{eff}/k_B = 74 K and the opening of a magnetic hysteresis below 2 K.[67] The ferromagnetic $[Fe(H_2L1^{NH2})\{Cr(L1^{Ph})(CN)_2\}]\cdot PF_6$ SCM was designed to ensure parallel orientation of the axial anisotropy of the PBP Fe units (Figure 8a). This nanomagnet is characterized by an energy barrier for demagnetization of U_{eff}/k_B = 113 K and the opening of a magnetic hysteresis loop below 5 K.[23]
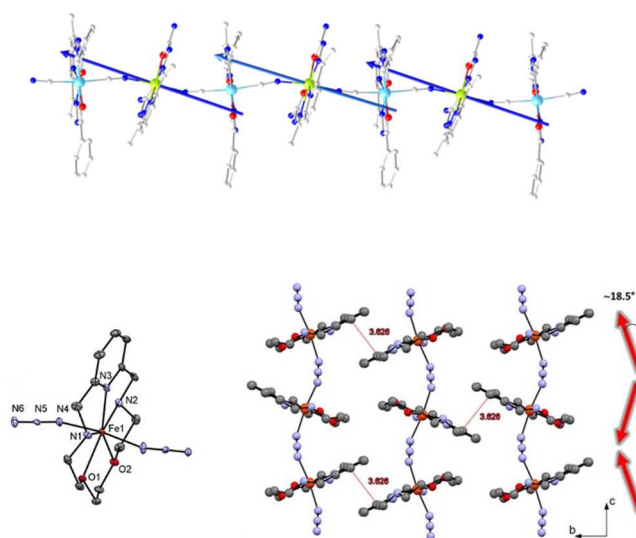
Figure 8. SCM involving PBP Fe^{II} centres as the source of magnetic anisotropy. *(top)* 1D-$[Fe(H_2L1^{NH2})\{Cr(L1^{Ph})(CN)_2\}]\cdot PF_6$ with local easy magnetic axes depicted as blue arrows (Fe in green, Cr in light-blue. Reprinted with permission from Ref.[23], Copyright 2022 American Chemical Society), *(bottom)* 1D-azido-bridged $[Fe(L5^H)(N_3)]\cdot ClO_4$, the red arrows represents the easy axis of magnetization of a Fe^{II} center positioned along $N_{azido}-Fe-N_{azido}$ axis, thus highlighting the tilt angle at the origin of weak ferromagnetism and SCM behavior (Adapted with permission from Ref.[76], copyright 2021 American Chemical Society).

Compounds	Arrhenius parameters		Applied DC field (kOe)	Coercive field (kOe)	Ref.
SMMs	U_{eff}/k_B (K)	τ_0 (s)		(*T*)	
$[Fe(tpa)\{ReCl_4(CN)_2\}]$	n.a.	n.a.	0		71
$[\{Fe(L4)(H_2O)\}_2\{Cr(CN)_6\}]$	44.3	1.4×10^{-9}		butterfly	79
$[\{Fe(H_2L1^{NH2})\}\{CrL1^{Ph}(CN)_2\}_2]$	22	3.8×10^{-8}	0		23
$[\{Fe(H_2L1^{mand})\}\{CrL1^{Ph}(CN)_2\}_2]$	19	3.5×10^{-7}	0		24
	35	6.8×10^{-8}	1		
mand =					
$[\{Fe(H_2L1^{Cyclohex})\}\{Cr(L1^{Ph})(CN)_2\}_2]$	n.a.				24
$[\{Fe(H_2L1^R)\}_3\{W(CN)_8\}_2]$					13
R = Ph	n.a.	n.a.			
R = biPh	35	4.6×10^{-10}	2		
SCMs					
$[\{Fe(L3)\}_2\{Nb(CN)_8\}]$	74	4.6×10^{-11}		4 (1 K)	67
$[\{Fe(H_2L1^{NH2})\}\{Cr(L1^{Ph})(CN)_2\}]\cdot PF_6$	113	1.6×10^{-11}		1.4 (2 K)	23
$[Fe(L3)CN]\cdot BF_4$	35.9	5.6×10^{-9}	0	0.68 (2 K)	80
	39.1	1.9×10^{-9}	2.2		
$[Fe(L4)CN]\cdot ABSA$	26.1	8.3×10^{-10}	0		73
$[Fe(L5^H)N_3]\cdot ClO_4$	87.5	5.2×10^{-10}	0	4.8 (2 K)	76

tpa: 6,6'-(pyridin-2-ylmethylazanediyl)bis-(methylene)bis(N-*tert*-butylpicolinamide); n.a.: not available

Table 5. Polynuclear nanomagnets involving PBP Fe^{II} units.

Homonuclear chains consisting solely of PBP Fe^{II} centers in antiferromagnetic interactions can exhibit SCM behavior. This occurs when the easy anisotropy axes of the Fe centers along the 1D coordination polymer are not collinear (Figure 8), leading to spin-canting in the ground state and to the emergence of a magnetization despite antiferromagnetic Fe-Fe interactions. Such a behavior is reminiscent of weak ferromagnetism. For instance, in cyanide-bridged 1D-$[Fe(L3)CN]\cdot BF_4$ chain, the directions of the apical axes are tilted by 7° and the exchange interaction is of J_{FeFe} = -4.3 cm^{-1}. This SCM is characterized by U_{eff}/k_B = 35.9 K.[80] The closely related chain $[Fe(L4)CN]^+$ associated to 4-aminobenzene-4'-sulfonic anion (ABSA$^-$) is a SCM with U_{eff}/k_B = 26.1 K.[73] In $\mu_{1,3}$-azido-bridged $[Fe(L5^H)N_3]\cdot ClO_4$ zig-zag chain, antiferromagnetic interactions of J_{FeFe} = -2.1 cm^{-1} take place and the angle between the axial directions is 18.5° (Figure 8, bottom). This compound is an SCM with U_{eff}/k_B = 87.5 K and exhibits a magnetic hysteresis loop below 3 K.[76]

I.7 d^7 ions (Co^{II})

A substantial number of heptacoordinated Co^{II} complexes with PBP coordination sphere are known and their magnetic anisotropy has been studied in detail (Table 6). Besides the derivatives using a pentadentate equatorial ligand to stabilize a PBP coordination polyhedron, a series of complexes comprising a heterocyclic amine (pyridine, bipy, *etc*...) and κ^2-NO_3^- anions in their coordination spheres have been investigated. All these complexes are characterized by large positive D parameters, typically between 25 and 40 cm^{-1}. The observed modulation of D does not seem to be directly related to the degree of distortion of the coordination geometry.[81] The seminal theoretical calculations performed for $[Co(H_2L1^{Ph})(H_2O)NO_3]\cdot NO_3$ indicated that the large positive value of D for this complex (31 cm^{-1}) results mainly from the contributions of three excited states, all positive (Figure 9).[10] These theoretical insights lead to the conclusion that the magnetic anisotropy of the Co ion could be modulated by tuning the coupling of the ground state and the excited states through the characteristics of the ligand set. For example, weak σ-donor ligands in apical positions would shift the d_{z^2} orbital downwards, reducing the energy difference with the other orbitals, thereby strengthening their coupling and resulting in a larger D value. Similarly, a more symmetric pentadentate ligand coordinated in equatorial positions would reduce the energy difference between the d_{xy} and $d_{x^2-y^2}$ orbitals, and enhance the positive contribution to D from the 1st excited doublet.

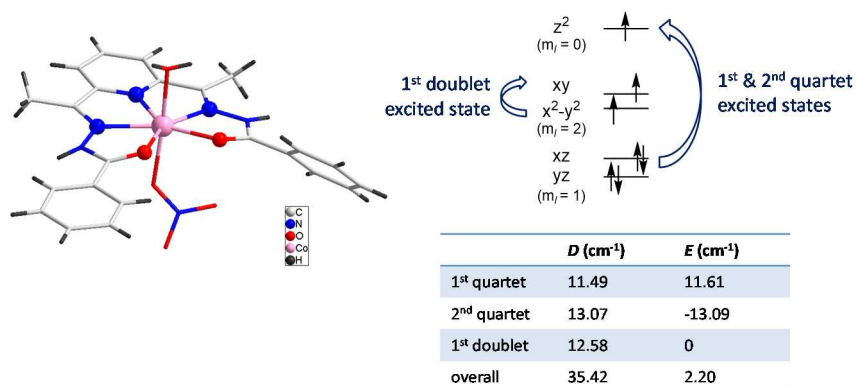|	D (cm^{-1})	E (cm^{-1})
1st quartet	11.49	11.61
2nd quartet	13.07	-13.09
1st doublet	12.58	0
overall	35.42	2.20

Figure 9. $[Co(H_2L1^{Ph})(H_2O)NO_3]\cdot NO_3$: *(left)* molecular complex, and *(right)* the three main positive contributions to the overall *ab initio* calculated ZFS parameters.[10]

These considerations have been used to account for variations in the D values found experimentally. For instance, replacement of oxygen-ligands at apical positions of $[Co(H_2L1^{Ph})(H_2O)NO_3]^+$ by NCS$^-$ led to a decrease of D from 32 cm^{-1} to 15.9 cm^{-1} that was attributed to the more σ donor nature of thiocyanate ligands.[82] A related effect has been found for a series of $[Co(L7^{Me})Y_2]^{n+}$ (Y = SPh$^-$, H$_2$O, NCS$^-$, pyridine, CN$^-$) complexes by altering Y ligands from weak-field SPh$^-$ to strong σ-donor CN$^-$ ligands leading to a gradual decrease of D from 34.5 cm^{-1} to 17.3 cm^{-1}.[83, 84] Still with the idea of modulating the ligand field strength in the axial positions, the effect of the halogen ligands in $[Co(L5^H)X_2]$ was found to induce lesser changes on D with values of 38, 41, and 35 cm^{-1}, respectively for X = Cl$^-$, Br$^-$, and I$^-$.[85] However, the increase of D does not simply follow the order of the ligand field reduction given by spectrochemical series (Cl > Br > I) but rather the trend suggested by the Mayer bond order[86] (Co-I > Co-Cl > Co-Br).

Such trends can only be deduced for a series of compounds whose alterations are strictly limited to the substitution of apical positions. The $[Co(L5^R)]^{n+}$ complexes based on the heptadentate ligand L5^R, where R consists of two arms allowing the coordination of specific groups in the apical positions of Co(II), are a good illustration.[52] Changing the apical ligands from pyridine to benzimidazole induced an increase of D from 34 to 40 cm^{-1}, in apparent contradiction with the decrease anticipated for stronger σ donor groups. The origin of this effect has been found in structural distortions that alter the axial and equatorial ligand fields. An *ab initio* modeling revealed that axial or equatorial bond length variations can have a significant influence on the overall D value. Obviously in these complexes, the effect on D of the bond characteristics of the apical benzimidazole ligands is largely offset by the contribution due to a modification of the equatorial field.

Chemical alterations of the equatorial ligand may also have substantial effects on D. This is especially understandable for pentadentate H$_2$L1^R that can be neutral, mono-, or di-anionic (see Appendix 1). For instance, $[Co(H_2L1^{Ph})(H_2O)X]X$ complexes (X = NO$_3^-$, Br$^-$, I$^-$) involving the neutral ligand are characterized by D values in the range of 30-32 cm^{-1} whereas a significantly reduced magnetic anisotropy with D = 13.1 cm^{-1} was reported for the related complex $[Co(L1^{Ph})(H_2O)_2]$ with deprotonated ligand. This decrease was attributed to a shift to higher energies of the excited doublet state as a result of the shrinking of the equatorial metal-ligand bond distances due to the di-anionic ligand.[82]

Seven coordinated Co^{II} complexes have also been obtained when bidentate nitrate ions and aromatic heterocyclic amines (pyridine, bipy, phen, terpy, …) coordinate the metal center. Deviation from PBP geometry is often larger than for the complexes with pentadentate equatorial ligands[81] but ZFS parameters are similar (Table 6). For $[CoL_3(NO_3)_2]$ (with L = 3-tert-butylpyridine or isoquinoline), and $[CoL(NO_3)_2MeCN)]$ (with L = bipy or phen), the D values are in the narrow range of 31-36 cm^{-1}.[81, 87] Related complexes of formula $[CoL(NO_3)_2]$ with L = 2,6-dipyrazolyl-pyrazine or 2,6-dipyrazolyl-pyridine, exhibit magnetic bistability in the temperature range 230 – 240 K.[88, 89] A structural phase transition distorts the environment of the cobalt and alters the angular contribution to the magnetic moment of the complexes. For example, the derivative with pyrazine ligand has a distorted PBP coordination sphere (with a Shape parameter of 4.06)[90] at low T that rearranges to capped trigonal prim above the critical temperature. Unfortunately, the ZFS parameter D of these different phases does not seem to have been determined.

Field-induced SMMs: Planar magnetic anisotropy (*i.e.,* D > 0) should not lead to blockage of magnetization since there is no energy barrier between the lowest energy ± M$_s$ states. However, many

of these PBP complexes were found to exhibit a slow relaxation of magnetization in a magnetic field. The origin of such field-induced SMM behavior in compounds with easy plane anisotropy (positive D) has been attributed to the van Vleck cancellation mechanism that hinders direct phonon-induced transitions between states of the ground state.[91] This situation results from the effect of a magnetic field on the electronuclear spin entanglement occurring in Co^{II}. Therefore, temperature dependence of the relaxation time is best modelled by a Raman model and possible contribution from a direct process. Nevertheless, the figure of merit for these field-induced Co SMMs has long been a pseudo-barrier for demagnetization (U_{eff}) obtained by analyzing the temperature dependence of the relaxation time (τ) by an Arrhenius low. Therefore, this pseudo energy barrier is also mentioned in Table 6.

PBP Co as building unit: Several examples of heteronuclear derivatives involving Co^{II} PBP units as a source of strong magnetic anisotropy have been described. A very elegant approach has been to functionalize a H_2L1^R ligand so that it can connect to several metal ions. A series of bimetallic $Co^{II}Ln^{III}$ complexes (Figure 10a) have been achieved by designing the R moieties of the ligand to contain an additional hexadentate [N2O4] pocket suitable for coordination to a Ln^{III} ion.[92] In $[Co(L1^{CMeN2HCONH2})Ln(NO_3)_2]NO_3$, the metal ions are bridged by the oxygen atoms common to both cavities. Ferromagnetic Co^{II}-Dy^{III} interactions have been observed, and the Co-Y derivate was found to behave as a field-induced SMM (Table 6).

Following the more classical building-block strategy, PBP Co^{II} complexes have been assembled with cyanometallate derivatives. A chiral magnet, $[\{Co(L4)\}_2\{Cr(CN)_6\}]\cdot ClO_4$, was obtained by assembling $[Co(L4)(H_2O)_2]^{2+}$ and $[Cr(CN)_6]^{3-}$ units.[93] This 3-D tubular network of cyano-bridged Co and Cr centers exhibited ferromagnetic ordering below T_c = 12 K and a magnetic hysteresis with a coercive field of 165 Oe at 1.8 K. The 2-D ferromagnet $[\{Co(L3)\}_3\{Cr(CN)_6\}_2]$ was reported to have similar characteristics with T_c = 15 K but small coercive field.[94] A 2-D metamagnet with honeycomb network was obtained with $[Co(TODA)]^{2+}$ (TODA stands for 1,4,10-Trioxa-7,13-diazacyclopentadecane) and $[Cr(CN)_6]^{3-}$. This compound showed antiferromagnetic ordering below 12 K but a butterfly-shaped hysteresis loop with coercive field of 720 Oe.[95] Assemblage with diamagnetic $[Co(CN)_6]^{3-}$ gave same structure topology. The absence of exchange interactions allowed confirming the magnetic anisotropy for the Co centers (D = 29.9 cm^{-1}) and resulted in field-induced SMM behavior. The preservation of the strong magnetic anisotropy of the PBP Co site (D = 32.9 cm^{-1}) with axial positions occupied by two cyanometallate-nitrogen atoms, was also confirmed in the 1D polymer $[\{Co(H_2L1^{Ph})\}\{Ni(CN)_4\}]$ formed with diamagnetic $[Ni(CN)_4]^{2-}$.[13] 2-D and 1-D hollows networks have been achieved with $[Co(L4)(H_2O)_2]^{2+}$ and $[Fe(CN)_6]^{3-}$ metallo-ligand.[96] Ferromagnetic Co-Fe interactions were found to take place but no SCM behavior was evidenced for the 1-D derivative. A chiral ligand derived from lactic acid hydrazide was used to impart chirality to 1-D $K[\{Co(H_2L1^{lact})\}\{Fe(CN)_6\}]$ (*lact* stands for lactic acid derived hydrazide group). This compound has ferroelectric properties and can be processed in an aqueous medium.[97]

Discrete heterometallic complexes in which Co^{II} is exchange coupled with another metal ion have also been reported. These comprise the pentanuclear complexes $[\{Co(H_2L1^{Ph})\}_3\{M(CN)_6\}_2]$ (M = Cr^{III} or Fe^{III}),[98] and $[\{Co(H_2L1^R)\}_3\{W(CN)_8\}_2]$ with R = Ph, BiPh (Figure 10b).[13] Ferromagnetic Co-M interactions have been observed in each case with J_{CoCr} = 5.4 cm^{-1} and J_{CoW} = 19 cm^{-1}, leading to large ground spin states but for none of these compounds slow relaxation of the magnetization was observed.

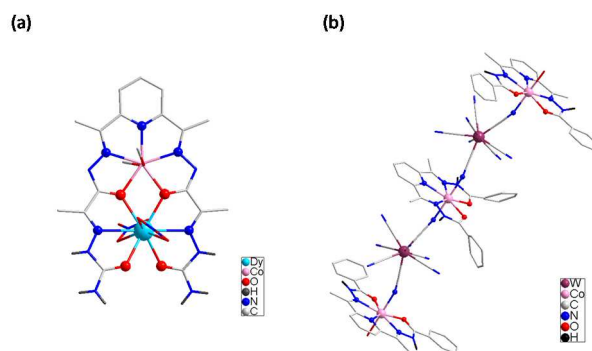**Figure 10.** PBP Co^{II} in polynuclear complexes: (a) [Co(L1^{CMeN2HCONH2})Ln(NO$_3$)$_2$]NO$_3$ derivatives obtained by ligand design,[92] (b) pentanuclear [{Co(H$_2$L1^{Ph})}$_3${W(CN)$_8$}$_2$] formed by building-block approach.[13]

Complexes	ZFS parameters (cm^{-1}) and g					SMM relaxation characteristics					Ref.
	experimental			Theory[c]		Orbach[f]	Raman[g]		Direct[h]	H_{DC}	
	$D^{(a)}$	$|E|$	g	D	E	U_{eff}/k_B (K)	A (K^{-n}s^{-1})	n	B (K^{-1}s^{-1}Oe^{-2})	(kOe)	
[Co(H$_2$L1^{Ph})(H$_2$O)X]X											
X = NO$_3^-$	31.0$^{(b)}$; 32.4	–	2.22; 2.33	35.42	2.20	50/81	n.a.	8.7		1.0	10, 99, 100
X = Br$^-$	30.0	0.3	2.18	–	–	–					98
X = I$^-$	30.0	0.3	2.24	–	–	–					98
1-D [{Co(H$_2$L1^{Ph})}{Ni(CN)$_4$}]	32.9	0.7	2.20			(i)	(i)	(i)	(i)		13
[Co(HL1'^{Ph})(H$_2$O)(EtOH)]BPh$_4$	27.6$^{(b)}$	–	2.25	28.5	–	–					101, 102
[Co(L1^{Ph})(H$_2$O)$_2$]	13.1	0	2.06	12.4$^{(e)}$	–	–					82
[Co(L1^{Ph})imidazole]	24.8	1.6.10^{-3}	2.21	–	–	89	n.a.	11.2		1.0	99
[Co(H$_2$L1^{R})(NCS)$_2$]											
R = Ph	15.9	0	2.14	14.6$^{(e)}$	–	–					82
R = PhOH	38.8	2.1	2.18	37.9	2.49	23.6$^{(d)}$	n.a.	3.7		1.0	103
[Co(H$_2$L1^{PhOH})(MeOH)NCS]ClO$_4$	41.5	1.5	2.21	38.0	1.32	28.4$^{(d)}$	n.a.	4.2		1.0	103
[Co(L1^{PhOH})(MeOH)$_2$]	43.1	3.3	2.27	38.0	3.2	33.5$^{(d)}$	n.a.	4.7		1.0	103
[Co(H$_2$L1^{BiPh})(MeOH)NO$_3$]NO$_3$	33.4	4.7	2.22	–	–	–	–	–	–		13
[Co(H$_2$L1^{NH2})X$_2$]											104
X = NCS$^-$	35.6	6.0	2.24	38.02	0.86		1.0×10^{-3}	9 (fixed)	1.03×10^{-3}	1.0	
X = NCSe$^-$	38.2	0	2.26	37.73	0.79		0.02	7.4	4.1×10^{-4}	1.5	
X = N(CN)$_2^-$	35.3	3.5	2.23	37.51	0.24		0.017	7.3	1.29×10^{-4}	1.5	
[Co(HL1^{NH2})(H$_2$O)X]·(2-y)NO$_3$			$g_{x,y}/g_z$								104
X = H$_2$O, y = 0	38.0	0.7	2.28/2.16	38.99	0.55		0.26	4.2	2.9×10^{-4}	1.2	
X = Cl$^-$, y = 1	35.6	5.7	2.45/2.11	38.94	0.52		2.43×10^{-4}	9 (fixed)	1.11×10^{-4}	1.4	
X = C(CN)$_3^-$, y = 1	33.6	5.0	2.26/ 2.0	37.49	0.35		0.4	5.6	7.7×10^{-5}	1.2	
[Co(HL1^{NH2})(H$_2$O)N$_3$]· [Co(L1^{NH2})(N$_3$)$_2$]N$_3$	40.4	–	$g_{x,y}$ = 2.48; g_z = 2.0	39.9/39.6	0.6/0.5		0.26	5.8	2.9×10^{-4}	1.5	104
[Co(H$_2$L1^{NHPh})(H$_2$O)Y]·2NO$_3$											105
Y = MeOH	37.2	0.9	2.3	36.1	0.5	15	n.a.	4.6		2.0	
Y = DMF	35.9	1.4	2.29	36.3	1.0	25	n.a	4.9		2.0	

Y = DEF	43.7	0.8	2.28	37.4	0.3	n.a.				2.0	
[Co(H$_2$L1^{CH2NMe3})(NCS)$_2$]X											61
X = 2 NCS$^-$	30$^{(b)}$	0	2.32	41.5	2.0	–					
X = [Co(NCS)$_4$]$^{2-}$	36.3$^{(b)}$	0.95	2.35	38.4	1.1	–					
[Co(L1^{CMeN2HCONH2})Ln(NO$_3$)$_2$]·3X											92
Ln = Y(III), X = NO$_3$				40.8	1.0	7	5.66	4.98	1.08×10^{-7}	1.0	
Ln = Dy(III) , X = NO$_3$				36.8	0.9	n.a.	–	–	–	1.0	
[Co(L3)(H$_2$O)$_2$]Cl$_2$	24.6	0.01	2.29	–	–	30	n.a.	4.9		1.0	99
[Co(L4)(MeCN)$_2$]·2BPh$_4$	36.9	0.2	$g_{x,y}$ = 2.18			32	0.15	6.2		1.2	68
			g_z = 2.01								
[Co(L5^H)X$_2$]			$g_{x,y}$ (g_z=2)								85
X = Cl$^-$	38	0	2.47	44.8	2.0					3.0	
X = Br$^-$	41	0	2.28	44.0	2.7		1.63×10^{-3}	2.79		1.0	
X = I$^-$	35	0	2.35	43.4	2.8		2.0×10^{-3}	2.82		2.0	
[Co(L5^R)]·2ClO$_4$										0	
R = CH$_2$Py	34	0	2.20	30.6	1.2	24	2.12×10^{-5}	2.84		1.0	74
R = 2-bzimidazolylmethyl	40.3	4	$g_{x,y}$ = 2.15	34.4	2.7	9	507	2.58		1.0	52
R = CH$_2$COO$^-$ (no ClO$_4$)	29.1	5.5	2.13	28.5	1.4	-	0.53	5.49	9.7×10^{-5}	1.0	75
[Co(L7^{Me})Y$_2$]$^{n+}$·nBF$_4^-$			$g_{x,y}$ (g_z=2)								84
Y = H$_2$O, n = 2	25.6	1	2.23	34.5	2.7	42 / 85$^{(c)}$	15.8	4.3	2.0×10^{-5}	1.5	
Y = CN$^-$, n = 0	17.3	0.6	2.12	35.1	3.4	49 / 76$^{(c)}$	2.9	5.1	6.5×10^{-6}	1.5	
Y = NCS$^-$, n = 0	26.3	0	2.26	37.7	3.6	49 / 82$^{(c)}$	60.5	4.8	1.2×10^{-5}	1.5	
Y = SPh$^-$, n = 0	34.5	1.8	2.24	39.7	6.8	55 / 99$^{(c)}$	0.8	5.5	7.9×10^{-6}	1.5	
1D-[Co(L7^{Me})Y]·2BF$_4$											83
Y = pyrazine	–	–	–			–					
Y = 4-NH$_2$Py	–	–	–			–					
Y = 1,2-diPy-ethane	21.7	0.4	2.12			19				1.0	
2D-[{Co(TODA)}$_2${Co(CN)$_6$}$_2$]	29.9	0.1	2.22	–	–	16				1.5	95
TODA = 1,4,10-Trioxa-7,13-diazacyclopentadecane											
[CoL3(NO$_3$)$_2$]			$g_{x,y}/g_z$								87
L = 3-^{t}BuPyridine	35.8$^{(b)}$	0.2	2.26/2.78			41.7$^{(d)}$	6.5	4.1	6×10^{-5}	1.0	

	D	E	$g_{x,y}/g_z$							Ref.
		0.07 [b]	2.21/1.98[b]	95[c] in Zn		1.4×10^{-3}	8.17	2×10^{-6}	1.0	
L = isoquinoline	35.7[b]	0.02	2.43/2.35	24[c]		127	3.6	1.4×10^{-3}	1.2	
		1.81[b]	2.21/2.0[b]							
2D-[Co(4,4'-bipy)$_{1.5}$(NO$_3$)$_2$]	69[b]	4	2.4[b]	36	–	–				102
[CoL(NO$_3$)$_2$MeCN)]			$g_{x,y}/g_z$							81
L = 2,2'-bipyridine	32.9	0.2	2.43/2.08	33.9	4.6	0.47	5.18	6.2×10^{-5}	1.0	
L = 1,10-phenanthroline	31.4	0.1	2.43/2.38	35.3	7.0	3.69	4.90	6×10^{-4}	1.0	
[Co(1,10-N$_2$-15C5-aniline)]X$_2$										106
X = NO$_3^-$	25	–	2.22							
X = ClO$_4^-$	26	–	2.15							
[Co(O3N)(H$_2$O)$_3$]	70.4	8.9	$g_{x,y}$ = 2.65	5.27						57
O3N = 8-carboxymethoxy-2-carboxylicquinoline			g_z = 2.12							

(a) from magnetic behavior; (b) EPR data available; (c) CASSCF/NEVPT2 calculations ; (d) multi-process relaxation analysis; (e) DFT calculations; (f) $\tau = \tau_0\exp(U_{eff}/k_BT)$; (g) $\tau^{-1} = AT^n$; (h) $\tau^{-1} = BH^2T$ (H in Oe; exponent is 2 due to the hyperfine interactions applying for this Kramers ion); DEF: diethylformamide; *n.a.*: not available; L1' stands for methyl pyrinide-4-carboxylate derivative.

Table 6. Magnetic anisotropy in high-spin PBP Co^{II} complexes, and their SMM characteristics.

I.8 d⁸ ions (Niⁱⁱ)

Heptacoordinate Ni^{II} complexes are much less common than other 3d ions.[107] This can be related to the Jahn-Teller effect which tends to strongly distort or even reshape the coordination polyhedron to favor geometries more favorable to a lifting of the degeneracy of partially occupied orbitals. This difficulty can be overcome when a pentadentate ligand is used to fix the equatorial positions and impose a PBP coordination sphere to the Ni^{II} ion.[108-110] This approach allowed obtaining PBP Ni^{II} complexes with the various ligands depicted in Figure 1. However, for the pentadentate ligands comprising oxygen as connecting atoms, Ni-O distances close or higher than 2.5 Å are usually observed which lead to an important distortion of the PBP geometry.[53, 68, 106, 110]

In PBP coordination sphere Ni^{II} has high-spin configuration with S = 1 (Figure 11) and exhibits a magnetic anisotropy characterized by a negative *D* parameter. Experimental *D* values span from -6 to -28 cm^{-1} (Table 7). Positive *D* values have been reported but these resulted from an analysis of the temperature dependence of $\chi_M T$ only, which does not allow discriminating the sign of *D* for powder samples.
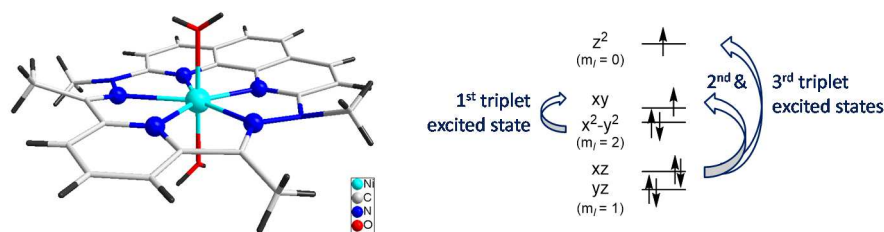

Figure 11. PBP Ni^{II} in [Ni(L7^{Me})(H$_2$O)$_2$]·2BF$_4$ (anions are not depicted),[33, 109] and sketch of the first three excited triplet states having main contributions to *D*.

Ab initio calculations showed that the main contributions to *D* come from the spin-orbit coupling of the ground state with first three triplet excited states (Figure 11).[10] The overall negative *D* value results from a large and negative contribution arising from the coupling between the ground state and the first excited triplet state, while the contributions from the other excited states are positive and much smaller. The observed *D* will therefore depend on the relative strengths of these opposite contributions that are governed by the differences of the energy levels of the involved orbitals. Based on this theoretical insights, it has been suggested that the negative contribution arising from the first excited triplet state could be increased by achieving a more symmetrical ligand field in the equatorial plane of Ni^{II}, thus reducing the energy difference between the d_{xy} and the $d_{x^2-y^2}$ orbitals. Additionally, the observed negative *D* value could be strengthened by reducing the positive contributions to *D*. This would be obtained using apical ligands with large σ-donor and less effective π-donor characteristic that increase the energy differences with the 2nd and 3rd excited triplet states.[10]

Complexes	PBP distortion[a]	ZFS parameters (cm^{-1}) and g						Ref.
		experimental			Theory[d]			
		D[b]	$\lvert E \rvert$	g	D	E	$g_{x,y,z}$	
[Ni(H$_2$L1^{Ph})(H$_2$O)$_2$]·2NO$_3$	0.51	-13.9	1.5	2.26	−16.8	1.15	–	10, 111
1-D [{Ni(H$_2$L1^{Ph})}{Ni(CN)$_4$}]	0.33	-17.7	1.0	2.18				13
[Ni(H$_2$L1^{BiPh})MeOH(NO$_3$)]·NO$_3$	0.34	-12.5	1.2	2.22				111
[Ni(H$_2$L1^{NH2})(H$_2$O)$_2$]·2NO$_3$	0.39	-12.5	1.7	2.26				13
		-15.6[c]	1.9[c]	$g_{x,y}$ = 2.2[c]				
				g_z = 2.3				
[Ni(H$_2$L1^{NH2})(H$_2$O)$_2$]·Cl·NO$_3$	0.71	-11.5	1.6	2.27	-17.8	3.5	2.26	112
		-10.5[c]	2.8[c]	g_y = 2.25[c]			2.30	
				g_z = 2.3			2.39	
[Ni(H$_2$L1^{NH2})(imidazole)$_2$]·2NO$_3$	0.34	-28.1	1.8	2.41	-43.5	-1.5	-	113
[Ni(H$_2$L1^{R})(NCS)$_2$](H$_2$O)$_n$								
R = Ph, n = 2	0.76	-12.4	1.5	2.28	-14.5	-1.7	–	113
R = NH$_2$, n = 2	0.90	-11.5	1.6	2.22	-19.0	-1.8	–	113
R = NH$_2$, n = 0	0.45	-15.5	0.76	2.19	-32.8	1.0	2.26	112
		-21.2[c]	2.1[c]	g_x = 2.0[c]			2.28	
				g_y = 2.1			2.48	
				g_z = 2.3				
[{Ni(H$_2$L1^{NH2})(H$_2$O)}$_2${WCN$_8$}]	0.69/0.38	-15.4	1.44	2.29	-19.8	1.6	2.25	112
		-15.0[c]	2.0[c]	g_x = 2.23[c]			2.27	
				g_y = 2.38			2.39	
				g_z = 2.27				
[Ni(H$_2$L1^{CH2NMe3})(NCS)$_2$]·2NCS	1.00	-11.7	1.5	2.31	-12.9	-2.8	2.22	61
							3 .27	
							2.34	
[Ni(L4)(MeCN)$_2$]·2BPh$_4$	0.48	-14.3	1.8	$g_{x,y}$ = 1.79	-15.4	3.23	1.74	68
				g_z = 2.39			1.91	
							2.59	

[Ni(L5^H)Cl$_2$]	1.0	-6.0	0.9	2.27	-6.08	1.19	2.18 2.24 2.27	[53]
[Ni(L5^{CH2Py})]·2ClO$_4$	1.24	-12.8	1.7	2.18	-19.11	2.60	1.98 2.10 2.19	[74]
[Ni(L5^{CH2COO})]·2ClO$_4$	2.99	-8.5	1.6	2.20	-13.3	2.40	2.27 2.24 2.35	[75]
[Ni(L5^{CH2bzIm})]·2ClO$_4$ ^{e}	1.20/1.11	-17.2	1.3	2.16	-23.8/ -25.6	1.59/ 1.10	2.25/2.24 2.23/2.23 2.40/2.41	[52]
[Ni(L7^{Me})(H$_2$O)$_2$]·2BF$_4$	0.38	-10.95	1.5	2.11				[33]
1D-[Ni(L7^{Me}){Ni(CN)$_4$}]$_\infty$	0.30	-14.4	1.8	2.13				[33]
[Ni(1,10-N$_2$-15C5-aniline)]X$_2$		|D|						[106]
X = NO$_3^-$	1.54	15		2.27				

(a) distortion parameter with respect to PBP geometry calculated by SHAPE;[90, 114] (b) from magnetic behavior or as specified; (c) from EPR data; (d) CASSCF/NEVPT2 calculations ; (e) the asymmetric unit contains two Ni centers.

Table 7. Magnetic anisotropy in PBP Ni^{II} complexes.

These guidelines motivated experimental work to gather quantitative data on achievable D values. For instance, in the series of complexes based on ligands H_2L1^R or $L5^R$, the more negative D values (respectively -28.1 cm^{-1} and -17.2 cm^{-1}) have been obtained when apical positions are occupied by imidazole units, which are good σ-donor ligands. Closely related values were found with N-bound cyanides in the apical positions. However, the structural distortion appears to have an effect too. This is suggested by the large difference in D found for $[Ni(H_2L1^{NH2})(imidazole)_2]^{2+}$ and $[Ni(L5^{CH2bzIm})]^{2+}$, both of which displaying imidazoles in their apical positions but the coordination sphere for the latter shows a larger deviation from reference geometry (shape parameters respectively of 0.34 and 1.2, Table 7). The effect of structural distortions is even better illustrated by the series of crystal phases obtained with $[Ni(H_2L1^{NH2})(NCS)_2]$ for which D changes from -15.5 cm^{-1} to -11.5 cm^{-1} as distortion increases (shape parameter of 0.45 and 0.90, respectively). The same trend is found for the $[Ni(H_2L1^R)(H_2O)_2]^{2+}$ derivatives, confirming the decrease of $|D|$ for these Ni complexes by structural distortions. Table 8 gathers the calculated contributions to D arising from the coupling with the three first triplet excited states for a series of complexes. For the H_2L1^R ligand-based complexes, substantial differences can be noticed in the contribution of the first triplet excited state, reflecting the effect of the coordination sphere distortion. These calculated contributions help to understand the differences in D values found experimentally for these complexes. A theoretical investigation pointed also to a strong effect of the equatorial ligand field, the magnetic anisotropy becoming more negative as the ligand field is weaker.[52]

For none of these complexes a SMM-type behavior was ever evidenced.

Complex	$D_{calculated}$ (cm^{-1})	Contribution of the excited triplet states			Ref.
		1st	2nd	3rd	
$[Ni(H_2L1^{NH2})(imidazole)_2]\cdot2NO_3$	-43.5	-93.6	20.5	18.5	[113]
$[Ni(L5^{CH2bzIm})]\cdot2ClO_4$	-23.8/-25.6	-72.0/-74.3	20.6/20.7	21.8/21.8	[115]
$[Ni(H_2L1^R)(NCS)_2]\cdot nH_2O$					
R = NH₂, n = 2	-19.0	-69.7	22.6	20.6	[113]
R = NH₂, n = 0	-32.8	-88.1	25.2	23.7	[116]
$[Ni(H_2L1^R)(H_2O)_2]\cdot XY$					
R = Ph, X = Y = NO₃⁻	-16.8	-66.2	22.5	23.2	[10]
R = NH₂, X = Cl⁻, Y = NO₃⁻	-17.8	-70.9	27.7	24.1	[116]
$[\{Ni(H_2L1^{NH2})(H_2O)\}_2\{W(CN_8)\}]$	-19.8	-71.6	25.1	23.8	[116]

Table 8: Main perturbative contributions of the triplet excited states to D for a selection of PBP Ni^{II} complexes.

PBP Ni^{II} as building unit: Pentanuclear $[Ni_3W_2]$ compounds were obtained by assembling $[Ni(H_2L1^R)(H_2O)_2]^{2+}$ and $[W(CN)_8]^{3-}$.[111] They are characterized by substantial ferromagnetic Ni-W interactions (up to 30 cm^{-1}) and the derivative with R = Ph was found to exhibit SMM-type behavior with an energy barrier for spin reversal of U_{eff}/k_B = 30 K. $[Ni(L7^{Me})(H_2O)_2]^{2+}$ and $[Cr(L1^{Ph})(CN)_2]^-$ resulted in the formation a 1D ferromagnetic coordination polymer behaving as an SCM with U_{eff}/k_B = 54 K (Figure 12a).[33] Here too ferromagnetic Ni-Cr interactions take place, of the order of J_{NiCr} = 10 cm^{-1} in a

trinulear [NiCr$_2$] complex. Chain compounds made up with diamagnetic [Ni(CN)$_4$]$^{2-}$ and [Ni(H$_2$L1^{Ph})(H$_2$O)$_2$]$^{2+}$ or [Ni(L7^{Me})(H$_2$O)$_2$]$^{2+}$ showed that PBP Ni units with N-bound cyanide ligands in the apical positions retain large magnetic anisotropy (respectively -17.7 and -14.4 cm^{-1}, Table 7).[13, 33] A related anisotropy, -15.4 cm^{-1}, was found in a trimetallic complex [{Ni(H$_2$L1^{NH2})(H$_2$O)}$_2${W(CN)$_8$}] involving a diamagnetic W^{IV} unit.[112]

A linear trinuclear Ni complex featuring a central ion with PBP geometry was obtained using a tri-compartmental ligand N,N'-bis(3-methoxysalicyl)-2,6-pyridine dicarbohydrazide (Figure 12b).[117] The magnetic behavior described for this compound is quite intriguing. It would correspond to the contribution of three S = 1 spins while two of the Ni ions are in a square-planar environment and, therefore, should be diamagnetic.
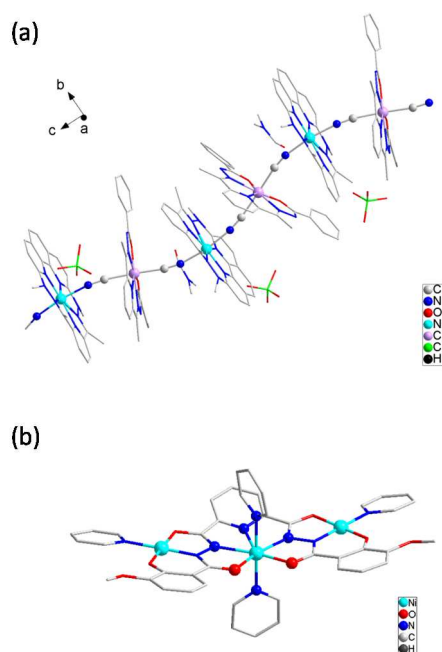

Figure 12. (a) Molecular arrangement in Single-Chain magnet [Ni(L7^{Me}){Cr(L1^{Ph})(CN)$_2$}].ClO$_4$; [33] (b) trinuclear complex featuring a central Ni^{II} with PBP coordination sphere (drawn from ref.[117]).
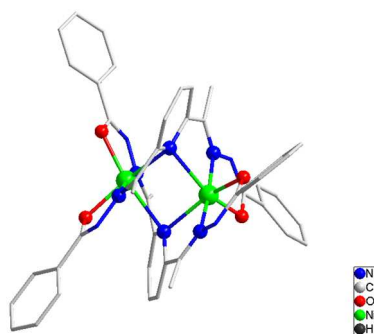
Figure 13. Hexacoordinated Ni-dimer formed by reorganization of PBP [Ni(H$_2$L1^R)(H$_2$O)$_2$]$^{2+}$ (redrawn from ref.[33]).·

The limited number of heterometallic compounds constructed with preformed PBP Ni^{II} complexes is likely related to the Jahn-Teller effect which leads to significant distortion of the coordination sphere of Ni^{II}. It may even favor a structural reorganization to an octahedral coordination polyhedron when

the chemical integrity of the PBP coordination sphere gets disturbed. For instance, a slightly basic medium (ex. in DMF or in the presence of some cyanometallates) induces an instantaneous rearrangement of $[Ni(H_2L1^{Ph})(H_2O)_2]\cdot 2NO_3$ to a bimetallic complex in which the Ni is 6-coordinated (Figure 13).[33, 118] However, this structural fragility seems to be reduced with a more rigid ligand to stabilize the equatorial coordination sphere.[33]

I.9. d^9 (Cu^{II})

Several examples of Cu^{II} complexes with PBP coordination polyhedron are known. As for the other transition metal ions, this geometry can be induced by a ligand constraining a pentagonal equatorial coordination arrangement (Table 9). A general feature of all these Cu^{II} complexes is their axially compressed PBP coordination sphere. As a consequence, the d_{z^2} orbital is highest in energy and accommodates the unpaired electron. The ground spin state S = ½ for PBP Cu^{II} excludes any contribution from ZFS. However, EPR revealed substantial g-anisotropy (Table 9) with $g_z < g_x$, g_y (*i.e.* $g_{||} < g_\perp$) in agreement with singly-occupied d_{z^2} orbital.[119]

Complexes	Cu-L axial *vs* equatorial mean-distances (Å)	g factors (EPR) $g_{x,y,z}$ or $g_{||}$, $g_\perp$	Ref.
$[Cu(H_2L^{N3O2R})(H_2O)_2]\cdot 2NO_3$			
R = NH$_2$	1.922 *vs* 2.296		108
R = Ph	1.942 *vs* 2.246		120
R = Me	1.942 *vs* 2.229		121
$[CuL^{N7}]\cdot 2ClO_4$	1.99 *vs* 2.356	2.02, 2.22[(b)]	122
$[Cu(L^{terpy})(imidazole)_2]^{2+}$	2.038 *vs* 2.206	2.26, 2.06[(a)]	123
$[Co(L^{COO})]$	1.925 *vs* 2.345	2.043, 2.106, 2.307[(a)]	107, 124
$[Cu(benzo15C5)Cl_2]$	2.248 *vs* 2.284	1.995, 2.294	125, 126
		2.321, 2.321, 1.995	119
$[Cu(15C5)Y_2]\cdot 2X$			
Y = Cl$^-$		2.372, 2.265, 2.00[(a)]	119
Y = H$_2$O, X = NO$_3^-$	1.93 *vs* 2.25	2.35, 2.36, 2.0[(b)]	127
$[CuL]\cdot 2ClO_4$	2.035 *vs* 2.220 (N atoms)		128
L = *N,N*-bis(2-aminobenzyl)-1,10-diaza-15C5			
$[Cu(L^{terpyNO})(H_2O)_2]\cdot 2BF_4$	2.271 *vs* 2.372 (O atoms)		129
$[Cu(Phen-2,9-COO)(H_2O)_3]$	1.929 *vs* 2.141		130

(a) in frozen solution, (b) solid state.

L^{N7} = ; L^{terpy} = ; H_2L^{COO} =
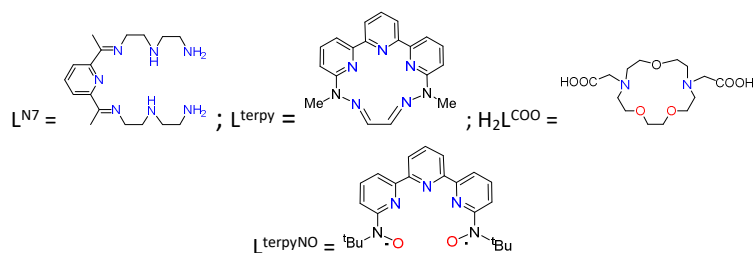
$L^{terpyNO}$ =

Table 9. PBP Cu^{II} complexes.

This overview of the magnetic anisotropies of transition metal ions shows that this property is directly related to the electronic configuration d^n. For this reason, it can be rationally imparted to a coordination complex. By adjusting the deformation of the PBP coordination sphere and possibly the ligand field in the axial and equatorial positions of the complex, values of the axial ZFS parameter D between -30 and +40 cm^{-1} are readily available by chemical design. This possibility is particularly interesting for the design of materials where the magnetic anisotropy has an important part in the magnetic behavior of the system, whether it is a nanomagnet (SMM or SCM) or a classical magnet.

II.   Lanthanide ions with pentagonal bipyramidal coordination sphere

Trivalent lanthanide ions are very attractive magnetic centers to achieve SMMs with high energy barrier for magnetization reversal, U_{eff}/k_B, and a significant blocking temperature, T_B. The 4f ions (except La^{III}, Gd^{III} and Lu^{III}) exhibit an inherent magnetic anisotropy due to a strong spin orbit coupling resulting from the unquenched orbital angular momentum.[131, 132] In contrast to transition metal ions, in lanthanide complexes the spin-orbit coupling energy is larger than the crystal field splitting by an order of magnitude of 10 to 100. Although crystal field effects (i.e. the electrostatic interaction between the ligand- and the f-electrons) are small, they are large enough to lift the degeneracy of the m_J states of the J multiplets and to be the real origin of the magnetic anisotropy in the f elements. Therefore SMM characteristics of a 4f compound are directly linked to crystal field considerations. The dynamic of the demagnetization is related to the $\pm m_J$ of lowest energy and to the energy difference between the ground and the first excited m_J microstate. Ideally, to ensure high blocking temperatures, ground m_J should have largest J value (i.e. $m_J = \pm 6$ for Tb^{III}, $\pm 15/2$ for Dy^{III}, etc…) and the energy gap with next m_J state must be as large as possible.

The role of the crystal field in optimizing the anisotropy for each Ln^{III} was discussed by Rinehart and Long.[133] For an Ln ion, each m_J state is characterized by a specific aspheric spatial distribution of its 4f electron density (Figure 14, bottom). The valence electron density distribution for the $\pm m_J$ state with largest J for each trivalent Ln is depicted in Figure 14.[134, 135] Their spatial shape is either axially compressed (i.e. oblate, for Ce^{III}, Pr^{III}, Nd^{III}, Tb^{III}, Dy^{III}, and Ho^{III}) or axially elongated (i.e prolate, for Pm^{III}, Sm^{III}, Er^{III}, Tm^{III}, and Yb^{III}), except that of Eu^{III}, Gd^{III} and Lu^{III} which is spherical. Since the electronic repulsion between the electron densities of the Ln center and the ligands results in a spatial distribution of the $4f^n$-electron cloud that minimizes these electrostatic interactions, it is possible to adjust the crystal field distribution to stabilize the ground m_J state with largest J. For instance, for an Ln^{III} with oblate density distribution of its ground m_J, electron density is larger in the *x,y*-plane directions than along the *z*-direction (Figure 14), therefore electrostatic interactions with its coordination sphere is minimal when ligand field is weak in the equatorial positions and strong along the *z* axis. Conversely, to stabilize an m_J state with a prolate electronic distribution, a stronger ligand field in the plane and weaker along the apical directions is required to minimize electrostatic interactions between the 4f electron cloud and its coordination sphere. When these conditions are met, the magnetic anisotropy is maximal and the reversal of magnetization via excited $\pm m_J$ states requires more energy, i.e. referring to an Arrhenius behavior, the energy barrier U/k_B is large.

The control of the coordination geometry around the 4f-ion is therefore of crucial importance, and with respect to the aforementioned model, low-coordinate lanthanide complexes with high order of symmetry are attractive, but challenging candidates to synthesize.[136-140] To circumvent those synthetic difficulties, Ln complexes belonging to an axial symmetry group such as trigonal and pentagonal bipyramids (D_{3h} and D_{5h}) are viable alternatives,[141, 142] the D_{5h} geometry being the point of interest of this review.

Focusing on complexes showing SMM-type magnetic behaviors, two families of rare earth complexes in PBP symmetry can be identified. The first family concerns complexes formed with monodentate ligands, the second family involves polydentate ligands. Dy^{III} derivatives have been most investigated and have been shown to exhibit largest axial anisotropy when strong-field ligands (alkoxide, siloxide, phosphine oxide, phosphonic diamide, phosphonic triamide, etc…) are located in the axial positions of the rare earth whereas equatorial positions are occupied by weak-field ligands (such as H_2O, THF, pyridine, polydentate ligands). Promising behaviors have also been obtained with other Ln ions. The most striking results are reviewed in the following.
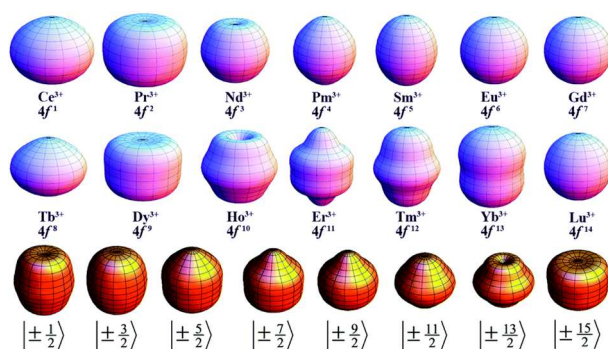

Figure 14. Shape of the 4f electron cloud for the ±m$_J$ state with the largest J for the trivalent 4f$^{1-14}$ Ln ions, and (bottom) for each m$_J$ state of Dy^{III}, showing the evolution from a prolate electron-density cloud for m$_{15/2}$ to an oblate spatial distribution for m$_{1/2}$ (reprinted from ref.[135] with permission from Royal Society of Chemistry).

II.1 PBP complexes with monodentate ligands

The reported examples of Ln^{III} complexes with PBP coordination polyhedron formed by only monodentate ligands and behaving as SMMs are listed in Table 10 with their characteristic magnetic and geometrical information. For this family of compounds, the dominating influence of the axial ligands is seen through the almost linear L_{ax}-Ln-L_{ax} arrangement (varying from 173.5°, entry 15, to 179.2°, entry 6) and through the L_{ax}-Ln bond distances shorter than the L_{eq}-Ln bond distances. This is perfectly illustrated by [Dy(CH$_3$CH(C$_6$F$_5$)O)$_2$(THF)$_5$][BPh$_4$][143] (Table 10, entry 34) which has one of the highest energy barrier (2114 K) and blocking temperature (22 K) reported for PBP complexes. For this derivative, the two axial ligands are fluorinated alkoxides with a L_{ax}-Dy-L_{ax} angle of 177.5°, and L_{ax}-Dy bond lengths of 2.102 Å, significantly shorter than the L_{eq}-Dy bond lengths (2.434 Å, Figure 15). The distortion of the Dy coordination polyhedron from the ideal D_{5h} geometry is small as supported by shape parameter of 0.461.
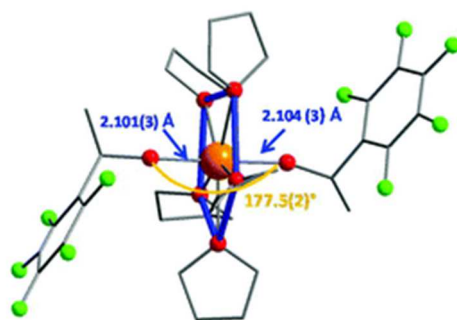
Figure 15. Molecular structures of the cationic complex [Dy(Me(C$_6$F$_5$)CHO)$_2$(THF)$_5$]$^+$. Colour code: orange, Dy; red, O; grey, C; green, F. Hydrogen atoms and the [BPh$_4$]$^-$ moieties have been omitted for clarity. (Reprinted from ref.[143] with permission from Royal Society of Chemistry).

Several important points are noted for this family of compounds. The nature of the negatively charged ligand coordinated in axial positions to the rare earth seems to be a predominant criterion for the optimization of the magnetic properties of these systems. This is clearly illustrated by the Dy^{III} complexes [DyX^{1}X^2(THF)$_5$]·BPh$_4$ (with X^1 = Cl, OPh, OCMe$_3$ and OSiMe$_3$; X^2 = Cl, Br, OPh, OCMe$_3$ and OSiMe$_3$; Table 10, entries 17, 18, 21-22, 27-28),[144-147] and [DyX^2(THF)$_5$]·BPh$_4$ (X^2 = CH$_3$(C$_6$F$_5$)CHO$^-$, pyrazolate, PhO$^-$, Me$_3$CO$^-$, Me$_3$SiO$^-$, Table 10, entries 19-20, 24, 26, 29-30, 34).[143-146] When one and then the two axial Cl$^-$ ligands of [DyCl$_2$(THF)$_5$]$^+$ are replaced by phenolate ligands to give [DyCl(PhO)(THF)$_5$]$^+$ and [Dy(PhO)$_2$(THF)$_5$]$^+$, respectively, the effective energy barrier for magnetization reversal, U$_{eff}$/k$_B$, increases from 83 K to 1329 K with a blocking temperature shift from 7 K to 12 K.[145] This trend is corroborated by the remarkable results obtained for [Dy(CH$_3$CH(C$_6$F$_5$)O)$_2$(THF)$_5$]·BPh$_4$ (entry 34), where the Dy-alkoxyl bond distance are shorter.

The nature of the second coordination sphere of the rare earth center is also a point of importance. For the series of complexes [Dy((Me$_2$N)$_3$PO)$_2$(H$_2$O)$_5$]$_n$·3nX (X = Cl, n = 1; X = Br, n = 2, and X = I, n = 1; Table 10 entries 7-9),[148, 149] [Dy(cy$_3$PO)$_2$(H$_2$O)$_5$]·3X (X = Cl, Br, CF$_3$SO$_3$, entries 14-16),[150, 151] and [Ho(pyr$_3$PO)$_2$(H$_2$O)$_5$]X$_3$ (X = Cl, Br, entries 12-13),[152] where various phosphonic triamide and phosphine oxide act as strong axial ligands and water molecules occupy the equatorial coordination sites of the Ln ions, the value of U$_{eff}$/k$_B$ was found to significantly change with the nature of the anions associated to the complex. Theoretical calculations of the energy barrier (U$_{cal}$) for model molecules derived from the two complexes [Dy((Me$_2$N)$_3$PO)$_2$(H$_2$O)$_5$]Cl$_3$·((Me$_2$N)$_3$PO)·H$_2$O and [Dy((Me$_2$N)$_3$PO)$_2$(H$_2$O)$_5$]I$_3$·2((Me$_2$N)$_3$PO),[148,149] showed that moving the second coordination sphere away from the magnetic center (i.e. reducing or even suppressing the H-bond interactions with the metal-bonded H$_2$O), reduces the negative-charge density of the O atom of the coordinated H$_2$O. This lessens the equatorial crystal field strength and, consequently, amplifies the axial field effect. An illustration is given by the two Ho complexes [Ho(pyr$_3$PO)$_2$(H$_2$O)$_5$]Cl$_3$ and [Ho(pyr$_3$PO)$_2$(H$_2$O)$_5$]Br$_3$.[152] The replacement of Cl$^-$ by Br$^-$ leads to a greater separation between the five equatorially coordinated water molecules and the counter ions (the O$_{eq\ water}$··· X$^-$ distances range from 3.014 to 3.119 with X = Cl$^-$ and from 3.182 to 3.262 Å for X = Br$^-$), which implies a weakening of the H-bond interactions. Concomitantly, the axial Ho-O bond distances are reduced and the axial O-Ho-O angle becomes more linear (entries 12 and 13 in Table 10). The stronger and more linear axial crystal field acting on Ho^{III} as a result of the reduced effect of the second coordination sphere leads to an increase in U$_{eff}$/k$_B$ from 350 K (X = Cl$^-$) to 418 K (X = Br$^-$).

The same arguments hold for the two Dy-based complexes [Dy(cy$_3$PO)$_2$(H$_2$O)$_5$]Cl$_3$·(cy$_3$PO)·H$_2$O·EtOH and [Dy(cy$_3$PO)$_2$(H$_2$O)$_5$]Br$_3$·2(cy$_3$PO)·2H$_2$O·2EtOH.[150] Furthermore, these complexes provide an illustration that the second coordination spheres can also modify the coordination polyhedron of the Ln^{III} center. For the complex with Cl$^-$ as a counter ion (Figure 16), the second coordination sphere consists in an asymmetrical 11-membered H-bonded ring formed by the five coordinated water molecules, four Cl$^-$, one free tricyclohexylphosphine oxide whereas with Br$^-$ as counter ion, a symmetrical 10-membered ring (a five-pointed star) is formed between the five water molecules, the three Br$^-$ ions and two free phosphine oxide molecules. In [Dy(cy$_3$PO)$_2$(H$_2$O)$_5$]Br$_3$, the PBP polyhedron around the Dy center is slightly more compressed than that in [Dy(cy$_3$PO)$_2$(H$_2$O)$_5$]Cl$_3$ (see entries 14 and 15 in Table 10) which results in a coordination geometry closer to the ideal D$_{5h}$ symmetry. The combined effects resulting from the modulation of the second coordination sphere lead to an increase of the blocking temperature from 11 K to 20 K for [Dy(cy$_3$PO)$_2$(H$_2$O)$_5$]Br$_3$.

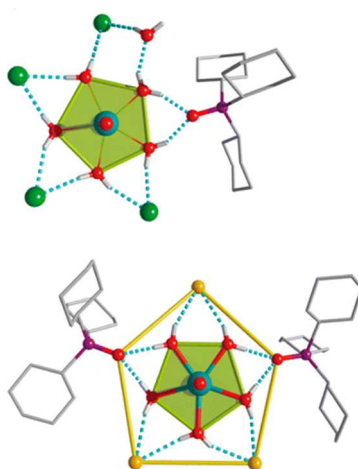**Figure 16.** Coordination environment of Dy^{III} and outer coordination sphere connected with hydrogen bonds, in (top) [Dy(cy$_3$PO)$_2$(H$_2$O)$_5$]Cl$_3$·(cy$_3$PO)·H$_2$O·EtOH and (bottom) [Dy(cy$_3$PO)$_2$(H$_2$O)$_5$]Br$_3$·2(cy$_3$PO)·2H$_2$O·2EtOH. H atoms of the ligands are omitted for clarity. Color codes: Dy, cyan; P, purple; Br, orange; Cl, green; O, red; C, gray; H, light gray. (Reprinted with permission from ref.[150], copyright 2022 American Chemical Society)

The alteration of the counter ions associated to a PBP Ln complex is the usual approach followed to modulate the influence of the second coordination sphere on the SMM behaviors (Table 10 and 11). The crystallization medium is another possibility that can be used because solvent molecules are often part of the crystal lattice and even involved in the composition of the second coordination sphere. This leads to emphasize the attention that must be paid to the aging of the samples; the loss of lattice solvent molecules can affect the second coordination sphere and significantly change the magnetic behavior of a compound even if the structure of the complex is apparently not modified.

		SMM relaxation characteristics					Structural information			
Entry	Complex	U_{eff}/k_B [a] (K)	τ_0 (s)	U_{cal}/k_B (K)	Hysteresis (field sweep Ts^{-1})	T_B [b] (K)	L_{ax}-Ln-L_{ax} (°)	Average Ln-L (Å)	Deviation from D_{5h} [c]	Ref
1	[Ho(^{t}Bu(NH^{i}Pr)$_2$PO)$_2$(H$_2$O)$_5$]I$_3$·2(^{t}Bu(NH^{i}Pr)$_2$PO)·H$_2$O	355	1.5x10^{-10}	374	Yes (0.027)	4	175.05	2.194 (L$_{ax}$) 2.343 (L$_{eq}$)	0.200	[153]
2	[Dy(^{t}Bu(NH^{i}Pr)$_2$PO)$_2$(H$_2$O)$_5$]I$_3$·2(^{t}Bu(NH^{i}Pr)$_2$PO)·H$_2$O	651 705 (2 kOe)	5.6x10^{-12} 5.8x10^{-12}	688	Yes (0.0018)	12	175.1	2.205 (L$_{ax}$) 2.363 (L$_{eq}$)	0.224	[154]
3	[Er(^{t}Bu(NH^{i}Pr)$_2$PO)$_2$(H$_2$O)$_5$]I$_3$·2(^{t}Bu(NH^{i}Pr)$_2$PO)·H$_2$O	45 (2 kOe)	1.1x10^{-8}	-	-	-	174.9	2.195 (L$_{ax}$) 2.334 (L$_{eq}$)	-	[154]
4	[Nd(^{t}Bu(NH^{i}Pr)$_2$PO)$_2$(H$_2$O)$_5$]I$_3$·2(^{t}Bu(NH^{i}Pr)$_2$PO)·H$_2$O	24.6 39.2 (2 kOe)	5x10^{-6} 9x10^{-7}	302	-	-	174.4	2.289 (L$_{ax}$) 2.441 (L$_{eq}$)	0.286	[155]
5	[Ho((Me$_2$N)$_3$PO)$_2$(H$_2$O)$_5$]Br$_3$·2((Me$_2$N)$_3$PO)·H$_2$O	320	1.4x10^{-11}	-	-	-	179.2	2.213 (L$_{ax}$) 2.348 (L$_{eq}$)	0.154	[156]
6	[Ho((Me$_2$N)$_3$PO)$_2$(H$_2$O)$_5$]$_2$Cl$_6$·2((Me$_2$N)$_3$PO)	290	7.5x10^{-11}	-	-	-	178.1 -176.7	2.208 (L$_{ax}$) 2.368 (L$_{eq}$)	0.127	[156]
7	[Dy((Me$_2$N)$_3$PO)$_2$(H$_2$O)$_5$]Cl$_3$·((Me$_2$N)$_3$PO)·H$_2$O (2 asym units)	460	2.0x10^{-11}	584	-	-	176	2.219 (L$_{ax}$) 2.408 (L$_{eq}$)	0.154 and 0.284	[148]
8	[Dy((Me$_2$N)$_3$PO)$_2$(H$_2$O)$_5$]I$_3$·2((Me$_2$N)$_3$PO)	600	1.2x10^{-11}	640	-	-	178	2.205 (L$_{ax}$) 2.359 (L$_{eq}$)	0.131	[148]
9	[Dy((Me$_2$N)$_3$PO)$_2$(H$_2$O)$_5$]$_2$Br$_6$·2((Me$_2$N)$_3$PO)·2H$_2$O	556	1.2x10^{-11}	-	Yes (0.002)	7	176.4 - 177.7	2.216 (L$_{ax}$) 2.357 (L$_{eq}$)	0.196 and 0.214	[149]
10	[Ho(cyPh$_2$PO)$_2$(H$_2$O)$_5$]I$_3$·2(cyPh$_2$PO)·H$_2$O·EtOH	237	1.7x10^{-11}	-	Yes (0.07)	3*	177.9	2.198 (L$_{ax}$) 2.364 (L$_{eq}$)	0.160	[157]
11	[Dy(cyPh$_2$PO)$_2$(H$_2$O)$_5$]Br$_3$·2(cyPh$_2$PO)·3H$_2$O·EtOH	508	8.6x10^{-12}	427	Yes (0.02)	19*	174.2	2.217 (L$_{ax}$) 2.364 (L$_{eq}$)	0.142	[158]
12	[Ho(pyr$_3$PO)$_2$(H$_2$O)$_5$]Cl$_3$·H$_2$O	351	7.2x10^{-11}		Yes (0.002)	8	177.94	2.210 (L$_{ax}$) 2.530 (L$_{eq}$)	0.112	[152]
13	[Ho(pyr$_3$PO)$_2$(H$_2$O)$_5$]Br$_3$·H$_2$O	418	1.8x10^{-11}	-	Yes (0.002)	15	178.80	2.195 (L$_{ax}$) 2.353 (L$_{eq}$)	0.132	[152]

14	[Dy(cy₃PO)₂(H₂O)₅]Cl₃·(cy₃PO)·H₂O·EtOH	472	8.7x10⁻¹²		Yes (0.02)	8	175.79	2.219 (L_ax) 2.359 (L_eq)	0.239	[150]

#	Compound									Ref
14	[Dy(cy₃PO)₂(H₂O)₅]Cl₃·(cy₃PO)·H₂O·EtOH	472	8.7×10^{-12}		Yes (0.02)	8	175.79	2.219 (L$_{ax}$) 2.359 (L$_{eq}$)	0.239	[150]
15	[Dy(cy₃PO)₂(H₂O)₅]Br₃·2(cy₃PO)·2H₂O·2EtOH	543	2.0×10^{-11}	-	Yes (0.02)	11	179.04	2.200 (L$_{ax}$) 2.352 (L$_{eq}$)	0.142	[150]
16	[Dy(cy₃PO)₂(H₂O)₅](CF₃SO₃)₃·2(cy₃OP)	562	1.7×10^{-11}	732	-	8.5	173.48	2.202 (L$_{ax}$) 2.363 (L$_{eq}$)	0.639	[151]
17	[DyCl₂(THF)₅][BPh₄]·0.5THF	83	4.1×10^{-10}	78	-	-	177.97	2.566 (L$_{ax}$) 2.413 (L$_{eq}$)	0.208	[145, 159]
18	[DyCl(PhO)(THF)₅]·BPh₄	737	4.5×10^{-11}	-	Yes (n.a.)	6.8	178.47	2.113/2.587 (L$_{ax}$) 2.415 (L$_{eq}$)	0.456	[145]
19	[Dy(PhO)₂(THF)₅][BPh₄]₂[Na(THF)₅]	1329	4.9×10^{-12}	-	Yes (n.a.)	12	176.34	2.127 (L$_{ax}$) 2.422 (L$_{eq}$)	0.556	
20	[Dy(PhO)₂(py)₅]·BPh₄	1302	3.6×10^{-13}	-	Yes (n.a.)	13	176.4	2.122 (L$_{ax}$) 2.534 (L$_{eq}$)	0.700	
21	[DyCl(Me₃CO)(THF)₅]·BPh₄	938	4.4×10^{-12}	-	Yes (n.a.)	7	178.26	2.043/2.662 (L$_{ax}$) 2.411 (L$_{eq}$)	0.293	[145]
22	[DyBr(Me₃CO)(THF)₅]·BPh₄	819	1.7×10^{-11}	-	Yes (n.a.)	4.5	178.0	2.023/2.814 (L$_{ax}$) 2.430 (L$_{eq}$)	0.386	
23	[DyCl(pz)(THF)₅]·BPh₄	470	2.0×10^{-10}	480-491	-	-	176.52	2.242 (L$_{ax}$) 2.443 (L$_{eq}$)	-	[146]
24	[Dy(pz)₂(THF)₅]·BPh₄	521	9.0×10^{-12}	503-558	Yes (0.0012)	4	174.23	2.296/2.278 (L$_{ax}$) 2.457 (L$_{eq}$)	-	
25	[DyCl(ᵗBuO)(THF)₅]·2BPh₄·2THF	950	3.0×10^{-12}	-	Yes (0.005)	7	178.26	2.043/2.662 (L$_{ax}$) 2.410 (L$_{eq}$)	-	[160]
26	[Dy(ᵗBuO)₂(py)₅]·BPh₄	1814 1805	1.7×10^{-12} 1.4×10^{-12}	1755	Yes (0.0012)	14	178.91	2.112 (L$_{ax}$) 2.561 (L$_{eq}$)	0.801	[144] [145]
27	[DyCl(Me₃SiO)(THF)₅]·BPh₄	801	2.8×10^{-11}	-	Yes (n.a.)	4.5	178.50	2.074/2.647 (L$_{ax}$) 2.414 (L$_{eq}$)	0.352	[145]
28	[DyBr(Me₃SiO)(THF)₅]·BPh₄	732	1.1×10^{-11}	-	Yes (n.a.)	4.5	178.95	2.092/2.797 (L$_{ax}$) 2.411 (L$_{eq}$)	0.483	
29	[Dy(Me₃SiO)₂(py)₅]·BPh₄	1596	1.5×10^{-12}	-	Yes (n.a.)	15	176.08	2.144 (L$_{ax}$) 2.550 (L$_{eq}$)	0.683	

No.	Compound	U_{eff}	τ_0		Hysteresis	T_B	angle	bond lengths	dev.	Ref.
30	[Dy(Me$_3$SiO)$_2$(4-Mepy)$_5$]·BPh$_4$	1498	3.0x10^{-12}	-	Yes (n.a.)	16	177.7	2.146 (L$_{ax}$) 2.548 (L$_{eq}$)	0.618	
31	[Ho(Me$_3$SiO)$_2$(py)$_5$]·BPh$_4$	715	1.3x10^{-12}	686	-	-	176.12	2.139 (L$_{ax}$) 2.520-2.557 (L$_{eq}$)	0.754	[161]
32	[Ho((C$_6$H$_5$)(CH$_3$)C(H)O)$_2$(py)$_5$]·BPh$_4$	499	6.8x10^{-12}	356	-	-	174.51	2.114 (L$_{ax}$) 2.532-2.564 (L$_{eq}$)	0.778	[161]
33	[Ho((C$_6$H$_5$)(CH$_3$)$_2$CO)$_2$(py)$_5$]·BPh$_4$	397	1.1x10^{-11}	300	-	-	175.68	2.141 (L$_{ax}$) 2.525-2.579 (L$_{eq}$)	0.881	
34	[Dy(CH$_3$CH(C$_6$F$_5$)O)$_2$(THF)$_5$]·BPh$_4$·2THF	2113	1.0x10^{-14}	-	Yes (0.002)	22	177.5	2.102 (L$_{ax}$) 2.434 (L$_{eq}$)	0.461	[143]
35	[Dy(4-MMNO)(H$_2$O)$_5$][M(CN)$_6$]									[162]
	M = Fe^{III}	592	1.9x10^{-10}	588	Yes (0.05)	20*	179.15	2.155 (L$_{ax}$) 2.369 (L$_{eq}$)	0.233	
	M = Cr^{III}	596	1.1x10^{-10}	592	Yes (0.05)	15*	178.6	2.154 (L$_{ax}$) 2.367 (L$_{eq}$)	0.269	
	M = Co^{III}	595	1.3x10^{-10}	595	Yes (0.05)	15*	178.1	2.148 (L$_{ax}$) 2.365 (L$_{eq}$)	0.264	

[a] U_{eff} is reported for H_{DC} = 0 Oe unless mentioned. [b] T_B is the temperature of the maximum of the zero field cooled (ZFC) susceptibility unless marked *, which corresponds to the highest temperature, T_H, with magnetic hysteresis cycle. [c] Deviation parameter obtained by the Continuous Shape Measures (CShM) method compared to the ideal D_{5h} symmetry configuration; n.a. = not available; cy : cyclohexyl; pyr : pyrrolidine; py : pyridine; pz :pyrazolate; 4-MMNO : 4-methylmorpholine N-oxide.

Table 10. PBP Ln SMMs formed from mono-dentate ligands with a selection of relevant magnetic (SMM characteristics) and structural information.

II.2 PBP complexes with polydentate ligands

The rare earth complexes in PBP symmetry obtained with polydentate ligands providing 2 to 6 donors atoms for metal coordination and exhibiting SMM behavior are gathered in Table 11. In most of these complexes, the multidentate ligand occupies the equatorial positions of the PBP coordination sphere around the rare earth ion, without necessarily involving full denticity. The axial positions are then occupied by anionic and/or neutral ligands (entries 1 to 12 and 30 to 47). These complexes can give rise to large energy barrier for magnetization reversal.

As mentioned before, pentadentate ligands are well suited to direct the formation of PBP coordination spheres, this also applies for Ln^{III} ions provided that the ligands in the apical positions are strictly monodentate.[163] For instance, Dy complex $[Dy(L^{N5})(Ph_3SiO)_2]\cdot BPh_4$[164] (Table 11, entry 31) is based on a cyclic pentadentate ligand (L^{N5} is an homologue of L3 (Figure 1) with propylene instead of ethylene units between the imine and amine N-atoms), with triphenylsilanolate in the apical positions, it was found to behave as an SMM with U_{eff}/k_B = 1108 K and a blocking temperature T_B = 5 K. In $[DyCu_5(quinha)_5(sal)_2(py)_2]\cdot CF_3SO_3$,[165] a more unusual metallacrown, $[15\text{-}MC_{Cu}\text{-}5]$ made of Cu^{II} ions and quinaldichydroxamic acid (H_2quinha), was involved as macrocyclic ligand to occupy the equatorial positions of the Dy^{III} ion whereas phenoxyl groups are in the apical positions. For this complex, an SMM behavior with energy barrier U_{eff}/k_B = 900 K (Table 11, entry 37) was evidenced.

Complexes with the axial positions occupied by moieties belonging to the multidentate ligand have been obtained with hexadentate ligands derived from ethylenediamine (entries 13 to 27),[166-170] propylenediamine (entry 27),[166] and tris(2-aminoethyl)amine (entries 28, 29).[171, 172] The five equatorial positions are occupied by remaining coordinating units of the multidentate ligands and additional ligands such as halide or solvent molecules. The complex series, $[Dy(bbpen\text{-}R)X]$[168-170] (Table 11, entry 14-26) is worth mentioning as several derivatives exhibit among the highest U_{eff}/k_B values for PBP complexes with values as large as 1162 K and blocking temperatures up to 21 K.

For these complexes involving polydentate ligands, the axial versus equatorial ligand-field strengths can be modulated too. The electrostatic potential in the equatorial plane can be modified by adapting the $Ln\text{-}L_{eq}$ bonds to have, for instance, a smaller crystal field contribution when coordinated to a Ln ion with oblate-shaped 4f-electron cloud for its largest m_J state (ex. Dy^{III}). This is nicely illustrated with the three series of compounds $[Dy(bbpen)X]$ (Table 11 entries 14-15, Figure 17)[168] and $[Dy(bbpen\text{-}CH_3)X]$ (entries 19-20),[169] and $[Dy(bbpen\text{-}OMe)X]$ (entries 21-26)[170] where the modification of the equatorial halogen ligand from Cl^- to weaker crystal field ligand Br^- leads to a large increase of U_{eff}/k_B and, to a lesser extent, of T_B. Same effect was observed for $[Zn_2Dy(TTT^{Cl})_2L]\cdot X$ (X = NO_3^-, $CF_3SO_3^-$, BPh_4^-, entry 29)[172] when equatorial ligand L was changed from methanol to weaker field ligands acetone, DMF, and finally N-methylpyrrolidone.
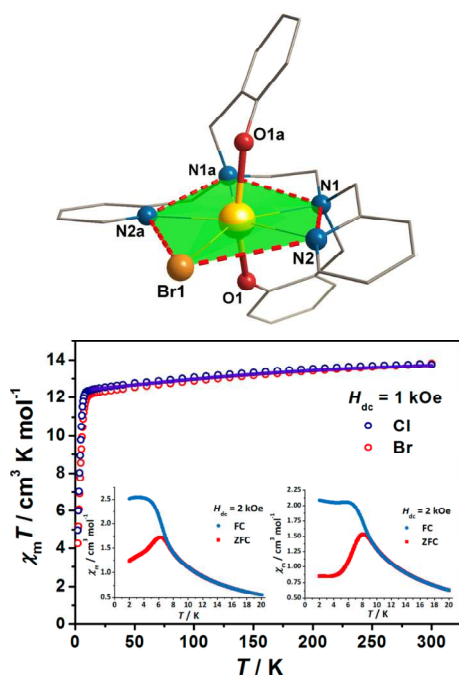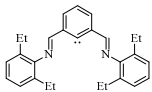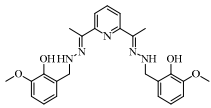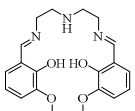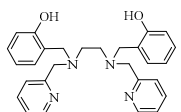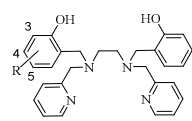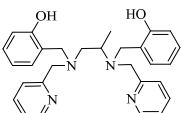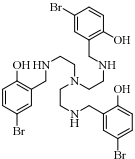
Figure 17 (left) Molecular structure for [Dy(bbpen)Br]. The equatorial plane of pentagonal bipyramidal coordination sphere is highlighted. Dy, yellow; Br, brown; O, red; N, blue; C, gray. Hydrogen atoms are omitted for clarity. (right) Variable-temperature molar magnetic susceptibility data for [Dy(bbpen)Br] and [Dy(bbpen)Cl]. Solid lines correspond to the *ab initio* calculation results. Inset: plot of magnetic susceptibility vs temperature during FC (blue) and ZFC (red) measurements for [Dy(bbpen)Br] (left) and [Dy(bbpen)Cl] (right) (Adapted with permission from ref.[168], copyright 2022 American Chemical Society).

A change of the ligand field can be obtained also by a modification of the donor atoms or functions of the polydentate ligand itself. For instance, changing imine to amine ligand can lower the crystal field contribution. This is illustrated by a series of Schiff-base Dy complexes and their amine-ligand homologues, [Dy(Bpen)Cl$_3$][173] (Table 11 entry 39) versus [Dy(HBpen)Cl$_3$][174] (entry 43), and [Dy(Bpen)Cl(OPhCl$_2$NO$_2$)$_2$][173] (entry 40) versus [Dy(Hbpen)Cl(OPhCl$_2$NO$_2$)$_2$][174] (entry 44) for which U_{eff}/k_B values of respectively, 22 K (H_{DC} = 800 Oe), 63 K (H_{DC} = 1600 Oe), 86 K (H_{DC} = 800 Oe), and 254 K (H_{DC} = 1200 Oe) have been obtained.

Finally, it can be noticed that the complexes involving polydentate ligands often exhibit slightly more distorted D_{5h} symmetry than those constructed with monodentate ligands. This is revealed by larger Shape parameters for the former (up to 2.327, Table 11 entry 15) while the same parameter does not exceed 0.801 (entry 26, Table 10) for the latter.

		SMM relaxation characteristics					Structural information			
Entry	Complex	U_{eff}/k_B[a] (K)	τ_0 (s)	U_{cal}/k_B (K)	Hysteresis (field sweep Ts^{-1})	T_B[b] (K)	L_{ax}-Ln-L_{ax} (°)	Average Ln-L (Å)	Deviation from PBP[c]	Ref
1	[(NCN)Dy(THF)$_2$Cl$_2$] NCN =	335	6.0x10^{-10}	384	Yes (not given)	1.9*	176.50	2.596 (L_{ax}) 2.393/2.448/ 2.668 (L_{eq})	-	147
2	[Dy(L1^{Ph})(Cy$_3$PO)Cl]	204 (1 kOe)	6x10^{-9}	223	-	-	169.62	2.237/2.625 (L_{ax}) 2.265/2.458 (L_{eq})	1.446	175
3	[Dy(L1^{Ph})(Ph$_3$PO)Cl]	241 (1.5 kOe)	2.3x10^{-10}	223	-	-	174.07	2.276/2.623 (L_{ax}) 2.283/2.460 (L_{eq})	1.505	175
4	[Yb(H$_3$Bmshp)(DMF)$_2$Cl$_2$]·DMF·1.5H$_2$O	14 (1.5 kOe)	2.38x10^{-5}	~ 288	-	-	165.54	2.622 (L_{ax}) 2.304 (L_{eq})	0.865	176
5	[Yb(H$_3$Bmshp)(DMF)$_2$Cl$_2$]·H$_4$Bmshp H$_4$Bmshp =	38 (0.6 kOe)	7.16x10^{-7}	~ 288	-	-	170.31	2.617 (L_{ax}) 2.304 (L_{eq})	1.094	
6	[Dy(H$_2$L1^{PhOH})Cl$_2$][Et$_3$NH]	70 (0.5 kOe)	1.9x10^{-6}	-	-	-	165.85	2.634 (L_{ax}) 2.365 (L_{eq})	1.159	163
7	[Er(L1$^{p\text{-}PhOMe}$)(H$_2$O)Cl]	23	6x10^{-9}		-	-	171.5	2.275/2.609(L_{ax}) 2.231/2.412(L_{eq})	1.171	177
8	[Er(L1$^{p\text{-}PhOMe}$)(MeOH)Cl]	16	1.7x10^{-7}		-	-	168.9	2.328/2.601(L_{ax}) 2.243/2.417(L_{eq})	1.457	
9	[Er(L1$^{p\text{-}PhOMe}$)(MeOH)N$_3$]	28	8x10^{-10}		-	-	179.5	2.316/2.232(L_{ax}) 2.263/2.432(L_{eq})	1.365	
10	[ErNa(valdien)Cl((PhO)$_2$PO$_2$)]$_n$	20 (1 kOe)	5.34x10^{-8}	-	-	-	163.19	2.427 (L_{ax}) 2.325 (L_{eq})	0.471	178
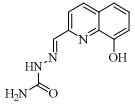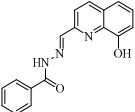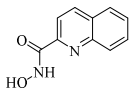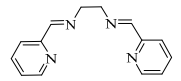
11	[DyNa(valdien)((PhO)$_2$PO$_2$)Cl]$_n$	20	2.56×10^{-7}	-	-	-	162.87	2.294/2.639 (L$_{ax}$) 2.396 (L$_{eq}$)	0.775	[179]
12	[Dy(valdien)((PhO)$_2$PO$_2$)]$_n$ H$_2$valdien =	20	6.12×10^{-7}	-	-	-	163.10	2.270 (L$_{ax}$) 2.400 (L$_{eq}$)	0.496	[179]
13	[Tb(bbpen)Cl] H$_2$bbpen =	33 (1 kOe)	8×10^{-8}	-	-	-	153.68	2.176 (L$_{ax}$) 2.617 (L$_{eq}$)	-	[166]
14	[Dy(bbpen)Cl]	708	9.46×10^{-11}	843	Yes (0.02)	7.5	154.3	2.166 (L$_{ax}$) 2.682/2.583 (L$_{eq}$)	2.048	[168]
15	[Dy(bbpen)Br]	1025	4.21×10^{-12}	1037	Yes (0.02)	9.5	155.8	2.163 (L$_{ax}$) 2.851/2.586 (L$_{eq}$)	2.327	[168]
16	[Dy$_2$(bbpen)$_2${Fe(CN)$_6$}]·PPh$_4$·3.5MeCN	628 962 (2 kOe)	8.42×10^{-10} 2.22×10^{-12} (2 kOe)	873	No (0.02)	-	159.4	2.153 (L$_{ax}$) 2.540/2.380 (L$_{eq}$)	1.359	[167]
17	[Dy$_2$(bbpen)$_2${Co(CN)$_6$}]·PPh$_4$·3.5MeCN	955 1054 (2 kOe)	4.13×10^{-12} 6.69×10^{-13} (2 kOe)	833	Yes (0.02)	15*	159.2	2.158 (L$_{ax}$) 2.533/2.385 (L$_{eq}$)	1.357	[167]

[Dy(bbpen-R)X]
H$_2$bbpen-R =

19	[Dy(bbpen-5-Me)X] X = Cl	723	2.36×10^{-10}	-	Yes (0.02)	9	158.07	2.155 (L$_{ax}$) 2.591/2.682 (L$_{eq}$)	1.824	[169]
20	X = Br	1162	1.02×10^{-12}	1179	Yes (0.02)	15	159.40	2.141 (L$_{ax}$) 2.586/2.852 (L$_{eq}$)	2.111	[169]
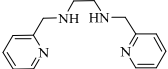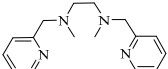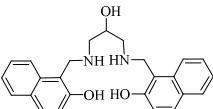
21	[Dy(bbpen-3-OMe)X] X = Cl	872	2.05×10^{-11}	1045	Butterfly (0.02)	5.5		2.154 (L_{ax}) 2.582/2.665 (L_{eq})	1.895	[170]
22	X = Br	1210	7.41×10^{-13}	1207	Butterfly (0.02)	8.5		2.142 (L_{ax}) 2.587/2.841 (L_{eq})	2.277	[170]
23	[Dy(bbpen-4-OMe)X] X = Cl	138	2.13×10^{-5}	1254	Butterfly (0.02)	2.5		2.169 (L_{ax}) 2.564/2.629 (L_{eq})	Capped trigonal prism	[170]
24	X = Br	602	3.28×10^{-8}	1388	Butterfly (0.02)	6.0		2.166 (L_{ax}) 2.569/2.789 (L_{eq})	Capped trigonal prism	[170]
25	[Dy(bbpen-5-OMe)X] X = Cl	907	1.22×10^{-11}	1022	Butterfly (0.02)	6.0		2.165 (L_{ax}) 2.583/2.664 (L_{eq})	1.866	[170]
26	X = Br	1216	7.43×10^{-11}	1200	21 K (0.02)	8.6		2.155 (L_{ax}) 2.582/2.823 (L_{eq})	2.152	[170]
27	[Tb(bbppn)Cl] H$_2$bbppen =	34 (1 kOe)	8×10^{-8}	-	-	-	165.83	2.187 (L_{ax}) 2.584 (L_{eq})	-	[166]
28	[Zn$_2$Dy(TTT^{Br})$_2$(MeOH)]·NO$_3$ ·3MeOH·H$_2$O TTT^{Br} =	439	-	424	Yes (0.02)	11*	168.6	2.208 (L_{ax}) 2.393 (L_{eq})	0.660	[171]
29	[Zn$_2$Dy(TTT^{Cl})$_2$L]·X·Solv TTT^{Cl} =	507 - 632	1.0×10^{-11} to 5.2×10^{-11}	-	Yes (0.02)	7.9 to 14.0	169.65 to 177.98	2.179 to 2.202 (L_{ax}) 3.370 to 3.396 (L_{eq})		[172]
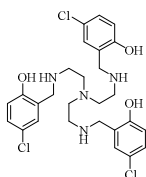
L = acetone, MeOH, DMF,
N-methylpyrrolidone
X = NO$_3^-$, CF$_3$SO$_3^-$, BPh$_4^-$

30	Dy(L^3)Cl$_3$·4H$_2$O	24	6.4x10^{-6}	-	-	-	No crystal structure	No crystal structure	-	[180]
31	[Dy(L^{N5})(Ph$_3$SiO)$_2$]·BPh$_4$·CH$_2$Cl$_2$ L^{N5} =	1108	1.56x10^{-11}	1040	Yes (0.01)	5 (14*)	174.83	2.153 (L$_{ax}$) 2.502 (L$_{eq}$)	1.487	[164]
32	[DyL(MeOH)Cl]$_2$ LH$_2$ =	88	2.65x10^{-7}	-	Yes (0.05)	5*	168.43	2.366/2.627 (L$_{ax}$) 2.520 (L$_{eq}$)	-	[181]
33	[Dy(LH$_3$)Cl$_2$]$_2$·2Et$_2$O (diluted at 10% in Y) LH$_4$ =	54	2x10^{-12}	344	-	-	169.78	2.618 (L$_{ax}$) 2.358 (L$_{eq}$)	0.479	[182]
34	[DyCl$_3$(HL^1)]·CH$_3$OH	52 (0.7 kOe)	1.12x10^{-10}	50	-	-	165.57	2.624 (L$_{ax}$) 2.459 (L$_{eq}$)	1.187	[183]
35	[Dy$_2$Cl$_4$(L^1)(MeOH)$_2$]·4C$_5$H$_5$N HL^1 =	120 (0.9 kOe)	8.62x10^{-10}	191	-	-	165.84	2.614 (L$_{ax}$) 2.390 (L$_{eq}$)	1.179	[183]

36	[Dy$_2$Cl$_4$(L^2)$_2$]·2CH$_3$CN HL^2 =	146 (0.9 kOe)	9.92x10^{-11}	204	-	-	163.30	2.600 (L$_{ax}$) 2.362 (L$_{eq}$)	1.088	[183]
37	[DyCu$_5$(quinha)$_5$(sal)$_2$(py)$_5$][CF$_3$SO$_3$]·py·4H$_2$O	899	2.0x10^{-11}	-	Yes (0.02)	12*	177.3	2.20 (L$_{ax}$) 2.41 (L$_{eq}$)	0.244	[165]
38	[Dy$_2$Cu$_{10}$(quinha)$_{10}$(sal)$_2$(OH)(py)$_9$][CF$_3$SO$_3$]$_3$ ·xpy· yCH$_3$OH·zH$_2$O quinha =	837	2.0x10^{-11}	-	Yes (0.02)	6*	172.5	2.17 (L$_{ax}$) 2.41 (L$_{eq}$)	0.394 and 0.531	
39	[Dy(Bpen)Cl$_3$]	22 (0.8 kOe)	3.72x10^{-6}	53	-	-	168.5	2.635/2.595 (L$_{ax}$) 2.509/2.611 (L$_{eq}$)	1.271	[173]
40	[Dy(Bpen)Cl(OPhCl$_2$NO$_2$)$_2$]	86 (0.8 kOe)	4.65x10^{-7}	442	-	-	165.6	2.174 (L$_{ax}$) 2.523/2.616 (L$_{eq}$)	1.904	
34 41	[Dy(Bpen)(OPhCl$_2$NO$_2$)$_3$]	34 (0.8 kOe)	2.40x10^{-6}	314	-	-	166.1	2.187/2.201 (L$_{ax}$) 2.203/2.503 (L$_{eq}$)	1.780	
42	[Dy(Bpen)(OPhNO$_2$)$_3$] H$_2$Bpen =	27 (0.8 kOe)	1.12x10^{-6}	336	-	-	164.5	2.193 (L$_{ax}$) 2.156 / 2.526 (L$_{eq}$)	1.355	

43	[Dy(Hbpen)Cl$_3$]	63 (1.6 kOe)	6.78×10^{-8}	71	-	-	170.4	2.622 (L$_{ax}$) 2.532/2.624 (L$_{eq}$)	0.828	[174]
44	[Dy(Hbpen)Cl(OPhCl$_2$NO$_2$)$_2$]	182 254 (1.2 kOe)	6.25×10^{-7} 4.76×10^{-8}	422	Yes (0.02)	3*	166.06	2.175 (L$_{ax}$) 2.534/2.620 (L$_{eq}$)	2.086	
45	[Dy(Hbpen)(OPhCl$_2$NO$_2$)$_3$] Hbpen =	21 (1.2 kOe)*	-	308	-	-	167.87	2.202 (L$_{ax}$) 2.517 (L$_{eq}$)	1.004	

46	[Dy(Mbpen)Cl$_3$] Mbpen =	37 (0.8 kOe)	9.47×10^{-7}	45	-	-	171.06	2.607 (L$_{ax}$) 2.572 (L$_{eq}$)	0.795	[174]

47	[Dy(H$_3$NAP)$_2$(H$_2$O)Cl$_2$]Cl·EtOH H$_3$NAP =	154 (1 kOe)	2.5×10^{-8} s	-	-	-	179.13	2.665 (L$_{ax}$) 2.319 (L$_{eq}$)	-	[184]

(a) U$_{eff}$/k$_B$ is reported for H_{DC} = 0 Oe unless mentioned; (b) T_B is the temperature of the maximum of the zero field cooled (ZFC) susceptibility unless marked *, which corresponds to the highest temperature, T_H, with magnetic hysteresis cycle; (c) deviation parameter obtained by the Continuous Shape Measures (CShM) method compared to the ideal D_{5h} symmetry configuration.

Table 11. PBP Ln SMMs involving polydentate ligands with a selection of relevant magnetic (SMM characteristics) and structural information.

II.3 PBP Ln complexes as building units

The use of Ln complexes as building units to achieve polynuclear nanomagnets taking advantage of the large axial magnetic anisotropy of the PBP Ln centers starts to be explored. For instance, trinuclear compounds $[\{Dy(bbpen)\}_2\{M(CN)_6\}]^-$ (M = Fe[III], Co[III])[167] (Figure 18) were formed by assembling of $[Dy(bbpen)]^+$ and either $[Fe(CN)_6]^{3-}$ or $[Co(CN)_6]^{3-}$, and the linkage takes place in the equatorial plane of the PBP coordination sphere of Dy. These complexes behave as SMMs characterized, for the Co derivative, by energy barriers for magnetization reversal as high as 955 K and a blocking temperature of 15 K (Table 11, entries 16 and 17). These values well compare with that of the mononuclear $[Dy(bbpen)X]$ complexes (Table 11, entries 14 and 15), whereas for Fe[III] derivative, the presence of exchange interactions was found to induce a faster relaxation of the magnetization.
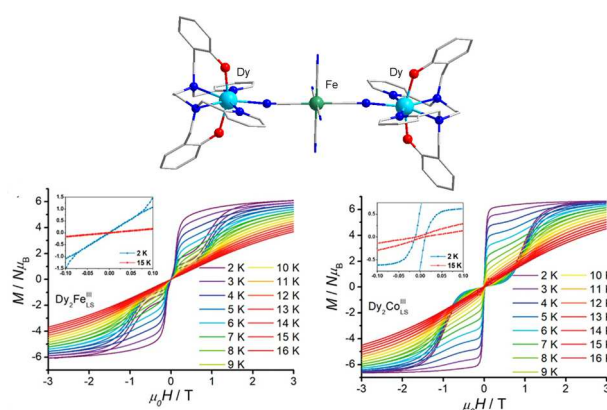

Figure 18. $[\{Dy(bbpen)\}_2\{M(CN)_6\}]\cdot PPh_4$: Molecular structure and magnetic hysteresis loops at various temperatures for the complexes with M = Fe[III] (left) and Co[III] (right). (Adapted with permission from ref.[167], copyright 2022 American Chemical Society)

$[Dy_2Cu_{10}(quinha)_{10}(sal)_2(OH)(py)_9]\cdot 3CF_3SO_3$ has been obtain by assembling two Dy[15-MC$_{Cu}$-5] metallacrowns by an hydroxyl group (Figure 19, Table 11 entry 38).[165] Each Dy[III] is located in the cavity of a metallocrown of five Cu[II] centers and exhibits a PBP coordination sphere where the bridging hydroxyl group occupies an apical position. This double-decker arrangement leads the anisotropy axes of the two Dy centers to be almost collinear, and to a ferromagnetic Dy-Dy interaction. This 3d-4f SMM is characterized by a U_{eff}/k_B = 837 K, and a magnetic hysteresis up to 6 K.
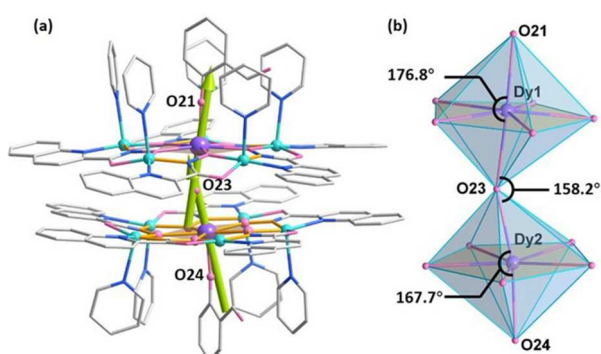
Figure 19: $[Dy_2Cu_{10}(quinha)_{10}(sal)_2(OH)(py)_9]\cdot 3CF_3SO_3$: a) molecular structure of the double-decker $[Dy\{15\text{-}MC_{Cu}\text{-}5\}]_2$ metallacrown complex. Yellow drawing shows the $[15\text{-}MC_{Cu}\text{-}5]$ metallacrown. The green arrows represent the orientations of the anisotropy axes for each of the Dy[III] ions as calculated by the MAGELLAN program. b) Coordination environment of the Dy[III] ions. H atoms are

omitted for clarity. Color codes: Dy lavender; Cu aqua; N light blue; O rose; C light grey. (Reproduced from ref.[165] with permission from John Wiley and Sons, copyright 2021)

III.   Final comments and outlook

This overview of the magnetic anisotropies associated to a pentagonal bipyramidal coordination sphere for transition metal and lanthanide ions permits to highlight some general trends that can guide the chemist for the design of a compound with determined properties.

For the transition metal ions, the magnetic anisotropy arising from zero-field splitting is directly related to the d^n electronic configuration. For this reason, it can be rationally imparted to a coordination complex. Complexes characterized by a D of a few cm^{-1} are accessible with V^{III} ($D > 0$) or Cr^{III} ($D < 0$) while larger anisotropies result from the use of Co^{II} ($D > 0$), Fe or Ni ($D < 0$). The ZFS parameters D and E are directly related to the effective energy diagram for the d orbitals of the considered metal ion, therefore adjusting the symmetry of PBP coordination sphere and possibly the ligand field in the axial and equatorial positions of the complex permits achieving larger anisotropies. For 3d ions, values up to -30 cm^{-1} (for Ni^{II}) and +40 cm^{-1} (for Co^{II}) of the axial ZFS parameter D are readily available by chemical design. The move to 4d and 5d metal ions leads to even larger anisotropies. Little information is currently available on these heavier ions, but they are very promising and could bridge the gap between the magnetic anisotropy exhibited by 3d ions and that of Ln ions in PBP geometry, thus opening new perspectives for efficient transition metal-based nanomagnets.

For rare-earth ions, the pentagonal bipyramidal geometry is especially interesting because its axial symmetry allows control of both the axial and equatorial components of the ligand field. The balance between axial and equatorial ligand field plays a key role in the anisotropy, and thus in the SMM characteristics of the complexes. To achieve largest magnetic anisotropy, it must be adapted to the spatial distribution of the 4f electron density of the ground m_J state of the considered Ln ion. This is well illustrated by the PBP Dy^{III} complexes for which optimization of the strong axial field ligands and weak field equatorial ligands has already yielded among the best SMMs after the Dy-metallocene derivatives.[185, 186] A large choice of ligands, monodentate or polydentate, enables to constrain a coordination polyhedron close to the ideal pentagonal bipyramidal geometry and allows fine control of the ligand field in the axial and equatorial positions.

The influence of the second coordination sphere, the H-bonds networks, etc. should not be neglected when optimizing the SMM behavior of Ln derivatives and this may apply too for transition metal complexes. Rigorous work combining a close correlation between the structures of the complexes, their magnetic properties and theoretical calculations has clearly demonstrated the significant effects of the second coordination sphere on the ligand field acting on the metal ion, and consequently on the SMM behavior. These effects should not be seen as necessarily negative, the second coordination sphere may be an additional way of engineering the ligand field acting on the Ln ion.

In addition to the flexibility of their chemical design, it is quite remarkable that complexes with PBP coordination geometry are generally stable and structurally robust. This allows involving these complexes as building units with controlled magnetic anisotropy in the assembly of polynuclear materials. This is particularly interesting for the design of materials where magnetic anisotropy plays

an important role in the intended magnetic behavior. There is no doubt that the involvement of PBP complexes in the construction of polynuclear magnetic systems represents an axis of development for these complexes in the near future.

Appendix 1: A geometrical parameter to ascertain the degree of protonation of the hydrazide units in $(H_{2-x}L1^R)^{x-}$ ligand (x = 0, 1 or 2)

The 2,6-diacetylpyridine-bis(R-acylhydrazone) ligand can be involved in coordination to a metal ion in its neutral form, H_2L1^R, or as mono-, $(HL1^R)^-$, or doubly-deprotonated, $(L1^R)^{2-}$ species. Due to the possible ambiguity in determining with certainty the degree of protonation of the ligand in coordination complexes by a structural study by X-ray diffraction, we have conducted a statistical study on the geometrical characteristics (distances and angles) of the ligand for the structures available in the CCDC data base. It appeared that the most selective geometrical criterion was the value of the N_a-N_b-C_b angle (Figure 20) because it seems to depend little on the multiple factors that are the nature of the metal, the temperature of the measurement, the quality of the refinement. Thus, for transition metal complexes about 98% of the 136 structures with a hydrogen on each of the hydrazide groups (x = 0) present N_a-N_b-C_b angles higher than 110°, with an average of about 114.5°. If we take into account only the structures with an angle >110°, the lower quartile is 113.8, the upper quartile is 115.2°, for a maximum value of 119.9°. Of the 52 structures assumed to have a fully deprotonated ligand (x = 2), 89% have a N_a-N_b-C_b angle < 110°, with an average value of 109.1°. For the remaining 11% values range up to 117°. Finally, of the 9 structures deposited with a partially deprotonated ligand (x = 1), eight show N_a-N_b-C_b angles greater than 110° for the H-bearing hydrazide and values less than 110° for the deprotonated moiety. For instance, in $[Cr(HL1^{Ph})(NCS)_2]$ (Figure 20) these angles are respectively 113.0(1)° and 108.2(1)°.[22]

From this statistical study, it appears that the threshold of 110° for the value of the N_a-N_b-C_b angle seems to be relevant to determine the protonated (> 110°) or deprotonated (< 110°) form of the hydrazide moieties of this ligand.

	M = TM	M = Ln^{III}
NH$_1$	> 110°	> 111°
NH$_0$	< 110°	< 111°
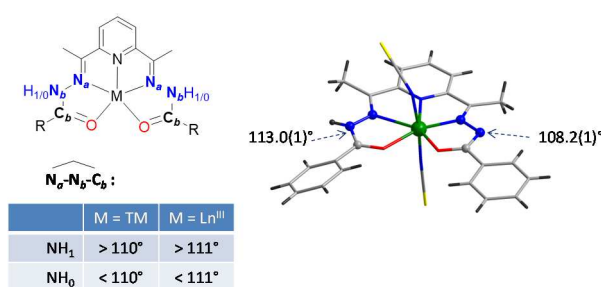
Figure 20. Selective geometrical criterion allowing to discriminate neutral versus deprotonated hydrazide moieties in $(H_{2-x}L1^R)^{x-}$ ligands; *(right)* example for mono-deprotonated ligand in complex $[Cr(HL1^{Ph})(NCS)_2]$.[22]

A very similar situation applies for the Ln^{III} complexes. Examination of 102 structures spanning over the whole 4f series lead to an average N_a-N_b-C_b angle of about 115.5° when each of the hydrazide groups carries a hydrogen (x = 0) and of 109.1° when the hydrazide is deprotonated (x = 1 or 2). No obvious differences were found along the Ln series, indicating no effect due to the size of the metal

ion. The threshold, 111°, relevant to determine the protonated (> 111°) or deprotonated (< 111°) form of the ligand is hardly different to that found for the transition metal derivatives.

REFERENCES

1. A. K. Bar, C. Pichon and J.-P. Sutter, Magnetic anisotropy in two- to eight-coordinated transition–metal complexes: Recent developments in molecular magnetism, *Coord. Chem. Rev.*, 2016, **308**, 346-380.
2. S. Gómez-Coca, D. Aravena, R. Morales and E. Ruiz, Large magnetic anisotropy in mononuclear metal complexes, *Coord. Chem. Rev.*, 2015, **289–290**, 379-392.
3. D. Wester and G. J. Palenik, Synthesis and characterization of novel pentagonal bipyramidal complexes of iron(II), cobalt(II), and zinc(II), *J. Am. Chem. Soc.*, 1973, **95**, 6505-6506.
4. M. G. Drew, H. Bin Othman, W. Hill, P. McIlroy and S. M. Nelson, Seven-coordinate complexes of iron(II) with pentadentate macrocyclic ligands, *Inorg. Chim. Acta*, 1975, **12**, L25-L26.
5. M. M. Bishop, J. Lewis, T. D. O'Donoghue, P. R. Raithby and J. N. Ramsden, X-Ray crystal structure of a planar, high-spin iron(II) complex of a pentadentate unsaturated macrocycle formed by reaction of 2,9-di(1-methylhydrazino)1,10-phenanthroline monohydrochloride with 2,6-diacetylpyridine, *Chem. Comm.*, 1978, 828-829.
6. I. Ivanovic-Burmazovic and K. Andjelkovic, in *Advances in Inorganic Chemistry*, ed. R. van Eldk, Elsevier, 2004, vol. 55, p. 315–360.
7. L. D. Popov, A. N. Morozov, I. N. Shcherbakov, Y. P. Tupolova, V. V. Lukov and V. A. Kogan, Metal complexes with polyfunctional ligands based of bis(hydrazones) of dicarbonyl compounds, *Russ. Chem. Rev.*, 2009, **78**, 643-658.
8. R. Bhula, P. Osvath and D. C. Weatherburn, Complexes of tridentate and pentadentate macrocyclic ligands, *Coord. Chem. Rev.*, 1988, **91**, 89-213.
9. E. L. Gavey and M. Pilkington, Coordination complexes of 15-membered pentadentate aza, oxoaza and thiaaza Schiff base macrocycles "Old Complexes Offer New Attractions", *Coord. Chem. Rev.*, 2015, **296**, 125-152.
10. R. Ruamps, L. J. Batchelor, R. Maurice, N. Gogoi, P. Jiménez-Lozano, N. Guihéry, C. de Graaf, A.-L. Barra, J.-P. Sutter and T. Mallah, Origin of the Magnetic Anisotropy in Ni(II) and Co(II) Heptacoordinate Complexes, *Chem. Eur. J.*, 2013, **19**, 950-957.
11. A. Sarkar, S. Dey and G. Rajaraman, Role of Coordination Number and Geometry in Controlling the Magnetic Anisotropy in Fe[II], Co[II], and Ni[II] Single-Ion Magnets, *Chem. Eur. J.*, 2020, **26**, 14036-14058.
12. **Note**: The magnetic quantum numbers for the d orbitals is $m_l = 0$ for d_z, $m_l = 1$ for d_{xz} and d_{yz}, and $m_l = 2$ for d_{xy} and d_{x2-y2}.
13. A. K. Bar, N. Gogoi, C. Pichon, V. M. L. D. P. Goli, M. Thlijeni, C. Duhayon, N. Suaud, N. Guihéry, A.-L. Barra, S. Ramasesha and J.-P. Sutter, Pentagonal Bipyramid FeII Complexes: Robust Ising-Spin Units towards Heteropolynuclear Nanomagnets, *Chem. Eur. J.*, 2017, **23**, 4380-4396.
14. M. S. Shongwe, H. N. R. Al-Kharousi, H. Adams, M. J. Morris and E. Bill, Unprecedented [V2O]6+ Core of a Centrosymmetric Thiosemicarbazonato Dimer: Spontaneous Deoxygenation of Oxovanadium(IV), *Inorg. Chem.*, 2006, **45**, 1103-1107.
15. R. L. R. Towns and R. A. Levenson, Structure of the seven-coordinate cyano complex of vanadium(III), *J. Am. Chem. Soc.*, 1972, **94**, 4345-4346.
16. R. A. Levenson and R. L. R. Towns, Crystal and molecular structure of potassium heptocyanovanadate(III) dihydrate, *Inorg. Chem.*, 1974, **13**, 105-109.
17. T. A. Bazhenova, L. Zorina, S. Simonov, V. S. Mironov, O. Maximova, L. Spillecke, C. Koo, R. Klingeler, Y. Manakin, A. N. Vasiliev and E. B. Yagubskii, The first pentagonal-bipyramidal vanadium (III) complexes with a Schiff-base N3O2 pentadentate ligand: synthesis, structure and magnetic properties, *Dalton Trans.*, 2020, **49**, 15287-15298
18. Y. Chen, X. Liu, J. Zhou, H.-h. Zou and B. Xiang, One-Dimensional Vanadium(III) Chalcogenidostannates Incorporating [V(tepa)]³⁺ Complexes as Bridging Groups, *Inorg. Chem.*, 2021, **60**, 2127-2132.
19. V. S. Mironov, T. A. Bazhenova, Y. V. Manakin, K. A. Lyssenko, A. D. Talantsev and E. B. Yagubskii, A new Mo(iv) complex with the pentadentate (N3O2) Schiff-base ligand: the first

non-cyanide pentagonal-bipyramidal paramagnetic 4d complex, *Dalton Trans.*, 2017, **46**, 14083-14087.

20. F. J. Birk, D. Pinkowicz and K. R. Dunbar, The Heptacyanotungstate(IV) Anion: A New 5 d Transition-Metal Member of the Rare Heptacyanometallate Family of Anions, *Angew. Chem. Int. Ed.*, 2016, **55**, 11368-11371.

21. T. A. Bazhenova, L. V. Zorina, S. V. Simonov, Y. V. Manakin, A. B. Kornev, K. A. Lyssenko, V. S. Mironov, I. F. Gilmutdinov and E. B. Yagubskii, A novel family of hepta-coordinated Cr(III) complexes with a planar pentadentate N3O2 Schiff base ligand: synthesis, structure and magnetism, *Inorg. Chim. Acta*, 2021, **522**, 120358.

22. C. Pichon, B. Elrez, V. Béreau, C. Duhayon and J.-P. Sutter, From Heptacoordinated CrIII Complexes with Cyanide or Isothiocyanate Apical Groups to 1D Heterometallic Assemblages with All-Pentagonal-Bipyramid Coordination Geometries, *Eur. J. Inorg. Chem.*, 2018, **2018**, 340-348.

23. C. Pichon, N. Suaud, C. Duhayon, N. Guihéry and J.-P. Sutter, Cyano-Bridged Fe(II)–Cr(III) Single-Chain Magnet Based on Pentagonal Bipyramid Units: On the Added Value of Aligned Axial Anisotropy, *J. Am. Chem. Soc.*, 2018, **140**, 7698-7704.

24. C. Pichon, N. Suaud, V. Jubault, C. Duhayon, N. Guihéry and J.-P. Sutter, Trinuclear Cyanido-Bridged [Cr2Fe] Complexes: To Be or not to Be a Single-Molecule Magnet, a Matter of Straightness, *Chem. Eur. J.*, 2021, **27**, 15484-15495.

25. Y. V. Manakin, V. S. Mironov, T. A. Bazhenova, K. A. Lyssenko, I. F. Gilmutdinov, K. S. Bikbaev, A. A. Masitov and E. B. Yagubskii, (Et$_4$N)[Mo^{III}(DAPBH)Cl$_2$], the first pentagonal-bipyramidal Mo(iii) complex with a N3O2-type Schiff-base ligand: manifestation of unquenched orbital momentum and Ising-type magnetic anisotropy, *Chem. Comm.*, 2018, **54**, 10084-10087.

26. M. B. Hursthouse, K. M. A. Maijk, A. M. Soares, J. F. Gibson and W. P. Griffith, The X-ray crystal structure of NaK$_3$[Mo(CN)$_7$],2H$_2$O and the structure of its anion in aqueous solution., *Inorg. Chim. Acta*, 1980, **45**, L81-82.

27. M. V. Bennet and J. R. Long, New cyanometalate building units: Synthesis and characterization of [Re(CN)$_7$]$^{3-}$ and [Re(CN)$_8$]$^{3-}$, *J. Am. Chem. Soc.*, 2003, **125**, 2394-2395.

28. J. David, F. Mendizabal and R. Arratia-Pérez, Electronic Structure and Molecular Properties of the Heptacyanorhenate [Re(CN)$_7$]$^{3-}$ and [Re(CN)7]4- Complexes, *J Phys Chem A*, 2006, **110**, 1072-1077.

29. H. I. Karunadasa and J. R. Long, Synthesis and Redox-Induced Structural Isomerization of the Pentagonal Bipyramidal Complexes [W(CN)$_5$(CO)$_2$]$^{3-}$ and [W(CN)$_5$(CO)$_2$]$^{2-}$, *Angew. Chem. Int. Ed.*, 2009, **48**, 738-741.

30. V. S. Mironov, New Approaches to the Problem of High-Temperature Single-Molecule Magnets, *Dokl. Phys. Chem.*, 2006, **408**, 130-136.

31. V. S. Mironov, Origin of Dissimilar Single-Molecule Magnet Behavior of Three Mn$^{II}_2$Mo^{III} Complexes Based on [Mo^{III}(CN)$_7$]$^{4-}$ Heptacyanomolybdate: Interplay of Mo^{III}–CN–Mn^{II} Anisotropic Exchange Interactions, *Inorg. Chem.*, 2015, **54**, 11339-11355.

32. V. S. Mironov, L. F. Chibotaru and A. Ceulemans, Mechanism of a Strongly Anisotropic Mo^{III}-CN-Mn^{II} Spin-Spin Coupling in Molecular Magnets Based on the [Mo(CN)$_7$]$^{4-}$ Heptacyanometalate: A New Strategy for Single-Molecule Magnets with High Blocking Temperatures, *J. Am. Chem. Soc.*, 2003, **125**, 9750-9760.

33. K. Bretosh, V. Béreau, C. Duhayon, C. Pichon and J.-P. Sutter, A ferromagnetic Ni(II)–Cr(III) single-chain magnet based on pentagonal bipyramidal building units, *Inorg. Chem. Front.*, 2020, **7**, 1503-1511.

34. J. Milon, M.-C. Daniel, A. Kaiba, P. Guionneau, S. Brandès and J.-P. Sutter, Nanoporous magnets of chiral and racemic [{Mn(HL)}$_2$Mn{Mo(CN)$_7$}$_2$] with switchable ordering temperatures (T_C = 85 K ↔ 106 K) driven by H$_2$O sorption (L = N,N-dimethylalaninol), *J. Am. Chem. Soc.*, 2007, **129**, 13872-13878.

35.   S. Tanase, F. Tuna, P. Guionneau, T. Maris, G. Rombaut, C. Mathonière, M. Andruh, O. Kahn and J.-P. Sutter, Substantial increase of the ordering temperature for [Mn(II)/Mo(CN)$_7$]-based magnets as a function of the 3d ion site geometry: Example of two supramolecular materials with T_c = 75 and 106 K., *Inorg. Chem.*, 2003, **42**, 1625-1631.

36.   K. Tomono, Y. Tsunobuchi, K. Nakabayashi and S.-i. Ohkoshi, Vanadium(II) Heptacyanomolybdate(III)-Based Magnet Exhibiting a High Curie Temperature of 110 K, *Inorg. Chem.*, 2010, **49**, 1298-1300.

37.   L. F. Chibotaru, M. F. A. Hendrickx, S. Clima, J. Larionova and A. Ceulemans, Magnetic Anisotropy of [Mo(CN)$_7$]$^{4-}$ Anions and Fragments of Cyano-Bridged Magnetic Networks, *J. Phys. Chem. A*, 2005, 7251-7257.

38.   M. Magott, K. R. Dunbar and D. Pinkowicz, Correlating magnetic anisotropy with [Mo(CN)$_7$]$^{4-}$ geometry of Mn^{II}–Mo^{III} magnetic frameworks, *Dalton Trans.*, 2019, **48**, 15493-15500.

39.   X.-Y. Wang, A. V. Prosvirin and K. R. Dunbar, A Docosanuclear {Mo$_8$Mn$_{14}$} Cluster Based on [Mo(CN)$_7$]$^{4-}$, *Angew. Chem. Int. Ed.*, 2010, **49**, 5081-5084.

40.   K. Qian, X.-C. Huang, C. Zhou, X.-Z. You, X.-Y. Wang and K. R. Dunbar, A Single-Molecule Magnet Based on Heptacyanomolybdate with the Highest Energy Barrier for a Cyanide Compound, *J. Am. Chem. Soc.*, 2013, **135**, 13302-13305.

41.   D.-Q. Wu, D. Shao, X.-Q. Wei, F.-X. Shen, L. Shi, D. Kempe, Y.-Z. Zhang, K. R. Dunbar and X.-Y. Wang, Reversible On–Off Switching of a Single-Molecule Magnet via a Crystal-to-Crystal Chemical Transformation, *J. Am. Chem. Soc.*, 2017, **139**, 11714-11717.

42.   L. Shi, D. Shao, X.-Q. Wei, K. R. Dunbar and X.-Y. Wang, Enhanced Single-Chain Magnet Behavior via Anisotropic Exchange in a Cyano-Bridged Mo^{III}–Mn^{II} Chain, *Angew. Chem. Int. Ed.*, 2020, **59**, 10379-10384.

43.   D. E. Freedman, D. M. Jenkins, A. T. Iavarone and J. R. Long, A Redox-Switchable Single-Molecule Magnet Incorporating [Re(CN)$_7$]$^{3-}$, *J. Am. Chem. Soc.*, 2008, **130**, 2884-2885.

44.   J. M. Zadrozny, D. E. Freedman, D. M. Jenkins, T. D. Harris, A. T. Iavarone, C. Mathonière, R. Clérac and J. R. Long, Slow Magnetic Relaxation and Charge-Transfer in Cyano-Bridged Coordination Clusters Incorporating [Re(CN)$_7$]$^{3-/4-}$, *Inorg. Chem.*, 2010, **49**, 8886-8896.

45.   G. J. Palenik, D. W. Wester, U. Rychlewska and R. C. Palenik, Pentagonal-Bipyramidal Complexes. Synthesis and Crystal Structures of Diaqua [2,6-diacetylpyridine bis(semicarbazone)] chromium(III) Hydroxide Dinitrate Hydrate and Dichloro [2,6-diacetylpyridine bis(semicarbazone)] iron(III) Chloride Dihydrate, *Inorg. Chem.*, 1976, **15**, 1814-1819.

46.   A. Bino, R. Frim and M. Van Genderen, Three coordination modes of the pentadentate ligand 2,6-diacetylpyridinedisemicarbazone, *Inorg. Chim. Acta*, 1987, **127**, 95-101.

47.   L. Y. Chung, E. C. Constable, M. S. Khan, J. Lewis, P. R. Raithby and M. D. Vargas, Structural characterisation of a pentagonal bipyramidal macrocyclic chromium(III) complex; an explanation of a chromium-mediated 'transient-template' effect, *Chem. Comm.*, 1984, 1425-1426.

48.   J. C. Dabrowiak, L. A. Nafie, P. S. Bryan and A. T. Torkelson, Accessibility of Manganese oxidation states. Control by pentaaza macrocyclic ligands, *Inorg. Chem.*, 1977, **16**, 540-544.

49.   M. L. Cofield and P. S. Bryan, Low-temperature magnetic susceptibility and zero-field splitting in some high-spin manganese(III) compounds, *Inorg. Chim. Acta*, 1986, **112**, 1-4.

50.   **Note**. Unpublished observations.

51.   O. Jiménez-Sandoval, D. Ramirez-Rosales, M. J. Rosales-Hoz, M. E. Sosa-Torres and R. Zamorano-Ulloa, Magnetostructural behavior of the complex [MnL(H$_2$O)$_2$]Cl$_2$, 4H$_2$O at variable temperature studied bu electron spin resonance (L = 2,13-dimethyl-3,6,9,12,18-pentaazabicyclo[12.3.1]octadeca-1(18),2,12,14,16-pentaene), *J. Chem. Soc., Dalton Trans.*, 1998, 1551-1556.

52.   B. Drahoš, I. Císařová, O. Laguta, V. T. Santana, P. Neugebauer and R. Herchel, Structural, magnetic, redox and theoretical characterization of seven-coordinate first-row transition

metal complexes with a macrocyclic ligand containing two benzimidazolyl N-pendant arms, *Dalton Trans.*, 2020, **49**, 4425-4440.

53. B. Drahoš, R. Herchel and Z. Trávníček, Structural, Magnetic, and Redox Diversity of First-Row Transition Metal Complexes of a Pyridine-Based Macrocycle: Well-Marked Trends Supported by Theoretical DFT Calculations, *Inorg. Chem.*, 2015, **54**, 3352-3369.

54. B. Drahos, R. Herchel and Z. Travnicek, Structural and magnetic properties of heptacoordinated MnII complexes containing a 15-membered pyridine-based macrocycle and halido/pseudohalido axial coligands, *RSC Advances*, 2016, **6**, 34674-34684.

55. M. V. Capparelli, P. De Meester, D. M. L. Goodgame, S. J. Gunn and A. C. Skapski, X-ray molecular structures of pentagonal bipyramidal M(DAPSC)(NCS)$_2$, M = Mn or Ni, and EPR spectra of seven-coordinate Mn(II) in these compounds, *Inorg. Chim. Acta*, 1985, **97**, L37-L39.

56. S. Naskar, D. Mishra, S. Kumar Chattopadhyay, M. Corbella and A. J. Blake, Versatility of 2,6-diacetylpyridine (dap) hydrazones in stabilizing uncommon coordination geometries of Mn(II): synthesis, spectroscopic, magnetic and structural characterization, *Dalton Trans.*, 2005, 2428-2435.

57. H. Lou, L. Yin, B. Zhang, Z.-W. Ouyang, B. Li and Z. Wang, Series of Single-Ion and 1D Chain Complexes Based on Quinolinic Derivative: Synthesis, Crystal Structures, HF-EPR, and Magnetic Properties, *Inorg. Chem.*, 2018, **57**, 7757-7762.

58. S. A. Cotton, EPR spectra of seven coordinate iron(III) complexes, *Chem. Phys. Lett.*, 1976, **41**, 606-608.

59. E. Fleischer and S. Hawkinson, The structure of two seven-coordinate complexes of iron(III), *J. Am. Chem. Soc.*, 1967, **89**, 720-721.

60. S. M. Nelson and D. H. Busch, Seven-Coordination in Some Mononuclear and Binuclear Iron(III) Complexes Containing a Pentadentate Macrocyclic Ring, *Inorg. Chem.*, 1969, **8**, 1859-1863.

61. D. Darmanović, I. N. Shcherbakov, C. Duboc, V. Spasojević, D. Hanžel, K. Anđelković, D. Radanović, I. Turel, M. Milenković, M. Gruden, B. Čobeljić and M. Zlatar, Combined Experimental and Theoretical Investigation of the Origin of Magnetic Anisotropy in Pentagonal Bipyramidal Isothiocyanato Co(II), Ni(II), and Fe(III) Complexes with Quaternary-Ammonium-Functionalized 2,6-Diacetylpyridine Bisacylhydrazone, *J. Phys. Chem. C*, 2019, **123**, 31142-31155.

62. E. C. Constable, M. S. Khan, J. Lewis, M. C. Liptrot and P. R. Raithby, Iron complexes of derivatised pentadentate macrocyclic ligands; the crystal and molecular structure of dichloro(6,13-(bis-2-hydroxyethyl)-6H, 13H-tripyrido[cd,fg,lm] [1,2,4,7,9,10,13] heptaaza-pent adecine)iron (III) chloride, *Inorg. Chim. Acta*, 1991, **181**, 207-212.

63. G. A. Craig, L. A. Barrios, J. S. Costa, O. Roubeau, E. Ruiz, S. J. Teat, C. C. Wilson, L. Thomas and G. Aromi, Synthesis of a novel heptacoordinated Fe(III) dinuclear complex: experimental and theoretical study of the magnetic properties, *Dalton Trans.*, 2010, **39**, 4874.

64. F. A. Deeney and S. M. Nelson, Relaxation effects in the mössbauer spectra of some seven-coordinate iron(III) complexes, *J. Phys. Chem. Sol.*, 1973, **34**, 277-282.

65. A. N. Scoville and W. M. Reiff, A low temperature magnetic suceptibility study of the zero field splitting in seven coordinate high-spin iron(III) complexes based on a pentadentate macrocyclic nitrogen ligand, *Inorg. Chim. Acta*, 1983, **70**, 127-131.

66. T. S. Venkatakrishnan, C. Duhayon, N. Gogoi and J. P. Sutter, Self-assembly of a Fe^{III}(L) complex with octacyano metallate [M$_{IV}$(CN)$_8$]$^{4-}$ (L = pentadentate macrocyclic ligand, M = Mo, W) : Crystal structure and magnetic properties, *Inorg. Chim. Acta*, 2011, **372**, 403-406.

67. T. S. Venkatakrishnan, S. Sahoo, N. Bréfuel, C. Duhayon, C. Paulsen, A.-L. Barra, S. Ramasesha and J.-P. Sutter, Enhanced Ion Anisotropy by Nonconventional Coordination Geometry: Single-Chain Magnet Behavior for a [{Fe^{II}L}$_2${Nb^{IV}(CN)$_8$}] Helical Chain Compound Designed with Heptacoordinate Fe^{II}, *J. Am. Chem. Soc.*, 2010, **132**, 6047-6056.

68. Y.-F. Deng, B. Yao, P.-Z. Zhan, D. Gan, Y.-Z. Zhang and K. R. Dunbar, Synthesis and magnetic studies of pentagonal bipyramidal metal complexes of Fe, Co and Ni, *Dalton Trans.*, 2019, **48**, 3243-3248.

69. A. Mondal, S.-Q. Wu, O. Sato and S. Konar, Effect of Axial Ligands on Easy-Axis Anisotropy and Field-Induced Slow Magnetic Relaxation in Heptacoordinated FeII Complexes, *Chem. Eur. J.*, 2020, **26**, 4780-4789.

70. A. K. Bar, C. Pichon, N. Gogoi, C. Duhayon, S. Ramasesha and J.-P. Sutter, Single-ion magnet behaviour of heptacoordinated Fe(II) complexes: on the importance of supramolecular organization, *Chem. Comm.*, 2015, **51**, 3616-3619.

71. T. D. Harris, H. S. Soo, C. J. Chang and J. R. Long, A cyano-bridged $Fe^{II}Re^{IV}(CN)_2$ cluster incorporating two high-magnetic anisotropy building units, *Inorg. Chim. Acta*, 2011, **369**, 91-96.

72. A. Mondal, A. K. Kharwar, P. K. Sahu and S. Konar, Alignment of Axial Anisotropy in a 1D Coordination Polymer shows Improved Field Induced Single Molecule Magnet Behavior over a Mononuclear Seven Coordinated Fe^{II} Complex, *Chem. As. J.*, 2020, **15**, 2681-2688.

73. D. Shao, X.-H. Zhao, S.-L. Zhang, D.-Q. Wu, X.-Q. Wei and X.-Y. Wang, Structural and magnetic tuning from a field-induced single-ion magnet to a single-chain magnet by anions, *Inorg. Chem. Front.*, 2015, **2**, 846-853.

74. P. Antal, B. Drahoš, R. Herchel and Z. Trávníček, Late First-Row Transition-Metal Complexes Containing a 2-Pyridylmethyl Pendant-Armed 15-Membered Macrocyclic Ligand. Field-Induced Slow Magnetic Relaxation in a Seven-Coordinate Cobalt(II) Compound, *Inorg. Chem.*, 2016, **55**, 5957-5972.

75. P. Antal, B. Drahoš, R. Herchel and Z. Trávníček, Structure and Magnetism of Seven-Coordinate FeIII, FeII, CoII and NiII Complexes Containing a Heptadentate 15-Membered Pyridine-Based Macrocyclic Ligand, *Eur. J. Inorg. Chem.*, 2018, 4286-4297.

76. B. Drahoš, R. Herchel and Z. Trávníček, Single-Chain Magnet Based on 1D Polymeric Azido-Bridged Seven-Coordinate Fe(II) Complex with a Pyridine-Based Macrocyclic Ligand, *Inorg. Chem.*, 2018, **57**, 12718-12726.

77. H. Wang, A. Grosjean, C. Sinito, A. Kaiba, C. Balde, C. Desplanches, J.-F. Letard and P. Guionneau, Towards synergy between spin-crossover and metal-ligand bond break in molecular crystals: structural investigations of eight seven-coordinated Fe(ii) macrocyclic complexes, *CrystEngComm*, 2015, **17**, 4075-4079.

78. R. Ababei, C. Pichon, O. Roubeau, Y.-G. Li, N. Bréfuel, L. Buisson, P. Guionneau, C. Mathonière and R. Clérac, Rational Design of a Photomagnetic Chain: Bridging Single-Molecule Magnets with a Spin-Crossover Complex, *J. Am. Chem. Soc.*, 2013, **135**, 14840-14853.

79. Y.-Z. Zhang, B.-W. Wang, O. Sato and S. Gao, First Fe(ii)-based cyano-bridged single molecule magnet [CrIIIFeII2] with a large anisotropy, *Chem. Comm.*, 2010, **46**, 6959-6961.

80. D. Shao, S.-L. Zhang, X.-H. Zhao and X.-Y. Wang, Spin canting, metamagnetism, and single-chain magnetic behaviour in a cyano-bridged homospin iron(II) compound, *Chem. Comm.*, 2015, **51**, 4360-4363.

81. J. Wang, H.-H. Cui, Y.-Q. Zhang, L. Chen and X.-T. Chen, Magnetic anisotropy and slow magnetic relaxation of seven-coordinate cobalt(II)–nitrate complexes, *Polyhedron*, 2018, **154**, 148-155.

82. M. Dey, S. Dutta, B. Sarma, R. C. Deka and N. Gogoi, Modulation of the coordination environment: a convenient approach to tailor magnetic anisotropy in seven coordinate Co(ii) complexes, *Chem. Comm.*, 2016, **52**, 753-756.

83. D. Shao, L. Shi, S.-L. Zhang, X.-H. Zhao, D.-Q. Wu, X.-Q. Wei and X.-Y. Wang, Syntheses, structures, and magnetic properties of three new chain compounds based on a pentagonal bipyramidal Co(ii) building block, *CrystEngComm*, 2016, **18**, 4150-4157.

84. D. Shao, S.-L. Zhang, L. Shi, Y.-Q. Zhang and X.-Y. Wang, Probing the Effect of Axial Ligands on Easy-Plane Anisotropy of Pentagonal-Bipyramidal Cobalt(II) Single-Ion Magnets, *Inorg. Chem.*, 2016, **55**, 10859-10869.

85. B. Drahoš, R. Herchel and Z. Trávníček, Impact of Halogenido Coligands on Magnetic Anisotropy in Seven-Coordinate Co(II) Complexes, *Inorg. Chem.*, 2017, **56**, 5076-5088.

86. A. J. Bridgeman, G. Cavigliasso, L. R. Ireland and J. Rothery, The Mayer bond order as a tool in inorganic chemistry *Dalton Trans.*, 2001, 2095-2108.

87.   L. Chen, S.-Y. Chen, Y.-C. Sun, Y.-M. Guo, L. Yu, X.-T. Chen, Z. Wang, Z. W. Ouyang, Y. Song and Z.-L. Xue, Slow magnetic relaxation in mononuclear seven-coordinate cobalt(ii) complexes with easy plane anisotropy, *Dalton Trans.*, 2015, **44**, 11482-11490.

88.   G. Juhasz, R. Matsuda, S. Kanegawa, K. Inoue, O. Sato and K. Yoshizawa, Bistability of magnetization without spin-transition in a high-spin cobalt(II) complex due to angular momentum quenching, *J. Am. Chem. Soc.*, 2009, **131**, 4560-4561.

89.   S.-Q. Su, T. Kamachi, Z.-S. Yao, Y.-G. Huang, Y. Shiota, K. Yoshizawa, N. Azuma, Y. Miyazaki, M. Nakano, G. Maruta, S. Takeda, S. Kang, S. Kanegawa and O. Sato, Assembling an alkyl rotor to access abrupt and reversible crystalline deformation of a cobalt(II) complex, *Nat. Comm.*, 2015, **6**, 8810.

90.   D. Casanova, P. Alemany, J. M. Bofill and S. Alvarez, Shape and symmetry of heptacoordinated transition-metal complexes: structural trends, *Chem. Eur. J.*, 2003, **9**, 1281-1295.

91.   S. Gómez-Coca, A. Urtizberea, E. Cremades, P. J. Alonso, A. Camón, E. Ruiz and F. Luis, Origin of slow magnetic relaxation in Kramers ions with non-uniaxial anisotropy, *Nat Commun*, 2014, **5**, 5300.

92.   F.-X. Shen, H.-Q. Li, H. Miao, D. Shao, X.-Q. Wei, L. Shi, Y.-Q. Zhang and X.-Y. Wang, Heterometallic MIILnIII (M = Co/Zn; Ln = Dy/Y) Complexes with Pentagonal Bipyramidal 3d Centers: Syntheses, Structures, and Magnetic Properties, *Inorg. Chem.*, 2018, **57**, 15526-15536.

93.   Y.-Z. Zhang and O. Sato, A cyano-bridges $Cr^{III}Co^{II}$ ferromagnet with a chiral nanotubular structure constituted of interlocked single and double helices, *Inorg. Chem.*, 2010, **49**, 1271-1273.

94.   R. Zhang, L. Xu, Z.-H. Ni, H. Chen and L.-F. Zhang, Synthesis, crystal structure and magnetic properties of a new cyanide-bridged two-dimensional CrIII2CoII3 ferromagnet, *Inorg. Chem. Comm.*, 2016, **67**, 99-102.

95.   D. Shao, Y. Zhou, Q. Pi, F.-X. Shen, S.-R. Yang, S.-L. Zhang and X.-Y. Wang, Two-dimensional frameworks formed by pentagonal bipyramidal cobalt(II) ions and hexacyanometallates: antiferromagnetic ordering, metamagnetism and slow magnetic relaxation, *Dalton Trans.*, 2017, **46**, 9088–9096.

96.   F. Pan, S. Gao and H. Z. Liu, A heterometallic nanosized tube $\{Fe[(CN)_6]_2[Co(L^{N3O2})]_3\}n$ and two of its lamellar polymorphous isomers, *CrystEngComm*, 2015, **17**, 7490-7495.

97.   A. Choudhury, C. Pichon, J.-P. Sutter, D. Pamu, B. Sarma, P. P. Mudoi and N. Gogoi, Accessing water processable cyanido bridged chiral heterobimetallic Co(II)–Fe(III) one dimensional network, *Chem. Comm.*, 2021, **57**, 207-210.

98.   L. J. Batchelor, M. Sangalli, R. g. Guillot, N. Guihéry, R. Maurice, F. Tuna and T. Mallah, Pentanuclear Cyanide-Bridged Complexes Based on Highly Anisotropic Co^{II} Seven-Coordinate Building Blocks: Synthesis, Structure, and Magnetic Behavior, *Inorg. Chem.*, 2011, **50**, 12045.

99.   X.-C. Huang, C. Zhou, D. Shao and X.-Y. Wang, Field-Induced Slow Magnetic Relaxation in Cobalt(II) Compounds with Pentagonal Bipyramid Geometry, *Inorg. Chem.*, 2014, **53**, 12671-12673.

100.   F. Habib, I. Korobkov and M. Murugesu, Exposing the intermolecular nature of the second relaxation pathway in a mononuclear cobalt(II) single-molecule magnet with positive anisotropy, *Dalton Trans.*, 2015, **44**, 6368-6373.

101.   F. Schleife, A. Rodenstein, R. Kirmse and B. Kersting, Seven-coordinate Mn(II) and Co(II) complexes of the pentadentate ligand 2,6-diacetyl-4-carboxymethyl-pyridine bis(benzoylhydrazone): Synthesis, crystal structure and magnetic properties, *Inorg. Chim. Acta*, 2011, **374**, 521.

102.   E. Bartolome, P. J. Alonso, A. Arauzo, J. Luzon, J. Bartolome, C. Racles and C. Turta, Magnetic properties of the seven-coordinated nanoporous framework material $Co(bpy)_{1.5}(NO_3)_2$ (bpy = 4,4[prime or minute]-bipyridine), *Dalton Trans*, 2012, **41**, 10382-10389.

103. A. K. Mondal, A. Mondal, B. Dey and S. Konar, Influence of the Coordination Environment on Easy-Plane Magnetic Anisotropy of Pentagonal Bipyramidal Cobalt(II) Complexes, *Inorg. Chem.*, 2018, **57**, 9999-10008.

104. V. A. Kopotkov, D. V. Korchagin, V. D. Sasnovskaya, I. F. Gilmutdinov and E. B. Yagubskii, A Series of Field-Induced Single-Ion Magnets Based on the Seven-Coordinate Co(II) Complexes with the Pentadentate (N3O2) H2dapsc Ligand, *Magnetochemistry*, 2019, **5**, 58.

105. A. Mondal, A. K. Kharwar and S. Konar, Sizeable Effect of Lattice Solvent on Field Induced Slow Magnetic Relaxation in Seven Coordinated CoII Complexes, *Inorg. Chem.*, 2019, **58**, 10686-10693.

106. C. Platas-Iglesias, L. Vaiana, D. Esteban-Gomez, F. Avecilla, J. A. Real, A. de Blas and T. Rodriguez-Blas, Electronic structure studiy of seven-coordinate first-row transition metal complexes derived from 1,10-diaza-15-crown-5: a successful marriage of theory with experiment, *Inorg. Chem.*, 2005, **44**, 9704-9713.

107. M. Regueiro-Figueroa, L. M. P. Lima, V. Blanco, D. Esteban-Gómez, A. de Blas, T. Rodríguez-Blas, R. Delgado and C. Platas-Iglesias, Reasons behind the Relative Abundances of Heptacoordinate Complexes along the Late First-Row Transition Metal Series, *Inorg. Chem.*, 2014, **53**, 12859-12869.

108. D. Wester and G. J. Palenik, Pentagonal Bipyramidal Complexes of Nickel(II) and Copper(II). The Relative Importance of Ligand Geometry vs. Crystal Field Effects, *J. Am. Chem. Soc.*, 1974, **96**, 7565-7566.

109. C. W. G. Ansell, J. Lewis, P. R. Raithby, J. N. Ramsden and M. Schroder, X-Ray crystal structure of the pentagonal bipyramidal nickel(II) complex [Ni(L)(H$_2$O)$_2$](BF$_4$)$_2$ and the selective stabilisation of the nickel(I) oxidation state by a quinquedentate macrocyclic ligand, *Chem. Comm.*, 1982, 546-547.

110. T. J. Giordano, G. J. Palenik, R. C. Palenik and D. A. Sullivan, Pentagonal-Bipyramidal Complexes. Synthesis and Characterization of Aqua(nitrato)[2,6-diacetylpyridinebis(benzoic acid hydrazone)]cobalt(II) Nitrate and Diaqua[2,6-diacetylpyridinebis(benzoic acid hydrazone)]nickel(II) Nitrate Dihydrate, *Inorg. Chem.*, 1979, **18**, 2445-2450.

111. N. Gogoi, M. Thlijeni, C. Duhayon and J.-P. Sutter, Heptacoordinated Nickel(II) as an Ising-Type Anisotropic Building Unit: Illustration with a Pentanuclear [(NiL)$_3${W(CN)$_8$}$_2$] Complex, *Inorg. Chem.*, 2013, **52**, 2283-2285.

112. M. Reczyński, M. Akaki, T. Fukuda, Y. Sawada, K. Nishii, M. Hagiwara, W. Nitek, B. Sieklucka and B. Nowicka, Hepta-coordinated Ni(II) assemblies – structure and magnetic studies, *Dalton Trans.*, 2021, **50**, 5251-5261.

113. M. Dey, P. P. Mudoi, A. Choudhury, B. Sarma and N. Gogoi, Deciphering the influence of structural distortions on the uniaxial magnetic anisotropy of pentagonal bipyramidal Ni(II) complexes, *Chem. Comm.*, 2019, **55**, 11547-11550.

114. M. Llunell, D. Casanova, J. Cirera, P. Alemany and S. Alvarez, *SHAPE: Program for the stereochemical analysis of molecular fragments by means of continuous shape measures and associated tools*, University of Barcelona, Barcelona, 2013

115. B. Drahoš, personal communication.

116. T. Fukuda and B. Nowicka, personal communication.

117. K. Wang, S. Tang, Z.-B. Hu, H.-H. Zou, X.-L. Wang, Y. Li, S.-H. Zhang, Z.-L. Chen and F.-P. Liang, A family of 3d metal clusters based on N-N single bonds bridged quasi-linear trinuclear cores: the Mn analogue displaying single-molecule magnet behavior, *RSC Advances*, 2018, **8**, 6218-6224.

118. S. Naskar, D. Mishra, A. J. Blake and S. K. Chattopadhyay, Synthesis, characterization, and crystal structure of [Ni(dap(A)$_2$)]$_2$ (dap(AH)$_2$: 2,6-diacetylpyridine bis(anthraniloyl hydrazone))—a molecule possessing an infinite double helical chain in the solid state, *Struct. Chem.*, 2007, **18**, 217-222.

119. K. Ishizu, T. Haruta, Y. Kohno, K. Mukai, K. Miyoshi and Y. Sugiura, Electron Spin Resonance Study of Cu(II)–Crown Ether Complexes with $3d_{Z^2}$ Ground State Doublet in Solution, *Bull. Chem.Soc. Jpn.*, 1980, **53**, 3513-3516.

120. X.-S. Gao, C.-C. Ni and X.-M. Ren, Syntheses, crystal structures, photoluminescent and magnetic properties of complexes of zinc(II) and copper(II) with Schiff-base ligands derived from 2,6-diacetylpyridine, *Polyhedron*, 2017, **138**, 225-231.

121. S. Ianelli, C. Pelizzi, G. Pelizzi and P. Tarasconi, Heptacoordination in MnII, NiII, and CuII complexes of 2,6-diacetylpyridine bis (acetylhydrazone), *J. Chem. Cryst.*, 1996, **26**, 195-201.

122. M. G. B. Drew, J. Nelson and S. M. Nelson, Synthesis of some pentagonal-bipyramidal complexes of manganese(II), iron(II), cobalt(II), nickel(II), copper(II), and zinc(II) with a heptadentate Schiff-base ligand and the crystal and molecular structures of a copper(II) complex, *Dalton Trans.*, 1981, 1685-1690.

123. V. E. Marquez, J. R. Anacona and D. Loroño, Crystal structure and electrochemistry of copper(II) macrocycles containing terpyridine, *Polyhedron*, 2004, **23**, 1317-1323.

124. Z. Urbańczyk-Lipkowska, P. Gluziński, J. W. Krajewski, R. A. Koliński, A. Kemme and A. Mishnyov, Crystal and molecular structure of 1,4,10-trioxa-7,13-diaza-cyclopentadecane-7,13-diacetatocopper (II) dihydrate, $C_{114}H_{24}N_2O_7Cu \cdot 2H_2O$, *J. Cryst. Spectro. Res.*, 1989, **19**, 387-397.

125. T. Sakurai, K. Kobayashi, S. Tsuboyama, Y. Kohno, N. Azuma and K. Ishizu, Structure of dichloro(5,6,8,9,11,12,14,15-octahydro-2,3-benzo-1,4,7,10,13-pentaoxacyclopentadec-2-ene)copper(II) chloroform solvate, $[Cu(C_{14}H_{20}O_5)Cl_2].CHCl_3$, a Cu^{II}-crown-ether complex with pentagonal-bipyramidal geometry, *Acta Cryst. C*, 1983, **39**, 206-208.

126. I. Kazuhiko, H. Tokuhiro, N. Kazuhiro, M. Kiyonori and S. Yukio, ESR g-ANISOTROPY INVERSION OBSERVED FOR Cu(II)-CROWN ETHER COMPLEX IN SOLUTION, *Chem. Lett.*, 1978, **7**, 579-582.

127. F. Dejehet, R. Debuyst, Y. Y. Wei, J.-P. Declercq and B. Tinant, Étude cristallographique et par RPE du diaqua(15-couronne-5 ether) cuivre(II) nitrate, *J. Chim. Phys.*, 1987, **84**, 975-979.

128. C. Rodríguez-Infante, D. Esteban, F. Avecilla, A. de Blas, T. Rodríguez-Blas, J. Mahía, A. L. Macedo and C. F. G. C. Geraldes, Copper complexes with bibracchial lariat ethers: from mono- to binuclear structures, *Inorg. Chim. Acta*, 2001, **317**, 190-198.

129. T. Konno, K. Koide and T. Ishida, A supramolecular switch between ground high- and low-spin states using 2,2′:6′,2′′-terpyridine-6,6′′-diyl bis(tert-butyl nitroxide), *Chem. Comm.*, 2013, **49**, 5156-5158.

130. C. Dey and R. Banerjee, POM-Catalyzed In Situ Ligand Synthesis for the Construction of Metal Complexes and Their Use in the Formation of Coordination Polymers, *ChemPhysChem*, 2013, **14**, 1009-1015.

131. D. N. Woodruff, R. E. P. Winpenny and R. A. Layfield, Lanthanide Single-Molecule Magnets, *Chem. Rev.*, 2013, **113**, 5110-5148.

132. S. T. Liddle and J. van Slageren, Improving f-element single molecule magnets, *Chem. Soc. Rev.*, 2015, **44**, 6655-6669.

133. J. D. Rinehart and J. R. Long, Exploiting single-ion anisotropy in the design of f-element single-molecule magnets, *Chem. Sci.*, 2011, **2**, 2078-2085.

134. J. Sievers, Asphericity of 4f-shells in their Hund's rule ground states, *Z. Phys. B, Cond. Mater.*, 1982, **45**, 289-296.

135. S.-D. Jiang and S.-X. Qin, Prediction of the quantized axis of rare-earth ions: the electrostatic model with displaced point charges, *Inorg. Chem. Front.*, 2015, **2**, 613-619.

136. P. Zhang, L. Zhang, C. Wang, S. Xue, S.-Y. Lin and J. Tang, Equatorially Coordinated Lanthanide Single Ion Magnets, *J. Am. Chem. Soc.*, 2014, **136**, 4484-4487.

137. A. J. Brown, D. Pinkowicz, M. R. Saber and K. R. Dunbar, A Trigonal-Pyramidal Erbium(III) Single-Molecule Magnet, *Angew. Chem. Int. Ed.*, 2015, **54**, 5864-5868.

138. P. Zhang, J. Jung, L. Zhang, J. Tang and B. Le Guennic, Elucidating the Magnetic Anisotropy and Relaxation Dynamics of Low-Coordinate Lanthanide Compounds, *Inorg. Chem.*, 2016, **55**, 1905-1911.

139. K. L. M. Harriman, J. L. Brosmer, L. Ungur, P. L. Diaconescu and M. Murugesu, Pursuit of Record Breaking Energy Barriers: A Study of Magnetic Axiality in Diamide Ligated DyIII Single-Molecule Magnets, *J. Am. Chem. Soc.*, 2017, **139**, 1420-1423.

140. A. K. Bar, P. Kalita, M. K. Singh, G. Rajaraman and V. Chandrasekhar, Low-coordinate mononuclear lanthanide complexes as molecular nanomagnets, *Coord. Chem. Rev.*, 2018, **367**, 163-216.

141. P. Kalita, J. Acharya and V. Chandrasekhar, Mononuclear pentagonal bipyramidal Ln(III) complexes: Syntheses and magnetic properties, *J. Magn. Magn. Mater.*, 2020, **498**, 166098.

142. Z. Zhu, M. Guo, X.-L. Li and J. Tang, Molecular magnetism of lanthanide: Advances and perspectives, *Coord. Chem. Rev.*, 2019, **378**, 350-364.

143. J. Long, A. O. Tolpygin, D. M. Lyubov, N. Y. Rad'kova, A. V. Cherkasov, Y. V. Nelyubina, Y. Guari, J. Larionova and A. A. Trifonov, High magnetization reversal barriers in luminescent dysprosium octahedral and pentagonal bipyramidal single-molecule magnets based on fluorinated alkoxide ligands, *Dalton Trans.*, 2021, **50**, 8487-8496.

144. Y.-S. Ding, N. F. Chilton, R. E. P. Winpenny and Y.-Z. Zheng, On Approaching the Limit of Molecular Magnetic Anisotropy: A Near-Perfect Pentagonal Bipyramidal Dysprosium(III) Single-Molecule Magnet, *Angew. Chem. Int. Ed.*, 2016, **55**, 16071-16074.

145. Y.-S. Ding, T. Han, Y.-Q. Zhai, D. Reta, N. F. Chilton, R. E. P. Winpenny and Y.-Z. Zheng, A Study of Magnetic Relaxation in Dysprosium(III) Single-Molecule Magnets, *Chem. Eur. J.*, 2020, **26**, 5893-5902.

146. Z.-H. Li, Y.-Q. Zhai, W.-P. Chen, Q.-C. Luo, T. Han and Y.-Z. Zheng, Breaking the axiality of pentagonal–bipyramidal dysprosium(iii) single-molecule magnets with pyrazolate ligands, *Inorg. Chem. Front.*, 2020, **7**, 4367-4376.

147. Y.-N. Guo, L. Ungur, G. E. Granroth, A. K. Powell, C. Wu, S. E. Nagler, J. Tang, L. F. Chibotaru and D. Cui, An NCN-pincer ligand dysprosium single-ion magnet showing magnetic relaxation via the second excited state, *Sci. Rep.*, 2014, **4**, 5471.

148. A. B. Canaj, M. K. Singh, C. Wilson, G. Rajaraman and M. Murrie, Chemical and in silico tuning of the magnetisation reversal barrier in pentagonal bipyramidal Dy(III) single-ion magnets, *Chem. Comm.*, 2018, **54**, 8273-8276.

149. L.-L. Li, H.-D. Su, S. Liu, Y.-C. Xu and W.-Z. Wang, A new air- and moisture-stable pentagonal-bipyramidal Dy^{III} single-ion magnet based on the HMPA ligand, *Dalton Trans.*, 2019, **48**, 2213-2219.

150. Y.-C. Chen, J.-L. Liu, L. Ungur, J. Liu, Q.-W. Li, L.-F. Wang, Z.-P. Ni, L. F. Chibotaru, X.-M. Chen and M.-L. Tong, Symmetry-Supported Magnetic Blocking at 20 K in Pentagonal Bipyramidal Dy(III) Single-Ion Magnets, *J. Am. Chem. Soc.*, 2016, **138**, 2829-2837.

151. I. F. Díaz-Ortega, J. M. Herrera, S. Dey, H. Nojiri, G. Rajaraman and E. Colacio, The effect of the electronic structure and flexibility of the counteranions on magnetization relaxation in [Dy(L)2(H2O)5]3+ (L = phosphine oxide derivative) pentagonal bipyramidal SIMs, *Inorg. Chem. Front.*, 2020, **7**, 689-699.

152. K. Jia, X. Meng, M. Wang, X. Gou, Y.-X. Wang, N. Xu, W. Shi and P. Cheng, Enhancing the energy barrier and hysteresis temperature in two benchtop-stable Ho(III) single-ion magnets, *Chem. Comm.*, 2021, **57**, 3607-3610.

153. S. K. Gupta, T. Rajeshkumar, G. Rajaraman and R. Murugavel, Is a strong axial crystal-field the only essential condition for a large magnetic anisotropy barrier? The case of non-Kramers Ho(III) versus Tb(III), *Dalton Trans.*, 2018, **47**, 357-366.

154. S. K. Gupta, T. Rajeshkumar, G. Rajaraman and R. Murugavel, An air-stable Dy(III) single-ion magnet with high anisotropy barrier and blocking temperature, *Chem. Sci.*, 2016, **7**, 5181-5191.

155. S. K. Gupta, T. Rajeshkumar, G. Rajaraman and R. Murugavel, An unprecedented zero field neodymium(III) single-ion magnet based on a phosphonic diamide, *Chem. Comm.*, 2016, **52**, 7168-7171.

156. L.-L. Li, H.-D. Su, S. Liu and W.-Z. Wang, Enhancing the energy barrier by replacing the counterions in two holmium(III)-pentagonal bipyramidal single-ion magnets, *Dalton Trans.*, 2020, **49**, 6703-6709.

157. Y.-C. Chen, J.-L. Liu, W. Wernsdorfer, D. Liu, L. F. Chibotaru, X.-M. Chen and M.-L. Tong, Hyperfine-Interaction-Driven Suppression of Quantum Tunneling at Zero Field in a Holmium(III) Single-Ion Magnet, *Angew. Chem. Int. Ed.*, 2017, **56**, 4996-5000.

158. Y.-C. Chen, J.-L. Liu, Y. Lan, Z.-Q. Zhong, A. Mansikkamäki, L. Ungur, Q.-W. Li, J.-H. Jia, L. F. Chibotaru, J.-B. Han, W. Wernsdorfer, X.-M. Chen and M.-L. Tong, Dynamic Magnetic and Optical Insight into a High Performance Pentagonal Bipyramidal Dy^{III} Single-Ion Magnet, *Chem. Eur. J.*, 2017, **23**, 5708-5715.

159. J. Long, A. N. Selikhov, E. Mamontova, K. A. Lyssenko, Y. Guari, J. Larionova and A. A. Trifonov, Single-molecule magnet behaviour in a Dy(III) pentagonal bipyramidal complex with a quasi-linear Cl–Dy–Cl sequence, *Dalton Trans.*, 2019, **48**, 35-39.

160. Y.-S. Ding, K.-X. Yu, D. Reta, F. Ortu, R. E. P. Winpenny, Y.-Z. Zheng and N. F. Chilton, Field- and temperature-dependent quantum tunnelling of the magnetisation in a large barrier single-molecule magnet, *Nat. Comm.*, 2018, **9**, 3134.

161. Y. Ma, Y.-Q. Zhai, Y.-S. Ding, T. Han and Y.-Z. Zheng, Understanding a pentagonal-bipyramidal holmium(III) complex with a record energy barrier for magnetisation reversal, *Chem. Comm.*, 2020, **56**, 3979-3982.

162. S. Li, J. Xiong, Q. Yuan, W.-H. Zhu, H.-W. Gong, F. Wang, C.-Q. Feng, S.-Q. Wang, H.-L. Sun and S. Gao, Effect of the Transition Metal Ions on the Single-Molecule Magnet Properties in a Family of Air-Stable 3d–4f Ion-Pair Compounds with Pentagonal Bipyramidal Ln(III) Ions, *Inorg. Chem.*, 2021, **60**, 18990-19000.

163. A. K. Bar, P. Kalita, J.-P. Sutter and V. Chandrasekhar, Pentagonal-Bipyramid Ln(III) Complexes Exhibiting Single-Ion-Magnet Behavior: A Rational Synthetic Approach for a Rigid Equatorial Plane, *Inorg. Chem.*, 2018, **57**, 2398-2401.

164. A. B. Canaj, S. Dey, C. Wilson, O. Céspedes, G. Rajaraman and M. Murrie, Engineering macrocyclic high performance pentagonal bipyramidal Dy(III) single-ion magnets, *Chem. Comm.*, 2020, **56**, 12037-12040.

165. J. Wang, Q.-W. Li, S.-G. Wu, Y.-C. Chen, R.-C. Wan, G.-Z. Huang, Y. Liu, J.-L. Liu, D. Reta, M. J. Giansiracusa, Z.-X. Wang, N. F. Chilton and M.-L. Tong, Opening Magnetic Hysteresis by Axial Ferromagnetic Coupling: From Mono-Decker to Double-Decker Metallacrown, *Angew. Chem. Int. Ed.*, 2021, **60**, 5299-5306.

166. L. E. d. N. Aquino, G. A. Barbosa, J. d. L. Ramos, S. O. K. Giese, F. S. Santana, D. L. Hughes, G. G. Nunes, L. Fu, M. Fang, G. Poneti, A. N. Carneiro Neto, R. T. Moura, R. A. S. Ferreira, L. D. Carlos, A. G. Macedo and J. F. Soares, Seven-Coordinate Tb3+ Complexes with 90% Quantum Yields: High-Performance Examples of Combined Singlet- and Triplet-to-Tb3+ Energy-Transfer Pathways, *Inorg. Chem.*, 2021, **60**, 892-907.

167. Y. Liu, Y.-C. Chen, J. Liu, W.-B. Chen, G.-Z. Huang, S.-G. Wu, J. Wang, J.-L. Liu and M.-L. Tong, Cyanometallate-Bridged Didysprosium Single-Molecule Magnets Constructed with Single-Ion Magnet Building Block, *Inorg. Chem.*, 2020, **59**, 687-694.

168. J. Liu, Y.-C. Chen, J.-L. Liu, V. Vieru, L. Ungur, J.-H. Jia, L. F. Chibotaru, Y. Lan, W. Wernsdorfer, S. Gao, X.-M. Chen and M.-L. Tong, A Stable Pentagonal Bipyramidal Dy(III) Single-Ion Magnet with a Record Magnetization Reversal Barrier over 1000 K, *J. Am. Chem. Soc.*, 2016, **138**, 5441-5450.

169. Z. Jiang, L. Sun, Q. Yang, B. Yin, H. Ke, J. Han, Q. Wei, G. Xie and S. Chen, Excess axial electrostatic repulsion as a criterion for pentagonal bipyramidal DyIII single-ion magnets with high Ueff and TB, *J. Mater. Chem. C*, 2018, **6**, 4273-4280.

170. Y. Dong, L. Zhu, B. Yin, X. Zhu and D. Li, Regulating the magnetic properties of seven-coordinated Dy(iii) single-ion magnets through the effect of positional isomers on axial crystal-field, *Dalton Trans.*, 2021, **50**, 17328-17337.

171. J.-L. Liu, Y.-C. Chen, Y.-Z. Zheng, W.-Q. Lin, L. Ungur, W. Wernsdorfer, L. F. Chibotaru and M.-L. Tong, Switching the anisotropy barrier of a single-ion magnet by symmetry change from quasi-D_{5h} to quasi-Oh, *Chem. Sci.*, 2013, **4**, 3310-3316.

172. G.-Z. Huang, Z.-Y. Ruan, J.-Y. Zheng, Y.-C. Chen, S.-G. Wu, J.-L. Liu and M.-L. Tong, Seeking magneto-structural correlations in easily tailored pentagonal bipyramid Dy(III) single-ion magnets, *Sci. China Chem.*, 2020, **63**, 1066-1074.

173. M. Li, H. Wu, Q. Yang, H. Ke, B. Yin, Q. Shi, W. Wang, Q. Wei, G. Xie and S. Chen, Experimental and Theoretical Interpretation on the Magnetic Behavior in a Series of Pentagonal-Bipyramidal DyIII Single-Ion Magnets, *Chem. Eur. J.*, 2017, **23**, 17775-17787.

174. H. Wu, M. Li, B. Yin, Z. Xia, H. Ke, Q. Wei, G. Xie, S. Chen and S. Gao, Fine-tuning the type of equatorial donor atom in pentagonal bipyramidal Dy(III) complexes to enhance single-molecule magnet properties, *Dalton Trans.*, 2019, **48**, 16384-16394.

175. P. Kalita, N. Ahmed, A. K. Bar, S. Dey, A. Jana, G. Rajaraman, J.-P. Sutter and V. Chandrasekhar, Pentagonal Bipyramidal Ln(III) Complexes Containing an Axial Phosphine Oxide Ligand: Field-induced Single-ion Magnetism Behavior of the Dy(III) Analogues, *Inorg. Chem.*, 2020, **59**, 6603-6612.

176. D.-Q. Wu, D. Shao, X.-Q. Wei, F.-X. Shen, L. Shi, Y.-Q. Zhang and X.-Y. Wang, Single-ion magnetism in seven-coordinate YbIII complexes with distorted D5h coordination geometry, *Dalton Trans.*, 2017, **46**, 12884-12892.

177. T. A. Bazhenova, V. A. Kopotkov, D. V. Korchagin, Y. V. Manakin, L. V. Zorina, S. V. Simonov, I. A. Yakushev, V. S. Mironov, A. N. Vasiliev, O. V. Maximova and E. B. Yagubskii, A Series of Novel Pentagonal-Bipyramidal Erbium(III) Complexes with Acyclic Chelating N3O2 Schiff-Base Ligands: Synthesis, Structure, and Magnetism, *Molecules*, 2021, **26**, 6908.

178. X.-C. Huang, S.-C. Yan, C.-L. Ji, Z.-Y. Qi, Y.-M. Guo and J.-Q. Tao, Two one-dimensional lanthanide compounds with pentagonal bipyramidal ErIII centers showing slow magnetic relaxation, *Polyhedron*, 2018, **139**, 289-295.

179. X.-C. Huang, M. Zhang, D. Wu, D. Shao, X.-H. Zhao, W. Huang and X.-Y. Wang, Single molecule magnet behavior observed in a 1-D dysprosium chain with quasi-D5h symmetry, *Dalton Trans.*, 2015, **44**, 20834-20838.

180. E. L. Gavey, Y. Beldjoudi, J. M. Rawson, T. C. Stamatatos and M. Pilkington, Slow relaxation in the first penta-aza Dy(III) macrocyclic complex, *Chem. Comm.*, 2014, **50**, 3741-3743.

181. Q. Chen, F. Ma, Y.-S. Meng, H.-L. Sun, Y.-Q. Zhang and S. Gao, Assembling Dysprosium Dimer Units into a Novel Chain Featuring Slow Magnetic Relaxation via Formate Linker, *Inorg. Chem.*, 2016, **55**, 12904-12911.

182. J. Acharya, N. Ahmed, J. Flores Gonzalez, P. Kumar, O. Cador, S. K. Singh, F. Pointillart and V. Chandrasekhar, Slow magnetic relaxation in a homo dinuclear Dy(III) complex in a pentagonal bipyramidal geometry, *Dalton Trans.*, 2020, **49**, 13110-13122.

183. Z.-F. Yang, Y.-M. Tian, W.-Y. Zhang, P. Chen, H.-F. Li, Y.-Q. Zhang and W.-B. Sun, High local coordination symmetry around the spin center and the alignment between magnetic and symmetric axes together play a crucial role in single-molecule magnet performance, *Dalton Trans.*, 2019, **48**, 4931-4940.

184. S. Yu, Z. Chen, H. Hu, B. Li, Y. Liang, D. Liu, H. Zou, D. Yao and F. Liang, Two mononuclear dysprosium(III) complexes with their slow magnetic relaxation behaviors tuned by coordination geometry, *Dalton Trans.*, 2019, **48**, 16679-16686.

185. C. A. P. Goodwin, F. Ortu, D. Reta, N. F. Chilton and D. P. Mills, Molecular magnetic hysteresis at 60 kelvin in dysprosocenium, *Nature*, 2017, **548**, 439-442.

186. F.-S. Guo, B. M. Day, Y.-C. Chen, M.-L. Tong, A. Mansikkamäki and R. A. Layfield, Magnetic hysteresis up to 80 kelvin in a dysprosium metallocene single-molecule magnet, *Science*, 2018, **362**, 1400-1403.